NAVAL POSTGRADUATE SCHOOL
MONTEREY, CALIFORNIA

THESIS

LASER ANEMOMETRY AND PRESSURE MEASUREMENTS IN THE ENDWALL REGION OF AN ANNULAR TURBINE CASCADE UTILIZING A PRESSURIZED AERODYNAMIC WINDOW

by

Michael H. Guerrera

September 1996

Thesis Advisor: Garth V. Hobson

Approved for public release; distribution is unlimited

REPORT DOCUMENTATION PAGE

Form Approved
OMB No. 0704-0188

1.AGENCY USE ONLY *(Leave blank)*	2.REPORT DATE	3.REPORT TYPE AND DATES COVERED
	September 1996	Master's Thesis

4.TITLE AND SUBTITLE LASER ANEMOMETRY AND PRESSURE MEASUREMENTS IN THE ENDWALL REGION OF AN ANNULAR TURBINE CASCADE UTILIZING A PRESSURIZED AERODYNAMIC WINDOW

5.FUNDING NUMBERS

6.AUTHOR(S)
Guerrera, Michael H.

7.PERFORMING ORGANIZATION NAME(S) AND ADDRESS(ES)
Naval Postgraduate School
Monterey CA 93943-5000

8.PERFORMING ORGANIZATION REPORT NUMBER

9.SPONSORING/MONITORING AGENCY NAME(S) AND ADDRESS(ES)
Naval Air Warfare Center Aircraft Division, AIR-4.4.3.1(Attn: D. Parish) Propulsion and Power Engineering, Building 106, Patuxent River, MD 20670-5304

10.SPONSORING/MONITORING AGENCY REPORT NUMBER

11.SUPPLEMENTARY NOTES The views expressed in this thesis are those of the author and do not reflect the official policy or position of the Department of Defense or the U.S. Government.

12a.DISTRIBUTION/AVAILABILITY STATEMENT
Approved for public release; distribution is unlimited.

12b. DISTRIBUTION CODE

13.ABSTRACT*(maximum 200 words)*

The purpose of this research was to compare previous laser-anemometry measurements obtained through an unpressurized laser window with the results from a pressurized laser window and to validate this innovative measuring technique in the endwall region of a confined annulus. Two-dimensional velocity, flow angle, and turbulence intensity measurements were obtained with a fiber-optics laser-Doppler velocimeter. The measurements were performed through a 1.09 mm opening in the endwall region of an annular turbine cascade at depths ranging from 0.01 mm to 0.89 mm with varying pressure applied to the chamber of the modified window. Cobra probe measurements were performed to validate the flow angles obtained by the laser anemometer. The cascade was modified to measure the inlet profile, which was performed with a three-hole probe.

14. SUBJECT TERMS	15.NUMBER OF PAGES
Annular Turbine Cascade, Surface Pressure Measurement, Laser-Doppler Velocimetry, Cobra Probe	108
	16.PRICE CODE

17. SECURITY CLASSIFICATION OF REPORT	18. SECURITY CLASSIFICATION OF THIS PAGE	19.SECURITY CLASSIFICATION OF ABSTRACT	20.LIMITATION OF ABSTRACT
Unclassified	Unclassified	Unclassified	UL

NSN7540-01-280-5500
Form 298 (Rev. 2-89)
Std. 239-18

Standard
Prescribed by ANSI
298-102

Approved for public release; distribution is unlimited.

LASER ANEMOMETRY AND PRESSURE MEASUREMENTS IN THE ENDWALL REGION OF AN ANNULAR TURBINE CASCADE UTILIZING A PRESSURIZED AERODYNAMIC WINDOW

Michael H. Guerrera
Lieutenant, United States Navy
B.S., United States Naval Academy, 1986

Submitted in partial fulfillment of the
requirements for the degree of

MASTER OF SCIENCE IN AERONAUTICAL ENGINEERING

from the

NAVAL POSTGRADUATE SCHOOL
September 1996

ABSTRACT

The purpose of this research was to compare previous laser-anemometry measurements obtained through an unpressurized laser window with the results from a pressurized laser window and to validate this innovative measuring technique in the endwall region of a confined annulus. Two-dimensional velocity, flow angle, and turbulence intensity measurements were obtained with a fiber-optics laser-Doppler velocimeter. The measurements were performed through a 1.09 mm opening in the endwall region of an annular turbine cascade at depths ranging from 0.01 mm to 0.89 mm with varying pressure applied to the chamber of the modified window. Cobra probe measurements were performed to validate the flow angles obtained by the laser anemometer. The cascade was modified to measure the inlet profile, which was performed with a three-hole probe.

TABLE OF CONTENTS

LIST OF FIGURES

LIST OF TABLES

ACKNOWLEDGMENTS

This work would not have been possible without the guidance and support of several dedicated individuals. I thank Professor Garth Hobson for his friendship, patience, and sincere passion for engineering. His ability to touch the lives of so many with his vast knowledge while motivating individual interests make him one of the finest instructors that I have ever had.

The combination of a friendly working environment and technical expertise make the Turbopropulsion Laboratory an outstanding place for research. My thanks to Professor Shreeve, Rick Still, Thad Best, and Don Harvey who assisted me numerous times during my project. ---"Don't Touch the Blue Knob!"

My greatest thanks go to my family. The continuous motivation instilled in me by my parents, Louis and Miyuki, and the sense of humor provided by my brother, Peter, will guide me for life. They have accomplished everything along with me and have made me a better person. Finally, my thanks to my best friend and wife, Eleanor. Her constant drive, continuous support, and smiling face will always be in my heart. Aloha to you all.

I. INTRODUCTION

Modern propulsion systems have improved rapidly over the last few decades which in turn have required continual developments in measurement techniques in turbomachinery. Non-intrusive measurement techniques are essential for providing the fundamental insight of the secondary flows in the annular blade rows of the next generation turbines. The design and performance of turbomachinery begin with this understanding. Secondary flows, together with tip leakage flows, produce considerable flow distortions in the endwall region which results in the majority of the losses within a turbine [Ref. 1]. By understanding the flow mechanics in this region, current CFD programs can be validated, improving both current blade designs and turbine efficiencies.

Three previous investigations of the flow through the annular turbine cascade (ATC) have been conducted at the Naval Postgraduate School [Ref. 2-4]. Reference 4 included design and manufacturing information of the annular turbine cascade that was developed to determine the limitations of laser-Doppler velocity (LDV) measurements in a confined annulus. Reference 3 included additional laser and pressure probe access modifications and initial LDV measurements within the same ATC. Reference 2 included further ATC modifications for midspan blade surface pressure measurements and LDV measurements of the endwall flow. The present study was of the feasibility of an innovative pressurized laser window and then to determine its effect on current LDV near-wall flow measurements. Three-hole pressure probe measurements were also conducted to compare with the LDV measurements. Radial LDV surveys were performed through a small access hole in the outer casing through the pressurized window to compare with previous results that used an open aerodynamic window (laser blank). Circumferential surveys were obtained at different radial locations close to the endwall. Blade midspan surface pressures were measured within one blade passage at various inlet total-to-downstream hub-static pressure ratios. Blade surface pressure and endwall flow measurements were compared with previous measurements.

II. EXPERIMENTAL APPARATUS

A. TEST FACILITY AND ANNULAR TURBINE CASCADE

The ATC was developed to provide small-scale testing of flow through a turbine stator. Airflow for the Annular Turbine Cascade experiment was provided by a VA-312 Allis-Chalmers 12-stage axial-flow compressor located at the Turbopropulsion Laboratory of the Naval Postgraduate School. The compressor was operated at 12,000 rpm at various discharge pressures and provided metered air to a plenum chamber. Air from the plenum was routed to a 232 mm (9.170 in) diameter bellmouth and test section through honeycomb flow straighteners in a 254 mm (10 in) flanged steel pipe as shown in Figure 1.

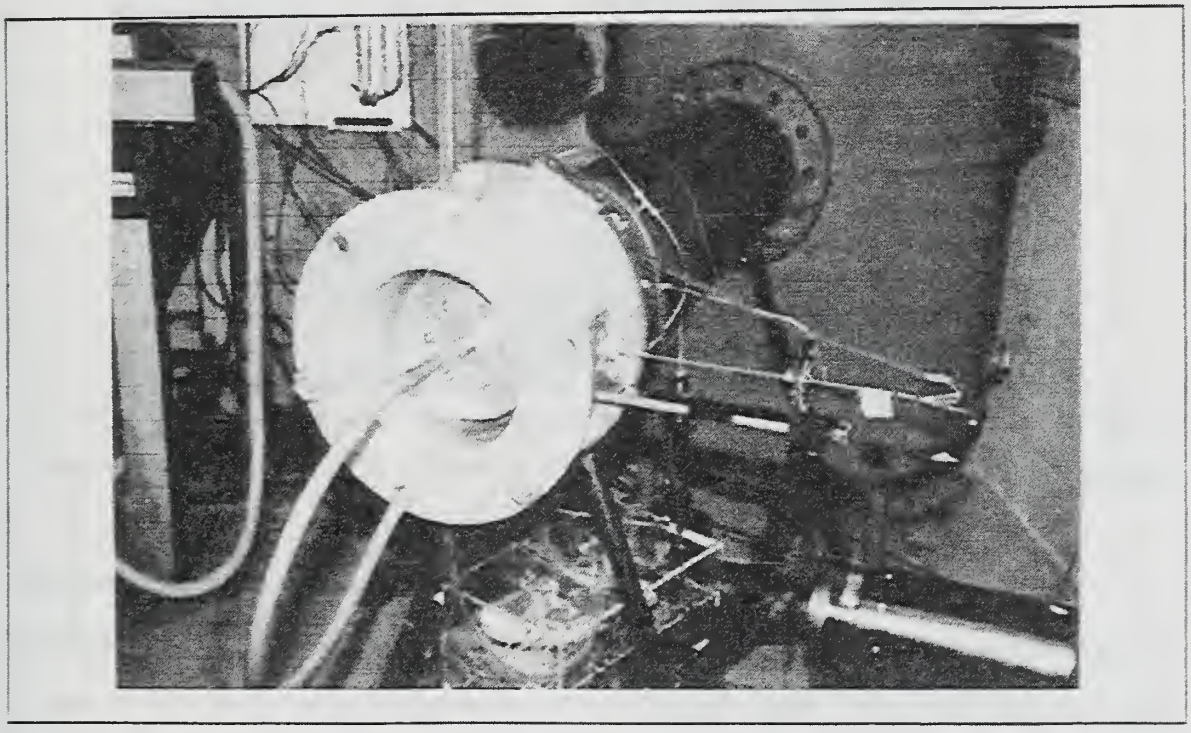

Figure 1. Annular turbine cascade (ATC)

Flow stagnation pressure was measured at two upstream locations. One combination probe provided pressure-setting information to a mercury manometer board and a digital readout of flow stagnation temperature, while the second probe was connected to a Scanivalve (Figure 2). Four (averaged) upstream static ports and four (averaged) inner hub downstream (one-half axial chord) static ports were also connected to the Scanivalve for automated pressure data acquisition.

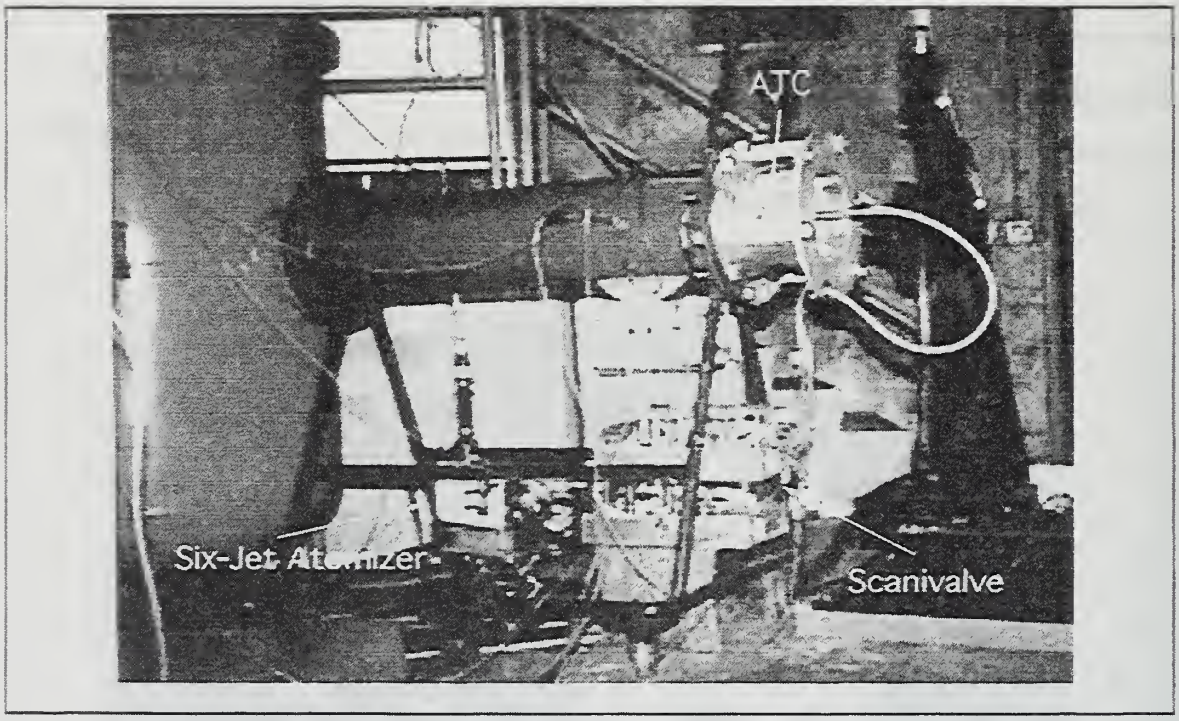

Figure 2. Side view of ATC, Scanivalve, and six-jet atomizer

Atomized glycerin particles constituted the LDV seed material which were introduced through a 8 mm (0.31 in) diameter copper tube approximately more than 100 tube diameters upstream of the test section. Seed atomization was performed using a commercial TSI, Inc., Six-Jet Atomizer connected to the laboratory compressed air supply as shown in Figure 2.

Each blade was designed with a combination of simple circular arcs and line segments and included a leading edge radius of 2 mm (0.095 in), trailing edge radius of 0.31 mm

(0.012 in), and axial chord of 25 mm (0.975 in). The annular stator row was manufactured from 2218-T61 aluminum and consisted of 31 blades with a midspan spacing of 22 mm (0.857 in), resulting in a blade solidity of 1.14. The inner hub radius was 99 mm (3.895 in) and the outer case radius was 116 mm (4.585 in) with the same profile at all radii [Ref. 2]. Reference 4 included the original set of ATC manufacturing drawings. Reference 3 included a description of the wake positioning system. Reference 2 included the location of the blade surface static pressure ports.

B. PRESSURE DATA ACQUISITION

The data acquisition system, for the blade surface pressure measurements, is shown schematically in Figure 3. All data acquisition was remotely controlled by a Hewlett-Packard 9000 computer system. Reference 2 contains the program utilized to conduct all pressure data acquisition.

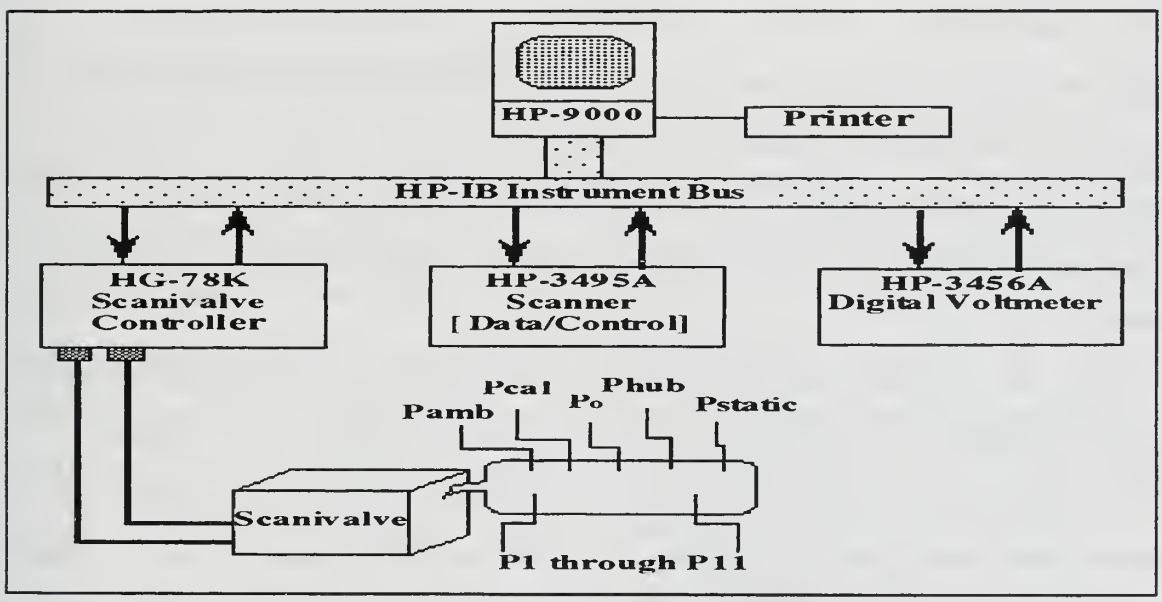

Figure 3. Hewlett Packard pressure data acquisition schematic

A Scanivalve was connected to a Model HG-78K Scanivalve controller, which in turn was connected to a Hewlett-Packard, Model 3456A Digital Voltmeter and Model 3495A Scanner

via a HP-IB instrument bus. Scanivalve calibration was performed to within an accuracy of +/- 0.1 inches mercury. Table A1 in Appendix A relates each Scanivalve port to its respective pressure measurement.

C. LASER-DOPPLER VELOCIMETER

The LDV system consisted of a LEXEL Model 95 four-Watt argon-ion laser connected to a TSI, Inc., Model 9201 ColorBurst multicolor beam separator (Figure 4). The beam separator divided the incoming light into shifted and unshifted beams, with the shifted beam receiving a 40 MHz frequency shift from a Bragg cell. The two beams were further split into three polarized pairs: green (514.5 nm), blue (488 nm), and violet (476.5 nm). The complete system was shown schematically in Figure 8.

Individual couplers on the ColorBurst directed each beam to the laser probe via a fiber-optic cable. Each fiber-optic probe contained receiving optics which directed the return signal to a TSI, Inc., Model 9230 ColorLink multicolor receiver (Figure 4). The ColorLink provided photomultiplier and frequency-shifting functions. All conditioned ColorLink signals were sent to a TSI, Inc., Model 1990C signal processor where valid Doppler signals were counted with reference to characteristics selected by the user. Utilizing only the green beam due to its greater strength, the MI-990 interface monitored the random criteria (1-component measurement) and then transferred the valid counter information to computer memory.

The laser apparatus included the laser probe and traverse mechanism. The fiber-optic probe was mounted to a LINTECH, Model 41583 traverse table (Figure 7). An Applied Motion Products System 1618 traverse controller was used to control the traverse table movement both manually and by computer. All ColorLink, MI-990 functions, and LDV data processing were accomplished remotely by computer using TSI's menu-driven software, FIND (FLOW INFORMATION DISPLAY) version 4.04.

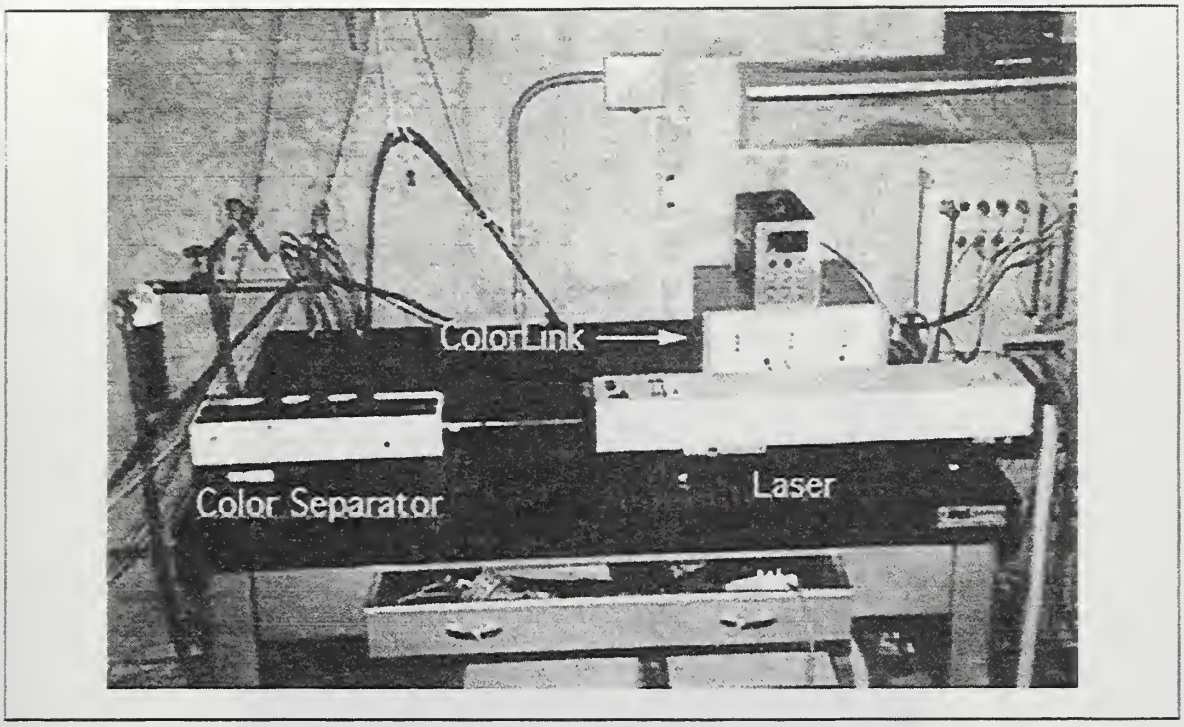

Figure 4. LDV bread board (with laser, color separator, and color link)

D. PRESSURIZED LASER WINDOW

A pressurized laser window was designed and manufactured in order to prevent the flow of air and seed material out of the 1.092 mm optical access hole. The new laser window entailed three modifications (Figure 5a). The first was to transform the previously flat laser blank into a chambered component. The second was to install internal plumbing into the chamber which included a .33 mm (.013 in) diameter static pressure port near the 1.092 mm (.043 in) diameter laser opening and two 1.27 mm (.05 in) diameter ports for pressurizing and sensing the chamber pressure. The third was to install a 6.35 mm (.25 in) acrylic window on a 1.58 mm (.0625 in) O-ring for sealing. The positioning of the new window and its components are depicted in Figure 5b. Appendix E shows the complete engineering drawings of the new pressurized LDV window.

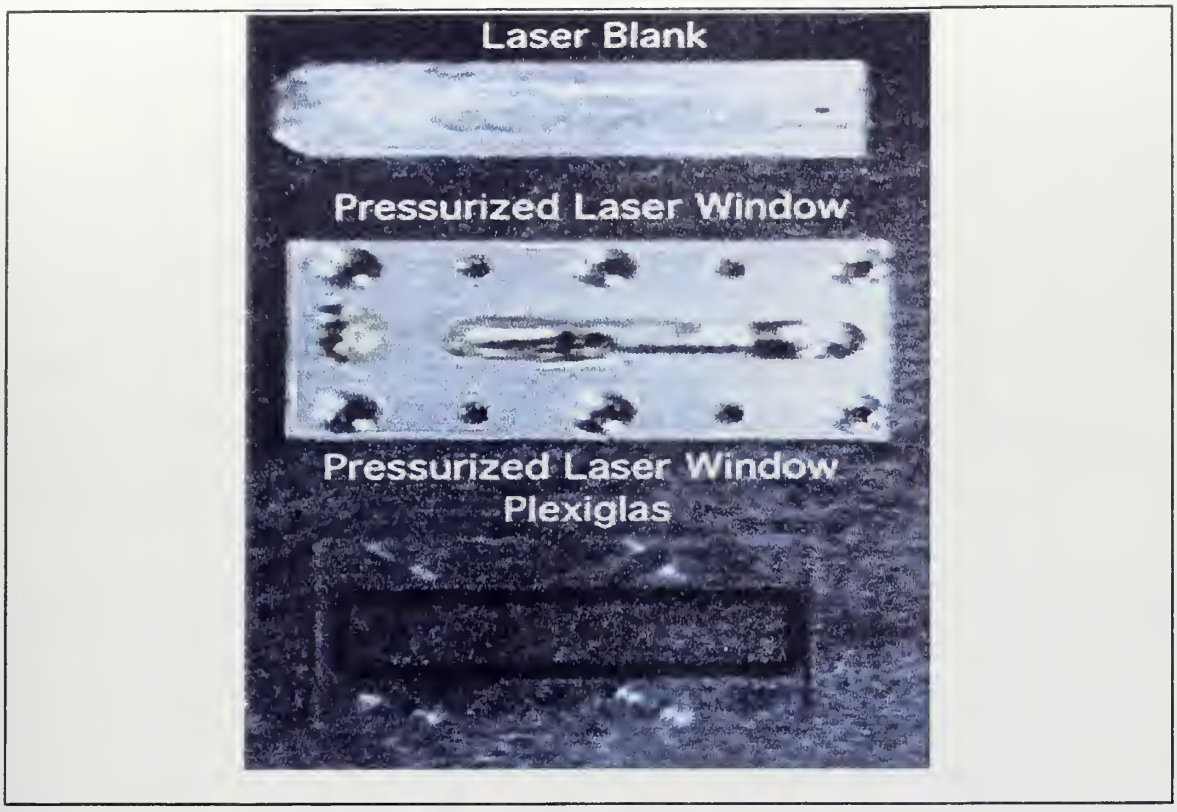

Figure 5a. Laser blank and pressurized LDV window

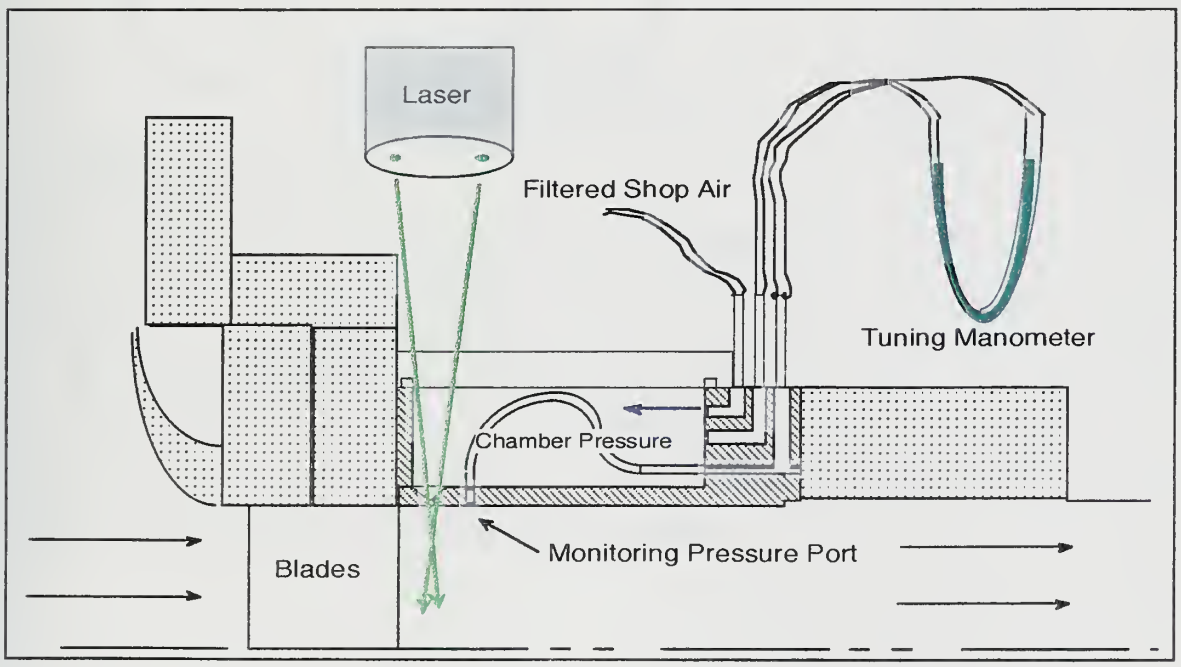

Figure 5b. Cross-section of pressurized LDV window

E. COBRA PROBE

Scanivalve control and data recording were accomplished using National Instruments' software, LabView, operating on a 486 PC system whose schematic is shown in Figure 6. Total pressure, non-dimensional velocity and flow angle measurements were performed with a three-hole yaw probe [Ref. 3]. All pressure taps were connected to a Scanivalve with a 2.5 psi differential pressure transducer. Probe calibration was also accomplished using this acquisition system. Appendix D contains the probe calibration measurement data and third-order calibration curves.

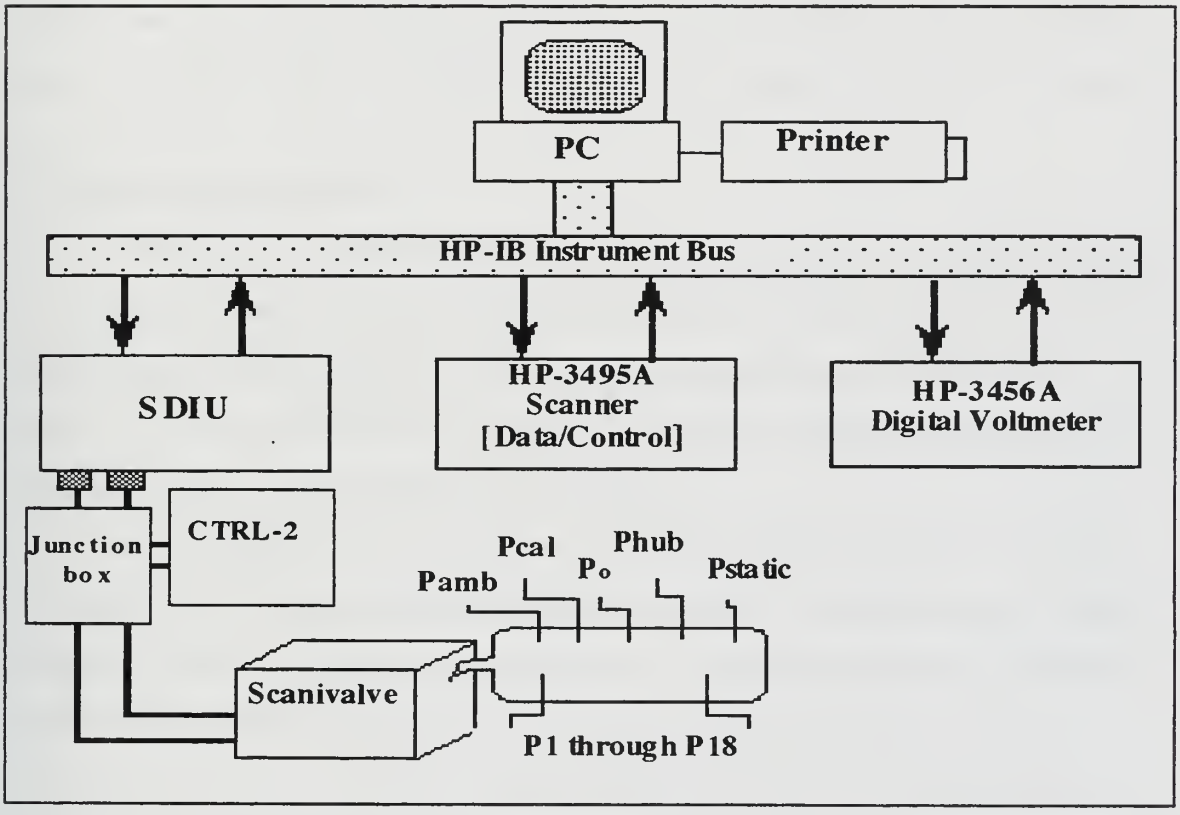

Figure 6. Cobra probe pressure data acquisition schematic

III. EXPERIMENTAL PROCEDURE

A. MIDSPAN SURFACE PRESSURE MEASUREMENTS

Midspan surface pressure measurements were obtained with the Hewlett Packard (HP) data acquisition system. The pressure ratio (P_{rat}) was defined as the downstream hub-static pressure (P_{hub}) divided by the upstream stagnation pressure (P_0). Each pressure ratio was achieved by metering the upstream stagnation pressure until a desired water column height was achieved. Twelve pressure ratios from 0.9826 to 0.9313 in steps of 0.0048 were considered and during each run all blade surface pressures, P_o, and P_{hub} were recorded. A midpoint P_{rat} of 0.9620 which was equivalent to 408.94 mm (16.1 in) of water was decided upon as the desired pressure ratio for the LDV surveys utilizing the pressurized laser window.

B. LASER MEASUREMENTS

LDV alignment for endwall flow measurements was accomplished as shown in Figure 9. The objective of the LDV alignment procedure was to center the probe volume into the 1.092 mm optical access hole and reset the traverse table coordinates to a relative home position. A one-component fiber-optic probe was attached to the traverse table (Figure 7) which was controlled both manually and by computer.

Using the laser blank as an alignment guide for the green laser beams, the traverse table was manually advanced radially until the beam separation was minimized on its surface, yet discernible with the naked eye (Figure 9, Point A). The traverse table was then manually positioned to the midpoint of the optical hole which placed the LDV probe volume at a consistent starting point. The traverse table was then homed relative to this new position. Once the horizontal measurements were completed, the LDV probe was then manually rotated and the alignment process was repeated for the vertical measurements. This alignment technique was repeatable and ensured that the probe volume was consistently positioned at the

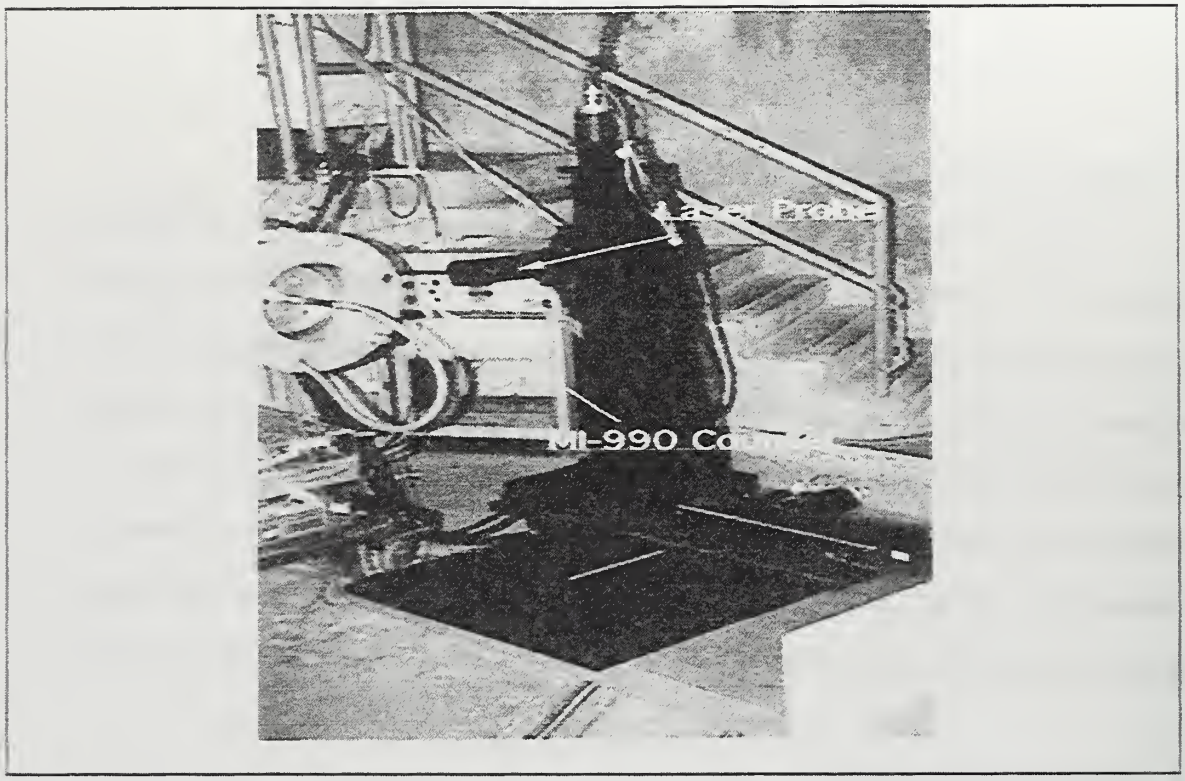

Figure 7. LINTECH traverse table

center of the optical access hole. Hole alignment and laser power (2.0 Watts) were periodically verified as these could drift due to temperature changes within the testing cell. Reference 3 described complete dimensions of the laser blank.

Radial traversing of the LDV positioned the measurement volume at various depths within the ATC and measurements were performed through the new pressurized window's optical access hole in the outer casing. These results were compared with previous measurements utilizing the laser blank. The circumferential LDV surveys were executed in a similar manner. The probe volume was first positioned by the traverse table to a fixed radial depth within the ATC. The stator ring was then circumferentially positioned from -8 to +8 degrees of its initial setting. These circumferential surveys were obtained at different radial locations close to the endwall. With both of these surveys completed, the measurement test matrix near the end wall was defined (Figure 10).

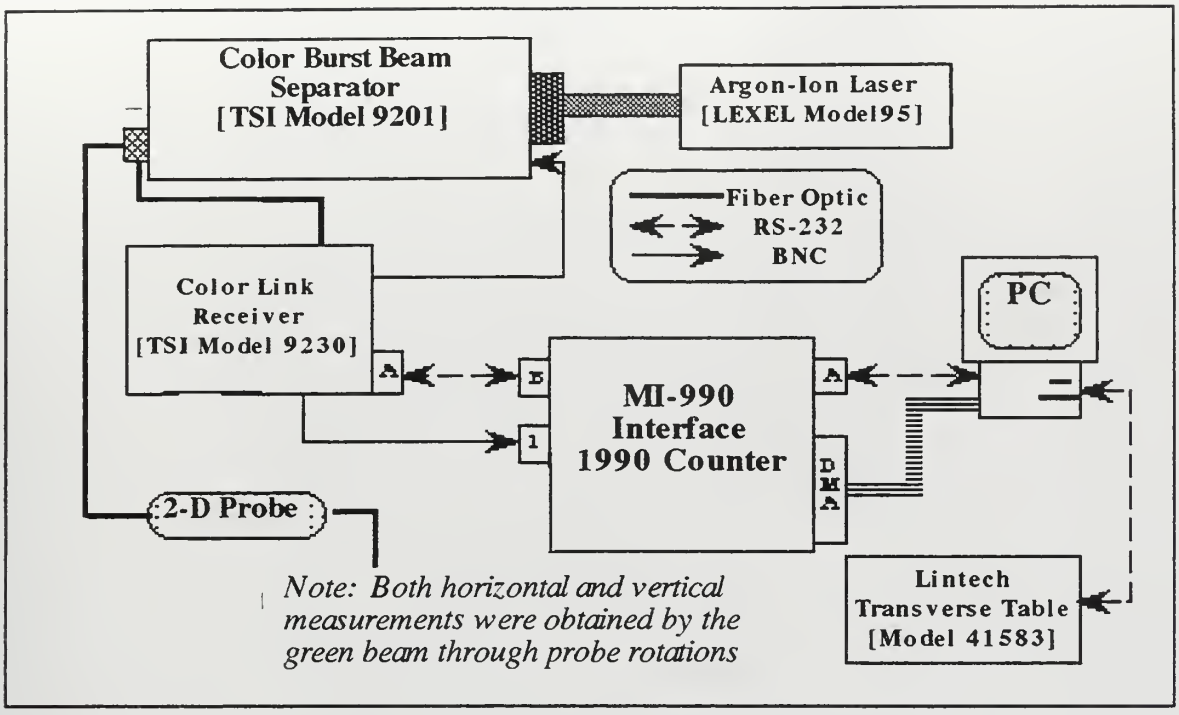

Figure 8. LDV system schematic

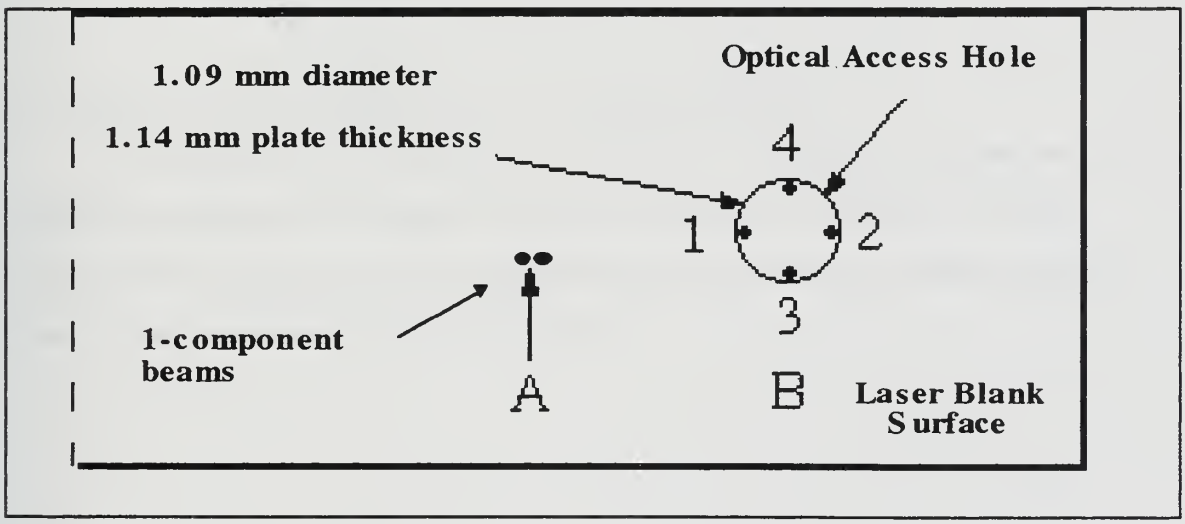

Figure 9. LDV alignment schematic

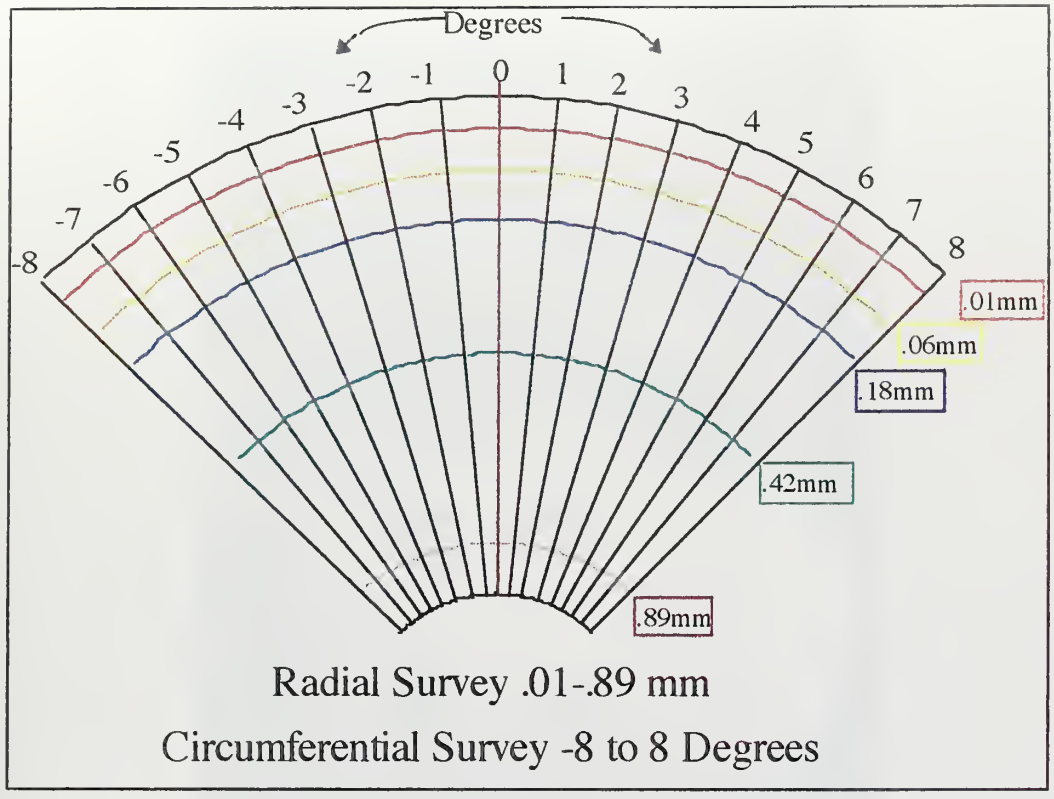

Figure 10. Measurement test matrix

C. COBRA PROBE CALIBRATION AND MEASUREMENTS

The calibration of the three-hole cobra probe was accomplished using the free-jet apparatus connected to the air supply previously used for the ATC (Figure 11). The LabView software program controlled the calibration procedure and the resultant data was transferred to a spreadsheet for further processing.

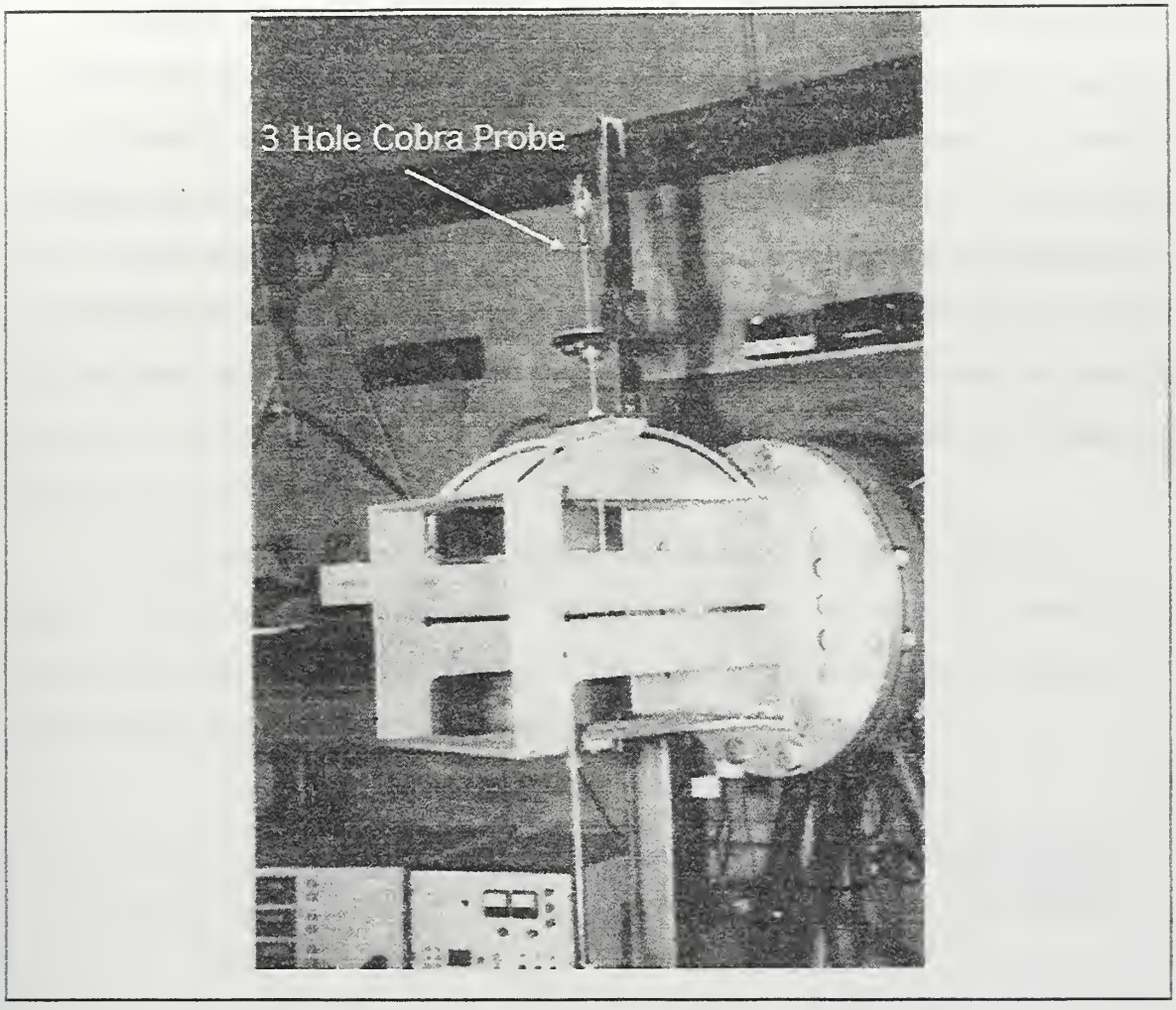

Figure 11. Three-hole cobra probe calibration apparatus

The probe was manually aligned in yaw using a water manometer at 406 mm (16.1 in) water of air pressure. Once the manometer equalized, the probe was checked at both pressure ratio extremes of the planned calibration. The probe was then calibrated at 101 mm (4 in) of water and in increments of approximately 101 mm (4 in) to 716 mm (28.2 in) of water. Reference 3 contains a description of the calibration variables and formulas. Third-order polynomials were fit through the calibration data and these are given in Appendix D.

Radial surveys of 0.42, 0.89, and 1.78 mm (0.016, 0.035, and 0.070 in) at a pressure ratio of 0.9620 were conducted to compare with previous LDV data from both the laser blank

and pressurized window. The probe measured total pressure and flow angle. Utilizing formulas from Reference 3, the values for velocity were calculated and non-dimensionalized. The total non-dimensional velocity (X) was defined as the measured velocity divided by the 'total' velocity. The total velocity was the square root of twice the total temperature multiplied by the specific heat at constant pressure. The same data acquisition system was used for both the surveys and the probe calibration. Flow angles were read from a vernier scale attached to the probe with an accuracy of plus or minus 0.2 degrees and recorded manually into the front panel of the LabView software program.

IV. RESULTS AND DISCUSSION

A. BLADE MIDSPAN SURFACE PRESSURE MEASUREMENTS

Experimental blade-surface pressure measurements were conducted over a range of pressure ratios which covered the pressure ratio at which LDV data were to be collected through the new laser window. Each blade static port reading was non-dimensionalized by the upstream stagnation pressure (P_0). Appendix B contains the pressure data for the 12 pressure ratios tested.

From the twelve pressure ratios measured, the middle pressure ratio of 0.9620 was selected to test the new pressurized window. Figure 12 shows the pressure profile around the blades for the above pressure ratio. Figures 13 and 14 show the remaining pressure ratios measured which show increased loading with decreased pressure ratio.

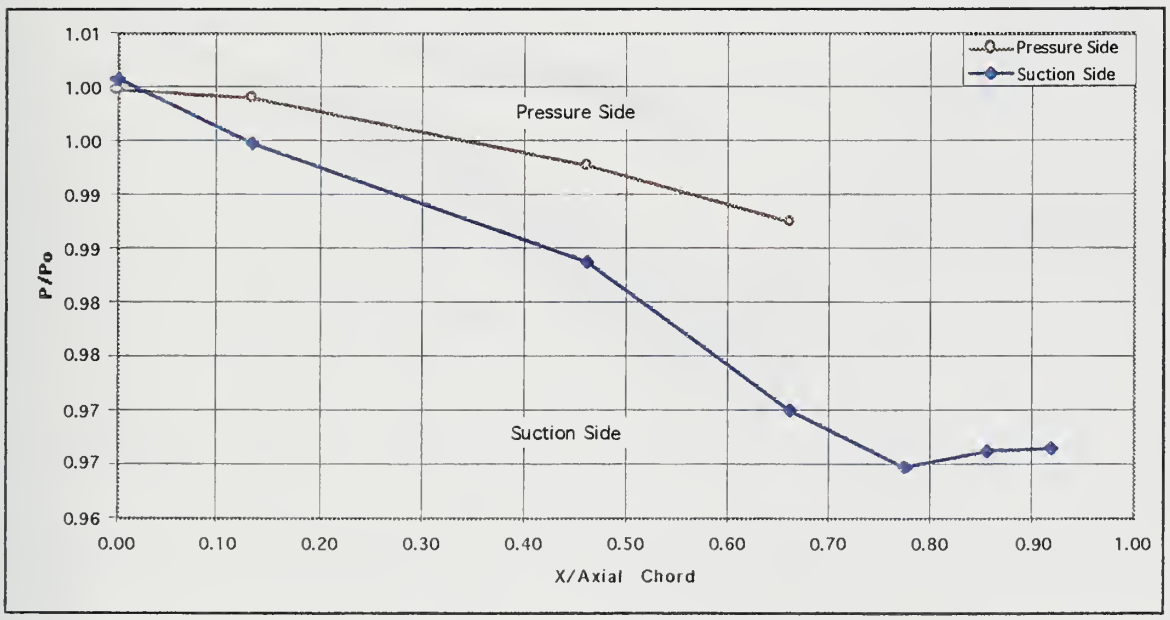

Figure 12. P/P_0 vs. x/c for 0.9620 pressure ratio

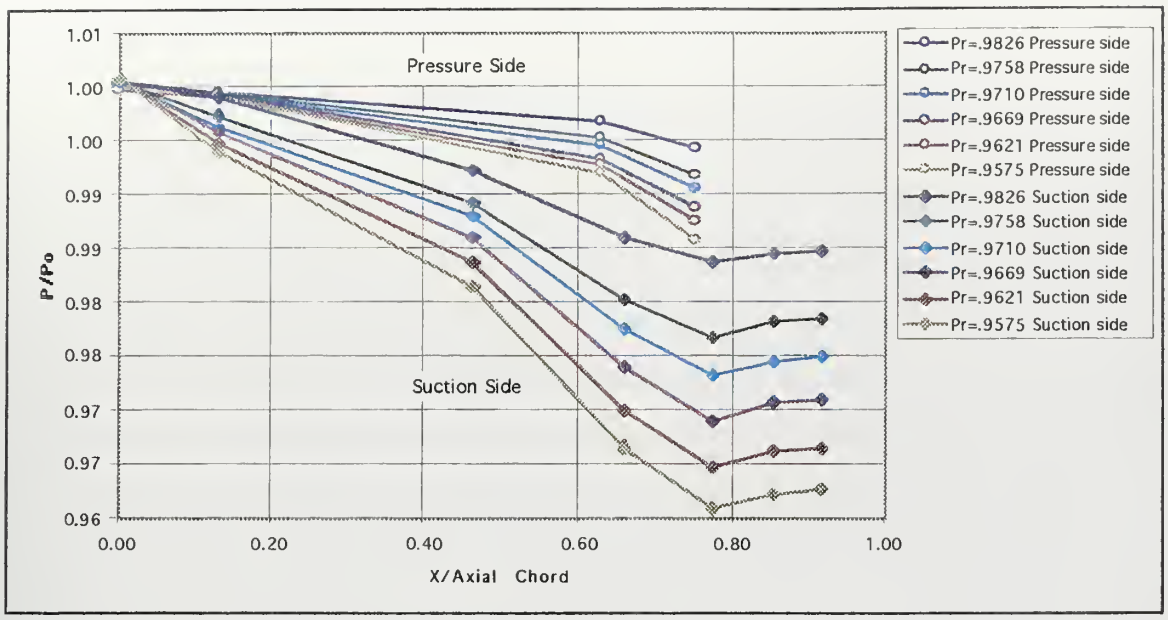

Figure 13. P/P_0 vs. x/c for 0.9826 through 0.9575 pressure ratios

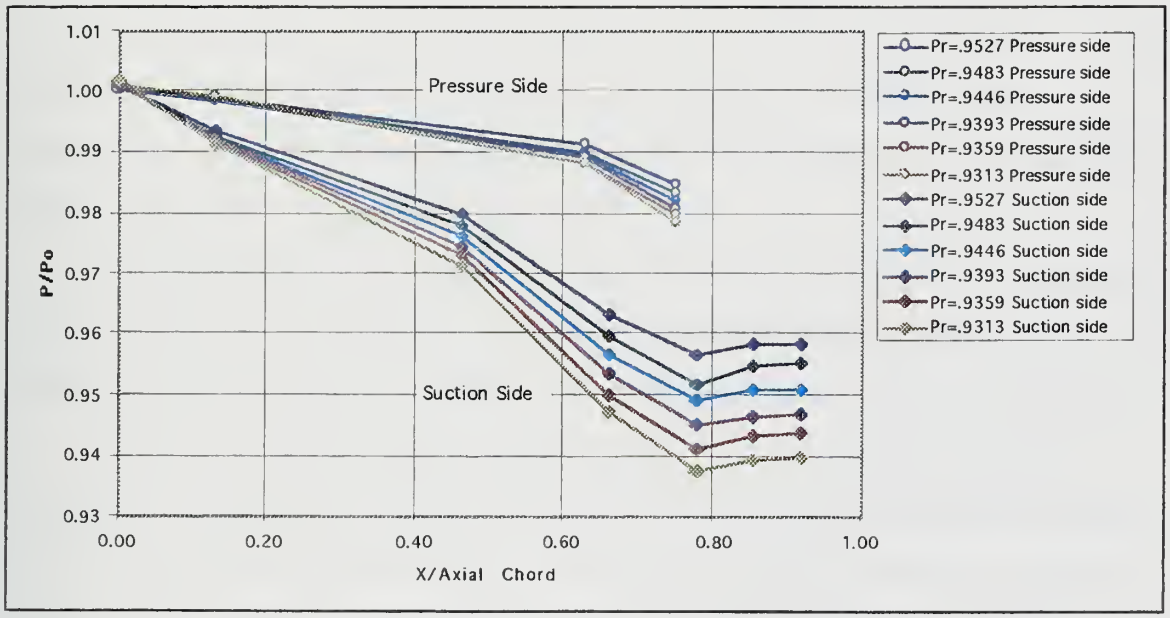

Figure 14. P/P_0 vs. x/c for 0.9527 through 0.9313 pressure ratios

B. LASER-DOPPLER VELOCIMETRY MEASUREMENTS

1. Comparison of a 1-D Procedure with 2-Component Measurements

The previous LDV experiments on the ATC were carried out using a two-component laser probe (both blue and green beams); however, due to the significant weakness in the signal strength of the blue beam and subsequent low data rates, this was abandoned. The current LDV measurements were conducted utilizing only the green beam for both horizontal (axial) and vertical (tangential) measurements of the flow field. Manual repositioning of the laser probe (Figure 7) allowed measurements in both directions. Initial LDV data were acquired at a pressure ratio of 0.9054 to allow comparisons with previous data taken in Reference 2.

LDV measurements were made first to determine the repeatability of the one-dimensional technique. The values of velocity, turbulence intensity, and flow angle were recorded and compared. Each velocity reading was non-dimensionalized by the total velocity based on the upstream stagnation temperature (T_0) to correct for varying conditions. Experimental repeatability was achieved by conducting runs on different days at both a zero degree and a pinned circumferential wake position.

The initial LDV radial measurement at the 0.9054 pressure ratio provided satisfactory seeding conditions and low ATC vibrations. Data rates ranged from approximately 100 samples per second at the 1.78 mm depth to 50 samples per second at the 0.01 mm depth.

Figures 15a and 15b contain the non-dimensionalized horizontal and vertical components of velocities that correlated over the different days of the experiment. Both the horizontal and vertical components seem to increase as the depth of the probe volume was increased. This is typical of an endwall boundary layer survey with the flow magnitude increasing to freestream conditions. The boundary layer was also distorted due to secondary flows , wake, and corner vortices that possibly formed within the blade passage.

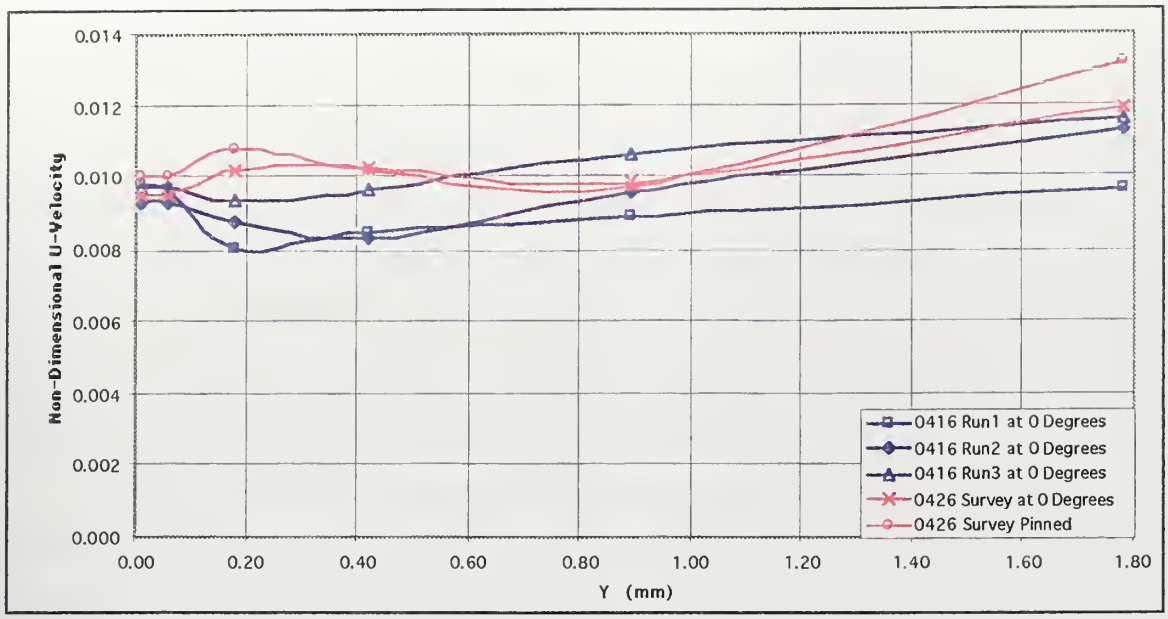

Figure 15a. A radial survey through the laser blank at a Prat of 0.9054

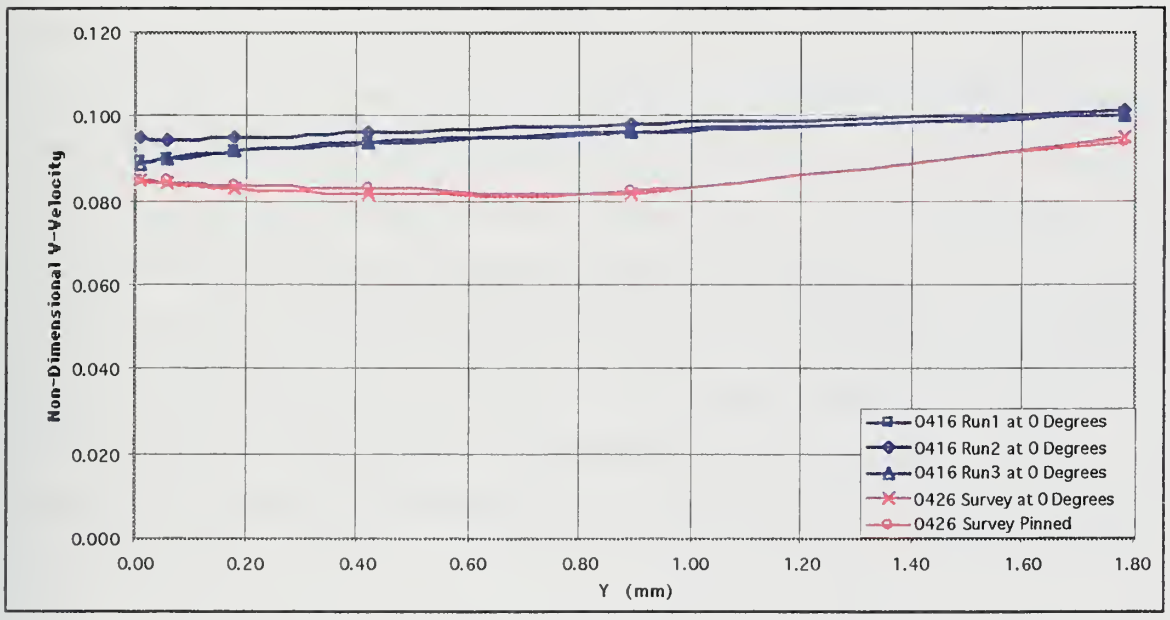

Figure 15b. A radial survey through the laser blank at a Prat of 0.9054

Figure 16a and 16b contain the horizontal and vertical turbulence intensities which also correlated well over the two days. The horizontal turbulence intensity was approximately 9% and was slightly less than the vertical turbulence intensity of about 10%. The horizontal turbulence intensity also remained relatively constant over the range of the radial survey where the vertical turbulence intensity was higher near the optical access hole and decreased as the survey point moved inwards. This indicated that the larger vertical velocity component was more susceptible to the complex and highly turbulent boundary layer and access hole interactions than the smaller horizontal component of the flow.

Figure 17 contains the mean angle from the two days and previous angles from Reference 2. The present data correlated well and indicated a flow angle of approximately 83.5 degrees. The previous flow angles were less, at about 75 degrees. The current flow angles started at a higher value near the endwall and then decreased as the survey point moved inwards. The previous angles [Ref. 2] started at lower flow values and increased as the survey point moved inwards. This former trend seemed to be inconsistent with the high turbulence intensity (lower velocities) currently found near the optical access hole and lower turbulence intensity (higher velocities) away from it. Initial velocity components would be expected to be low due to this highly turbulent location near the endwall. The measured velocity should then increase as the turbulence intensity decreased as the survey progressed. Endwall flow angle was defined as the arc tangent of the vertical (tangential) velocity divided by the horizontal (axial) velocity components. Since a greater change occurred in the horizontal than in the vertical velocity during the radial survey, the angles should first increase, but then decrease as the survey progressed. This is seen to be the case in the data given in Figure 17.

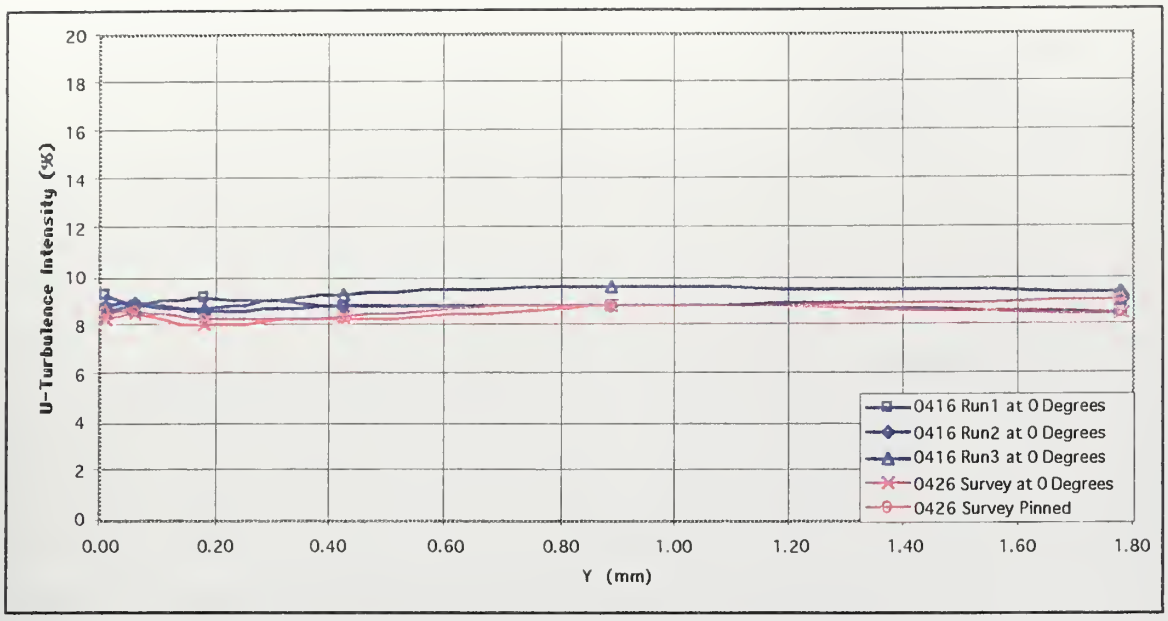

Figure 16a. A radial survey through the laser blank at a Prat of 0.9054

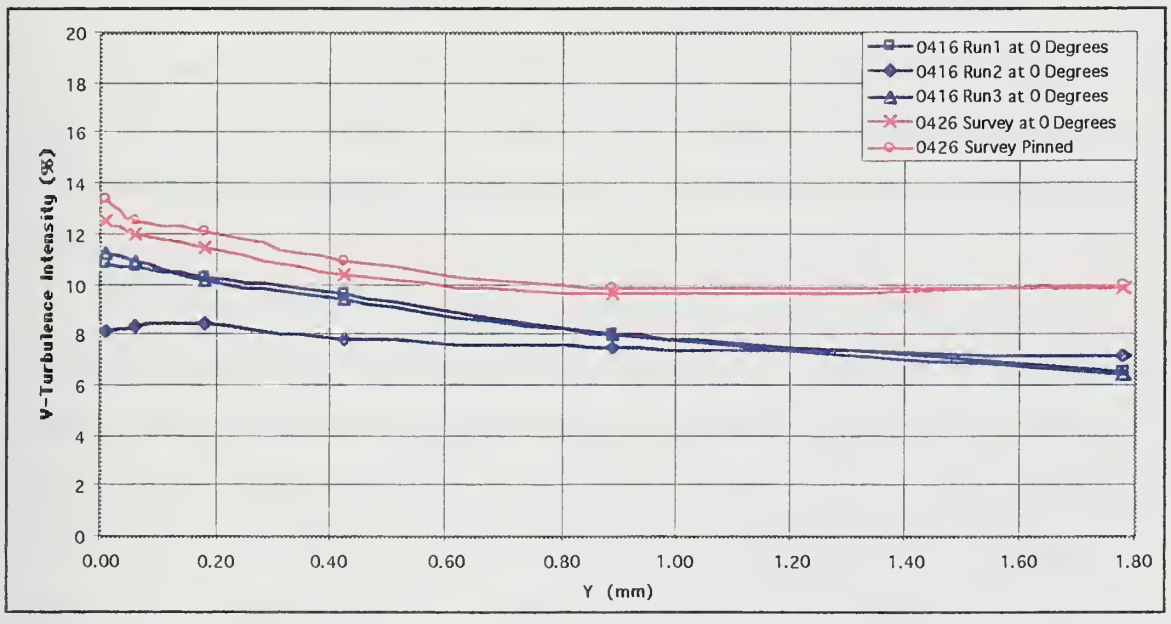

Figure 16b. A radial survey through the laser blank at a Prat of 0.9054

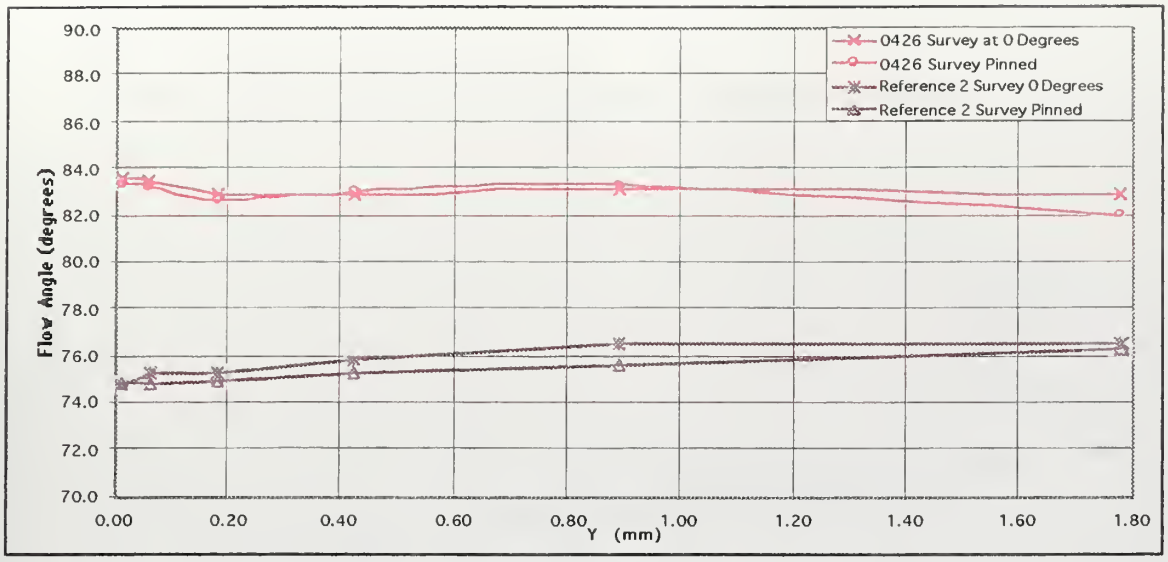

Figure 17. A radial survey through the laser blank at a Prat of 0.9054

2. Laser Blank Measurements at a Pressure Ratio of 0.9620

The laser blank was used and surveys were conducted at a pressure ratio of 0.9620, both radially and circumferentially, to provide data to compare with for later measurements with the pressurized laser window. The execution of these surveys was similar to the previous surveys at a pressure ratio of 0.9054.

Figures 18, 19, and 20 show the non-dimensional velocity, turbulence intensity, and flow angle respectively at 3 circumferential wake positions (0, 7,-8 degrees). Figure 18 shows similar velocity trends to those in Figures 15a and 15b; however, the turbulence intensities shown in Figure 19 were much higher, reaching values as high as 14%. Vertical turbulence intensity followed a similar trend to that in Figure 16b, starting high and then decreasing. Flow angles at this pressure ratio were 3 degrees higher than those in Figure 20. The LDV measurement at the 0.9620 pressure ratio provided much better seeding and improved data rates over those for the 0.9054 pressure ratio. Data rates ranged from approximately 175 samples per second at the 1.78 mm depth to 90 samples per second at the 0.01 mm depth.

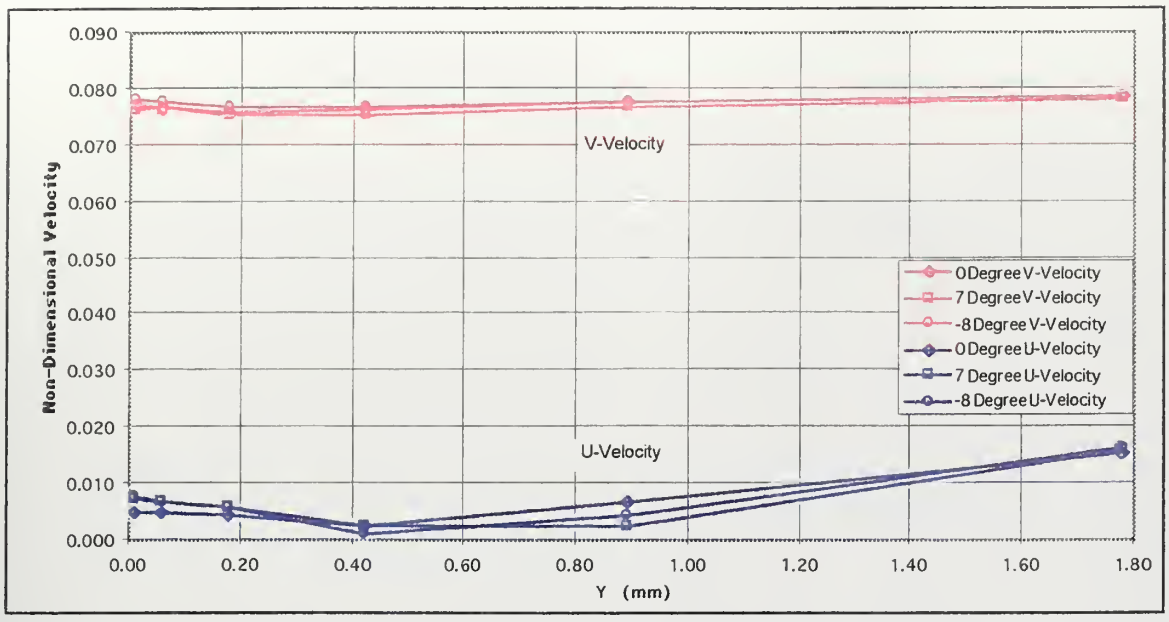

Figure 18. A radial survey through the laser blank at a Prat of 0.9620

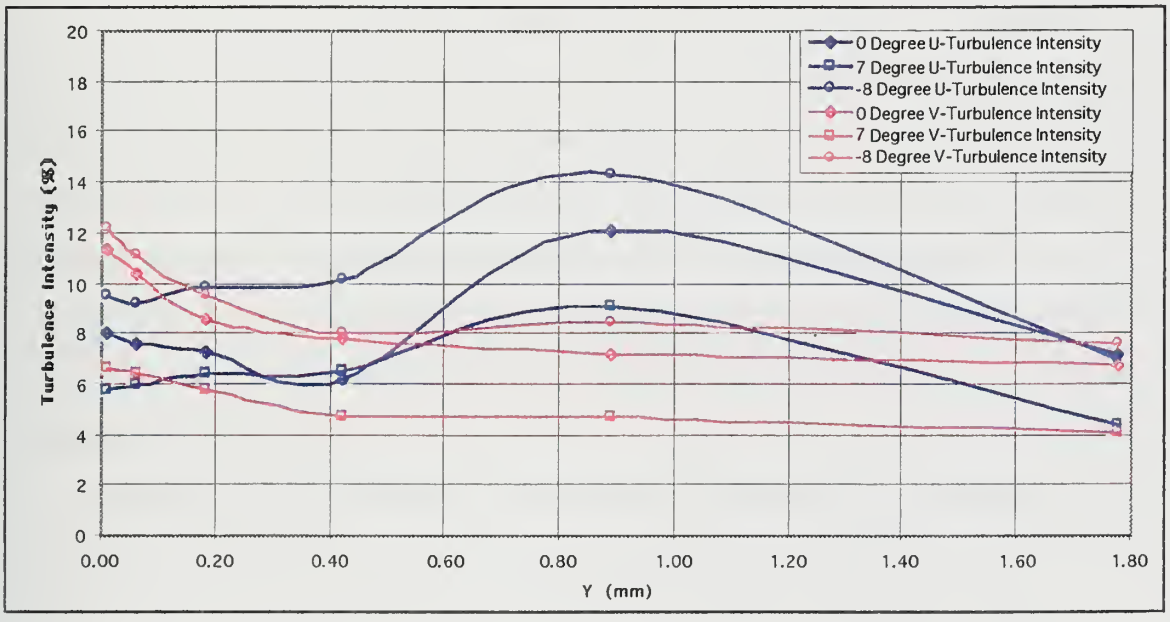

Figure 19. A radial survey through the laser blank at a Prat of 0.9620

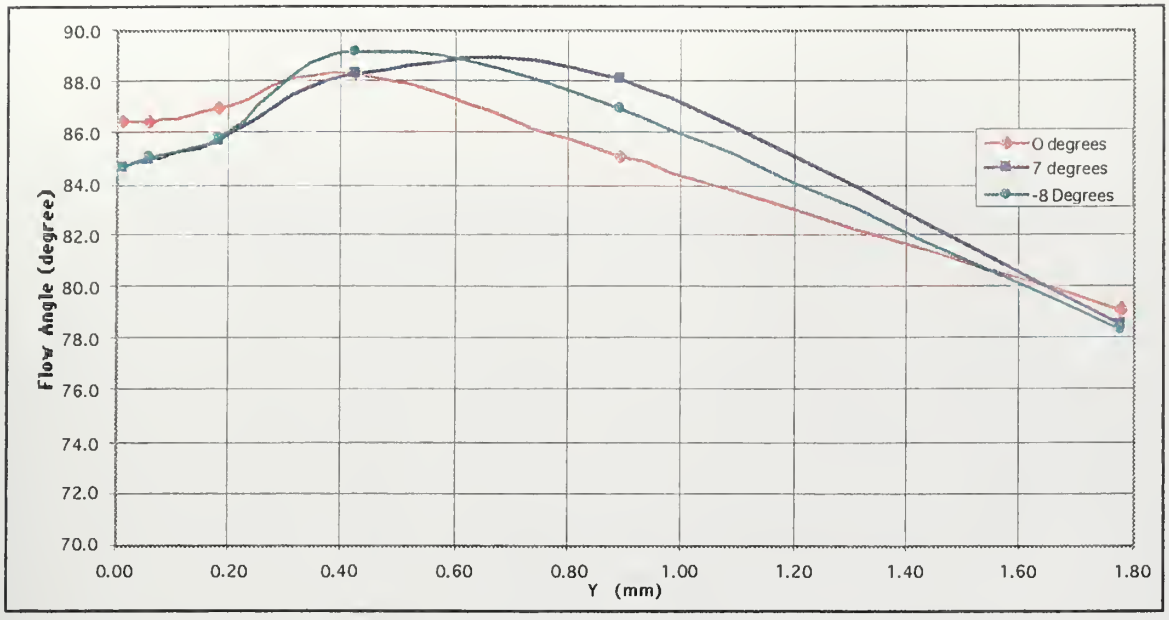

Figure 20. A radial survey through the laser blank at a Prat of 0.9620

A circumferential survey was conducted after the initial radial surveys to complete the test matrix (Figure 10) near the endwall. Figures 21 through 23 graphically depict velocity, turbulence intensity, and flow angle for circumferential wake positions of -8 to +8 degrees. Figures 21a and 21b once again show the lower velocity near the endwall which increased as the survey progressed. Horizontal turbulence intensity was consistent throughout the survey at about 6.5%. The vertical turbulence had a high of about 13% to a low of about 6% which, in showing a decrease in turbulence as the survey location moved further from the wall, was consistent to the previous surveys.

Figure 23 shows the flow angle to be varying only between 80 and 82 degrees, so the flow angle was relatively insensitive to circumferential variations of the ATC.

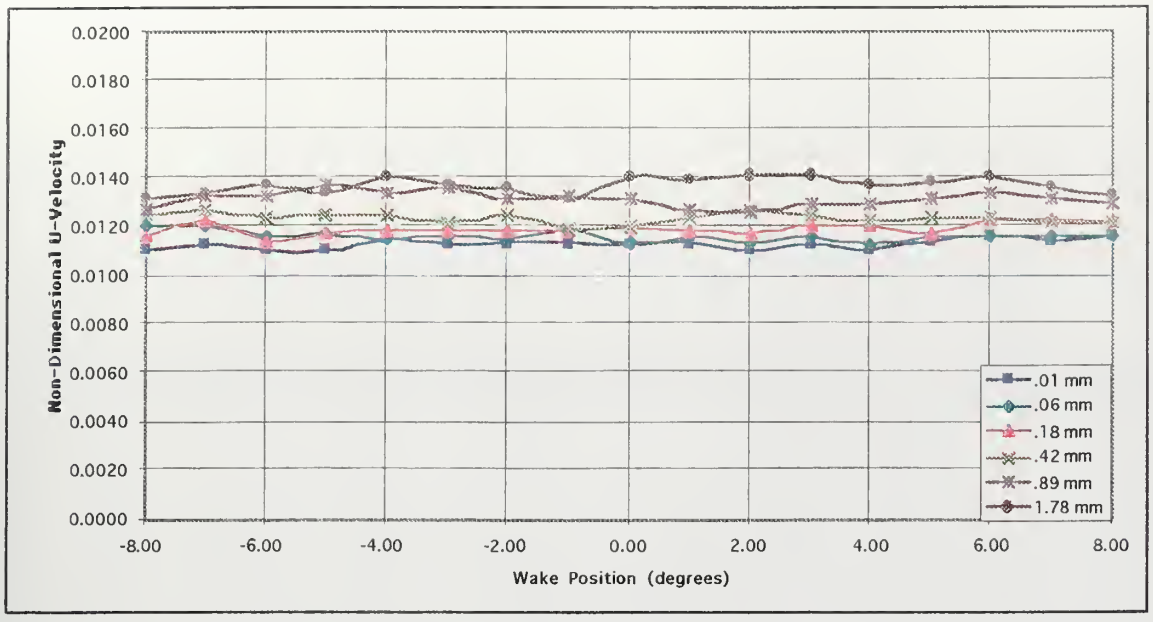

Figure 21a. A circumferential survey through the laser blank at a Prat of 0.9620

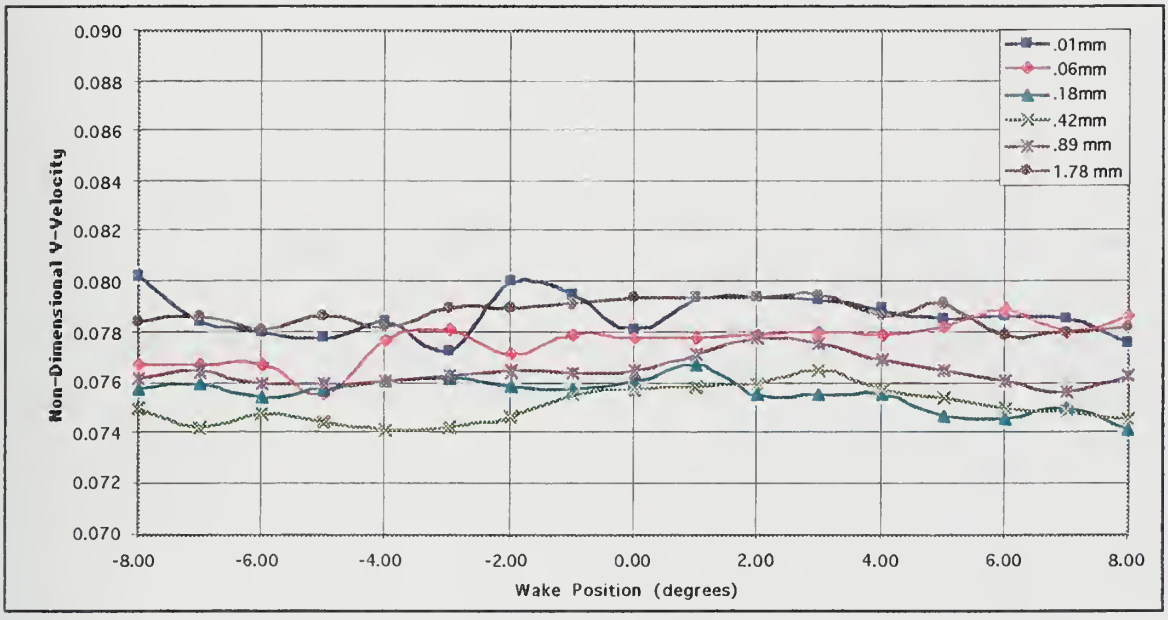

Figure 21b. A circumferential survey through the laser blank at a Prat of 0.9620

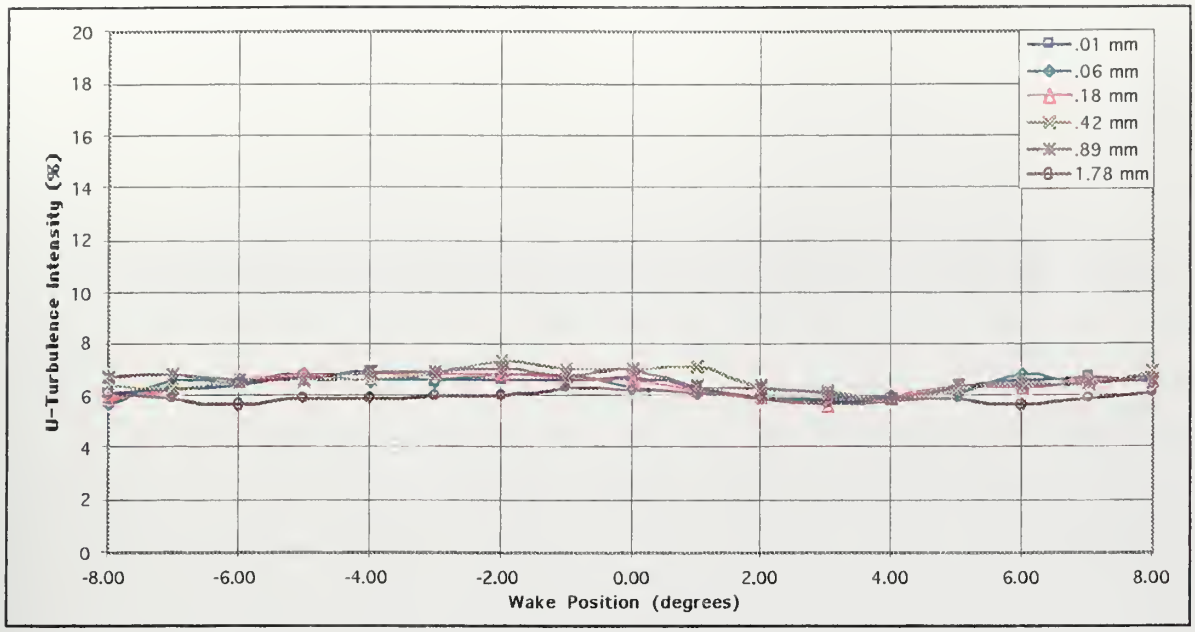

Figure 22a. A circumferential survey through the laser blank at a Prat of 0.9620

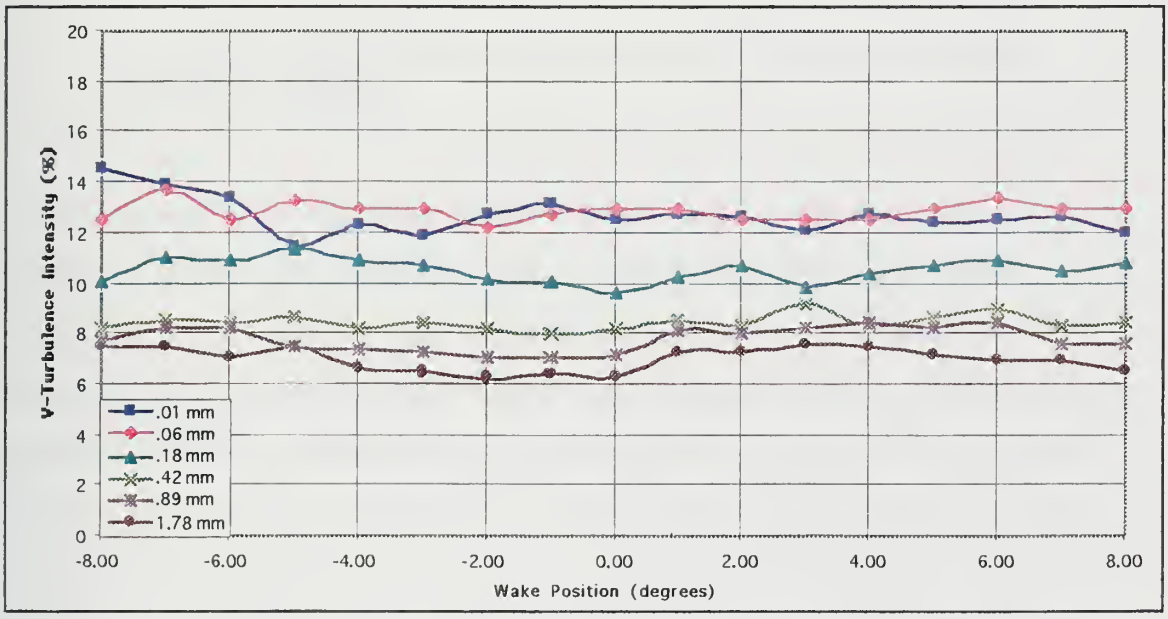

Figure 22b. A circumferential survey through the laser blank at a Prat of 0.9620

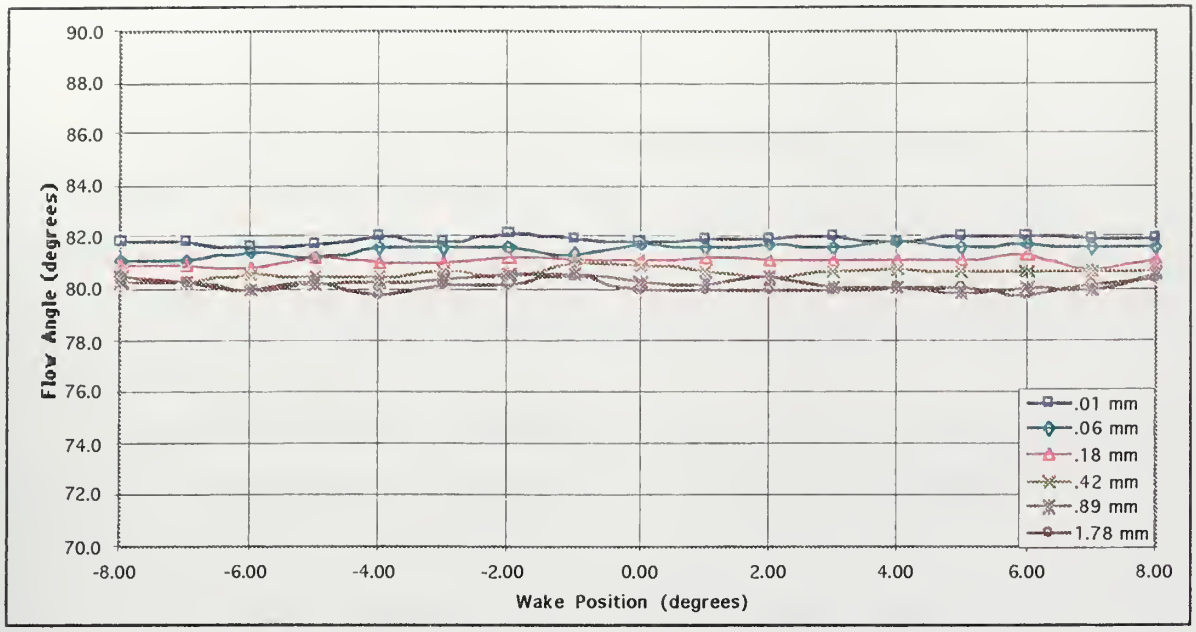

Figure 23. A circumferential survey through the laser blank at a Prat of 0.9620

3. Radial Measurements with Pressurized Window at Various Chamber Pressures

During both the radial and circumferential surveys with the laser blank, seeding material quickly accumulated inside the lower portion of the optical access hole and interfered with LDV data acquisition. The laser blank did not provide any pressure equalization across the optical access hole which allowed the flow to escape from it. The atomizer then had to be switched off to remove and clean the laser blank. Because of this problem, a window was designed which created a pressurized chamber between the optical access hole and the LDV. This resulted in a laser window that did not allow the air flow to escape from the ATC and never needed to be cleaned during the experiment. The window could also be pressurized to force air back into the flow to determine the effects of such a procedure.

A radial survey was conducted through the pressurized window at 3 chamber pressures to further investigate the effects of this optical device on LDV measurements. The

radial survey was decreased from the previous maximum depth of 1.78 mm to .89 mm due to the lack of accessibility at the 1.78 mm radial position.

Figures 24-26 show the influence of the increasing chamber pressure on the flow within the ATC. In both the horizontal and vertical velocities, the increase in chamber pressure led to a decrease in the measured velocity. This was especially evident in Figure 24b for the vertical (tangential) velocity which had a 3% decrease in magnitude due to the increased chamber pressure.

Figure 25a and 25b show the turbulence intensity remaining constant at about 6% for both velocities, implying that the pressurized window did not contribute significantly to increasing the turbulence of the flow near the endwall at this pressure ratio.

Figure 26 shows the flow angle results. The angle of the flow near the endwall tended to decrease initially as chamber pressure was increased, but followed the former trends of increasing near the end wall, and then decreasing. At 0 mm of pressure, the initial flow angle was about 79.8 degrees. At 152.4 mm, the angle was 79.5 degrees. With the exception of the one measurement at 79.8 degrees at 0 mm of pressure, all measurements of flow angle were constant (79.5) to within a tenth of a degree.

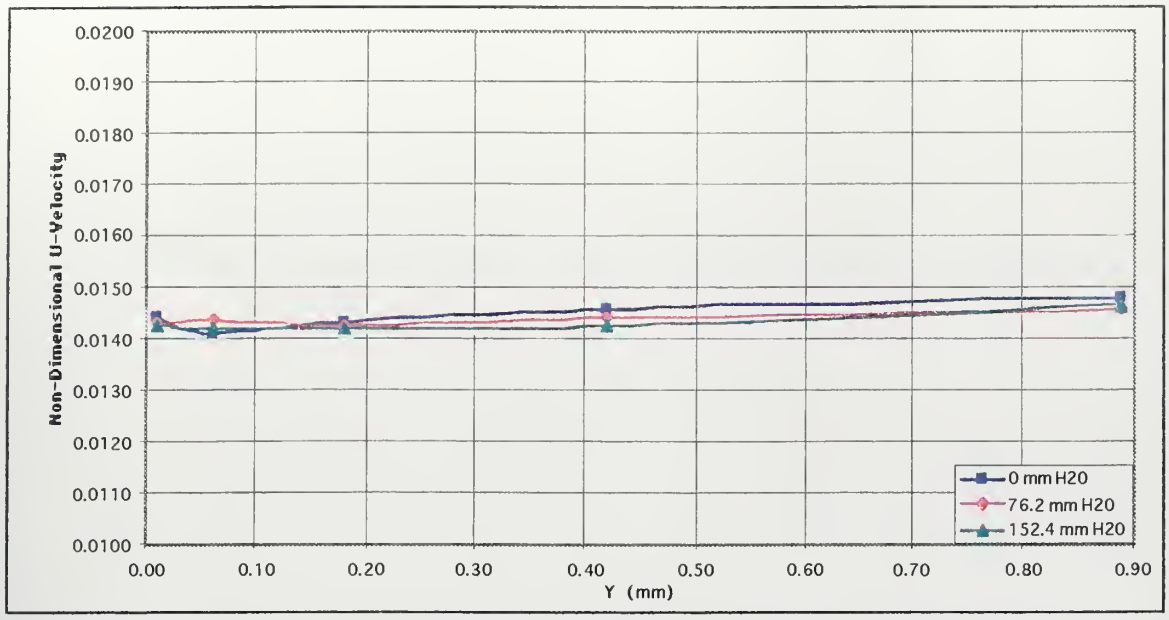

Figure 24a. A radial survey through the pressurized LDV window at a Prat of 0.9620

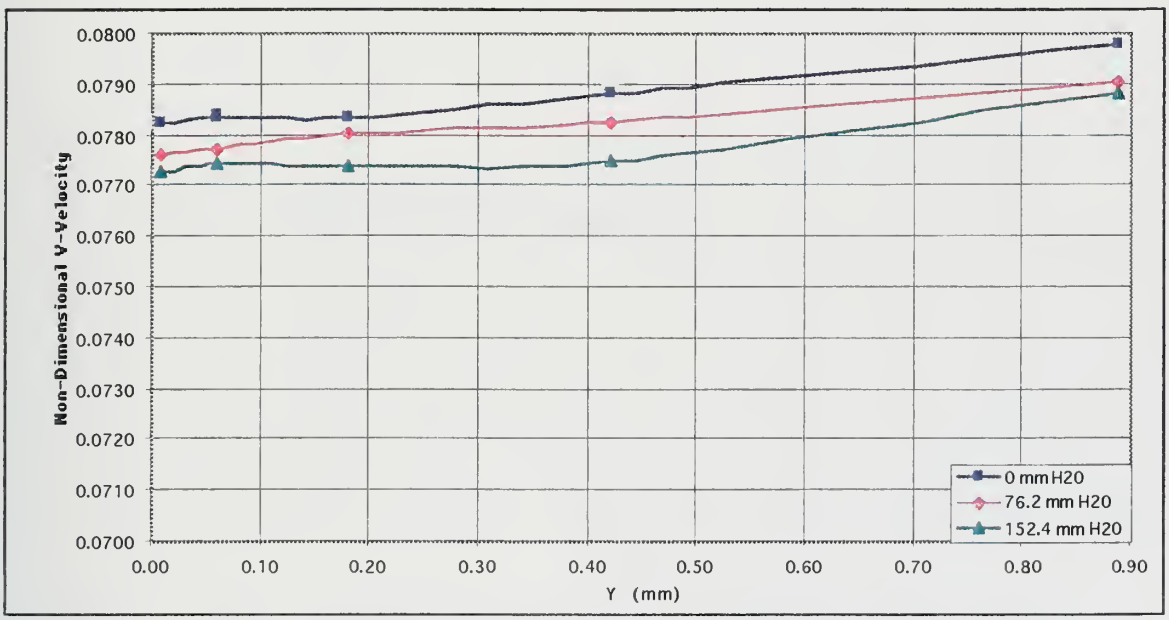

Figure 24b. A radial survey through the pressurized LDV window at a Prat of 0.9620

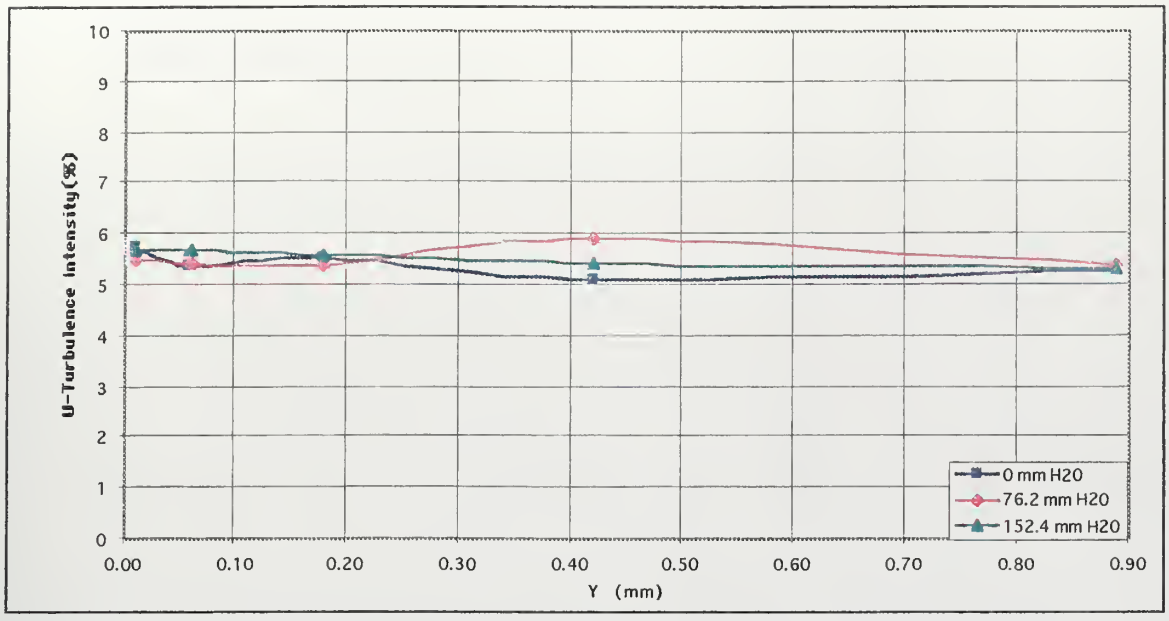

Figure 25a. A radial survey through the pressurized LDV window at a Prat of 0.9620

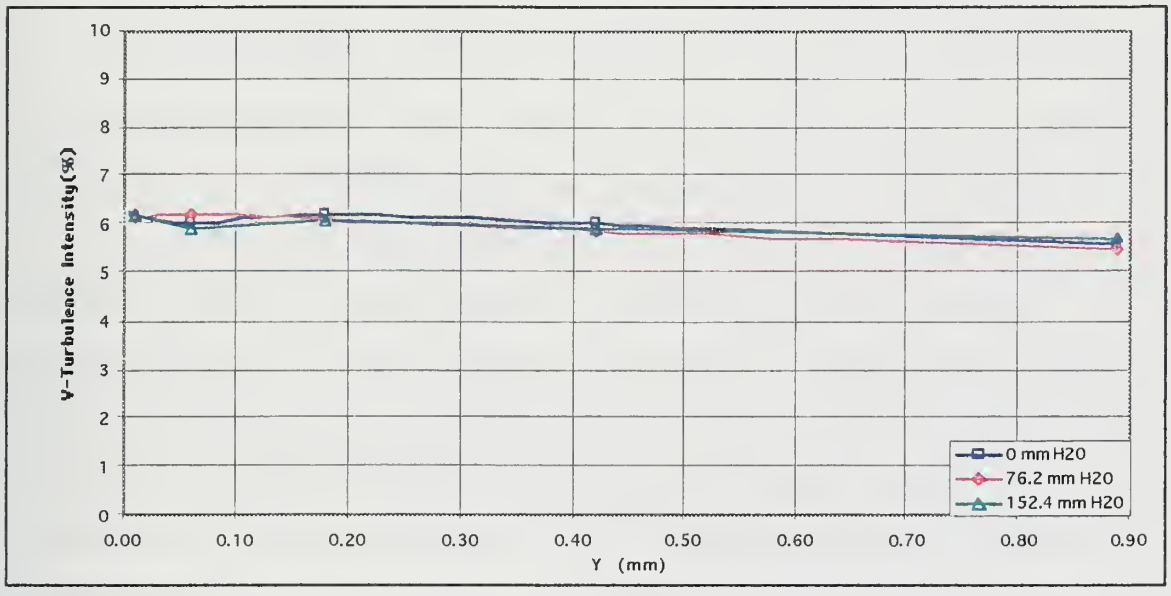

Figure 25b. A radial survey through the pressurized LDV window at a Prat of 0.9620

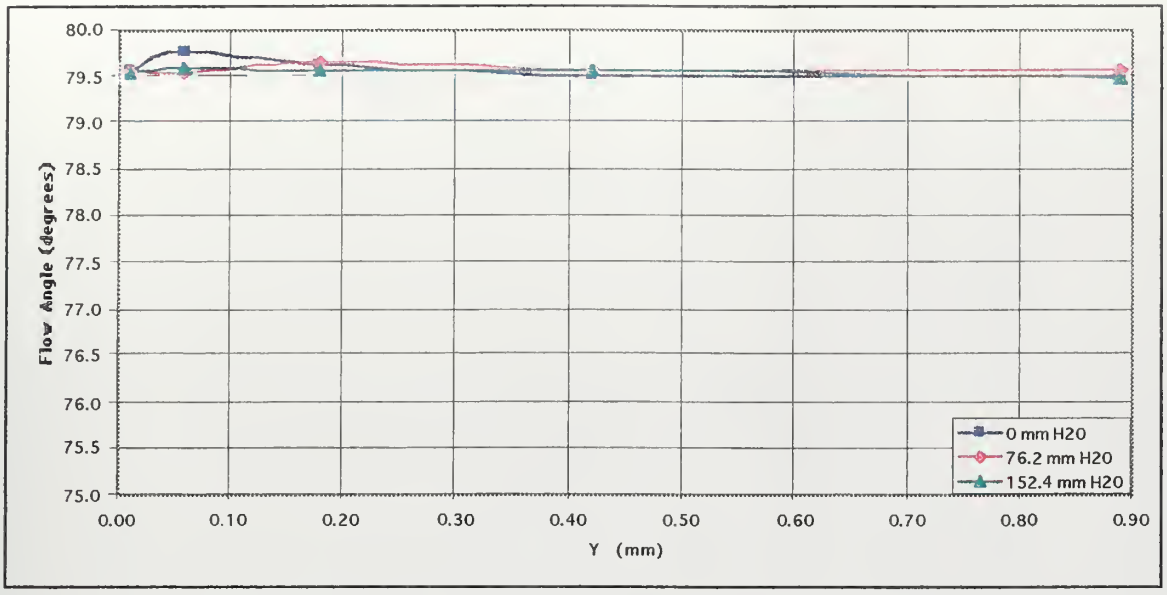

Figure 26. A radial survey through the pressurized LDV window at a Prat of 0.9620

4. Radial Survey Comparison between Pressurized Laser Window and Laser Blank

Radial surveys of flow velocity, turbulence intensity, and flow angle obtained using the new pressurized LDV window and the laser blank are compared in Figures 27-29.

Figures 27a and 27b show the pressurized window velocities were greater than the laser blank velocities at all chamber pressures. Figures 28a and 28b show turbulence intensities were about 6%, lower than with the laser blanks. This suggests that the pressurized window had little effect on the flow during the survey as compared to the laser blank. Figure 29 shows the flow angle with the laser blank to be about 87 degrees whereas with the pressurized window it was at 79.5 degrees. This 7.5 degree difference in flow angle was the result of the differences in the component velocities seen in Figures 27a and 27b.

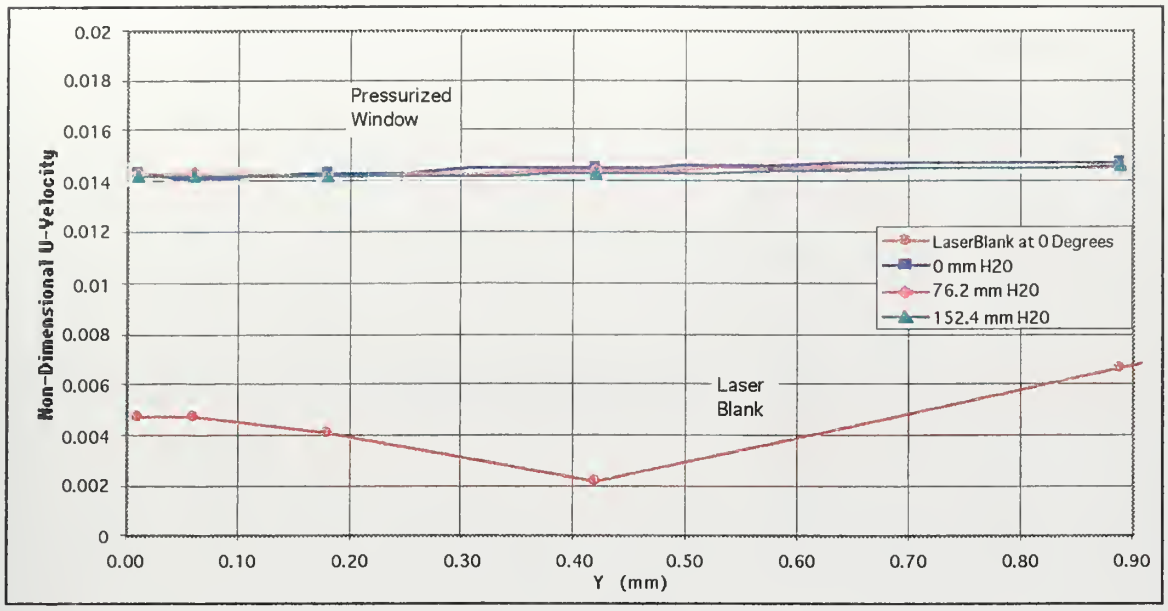

Figure 27a. Comparisons of radial surveys using the laser blank and pressurized LDV window at a Prat of 0.9620

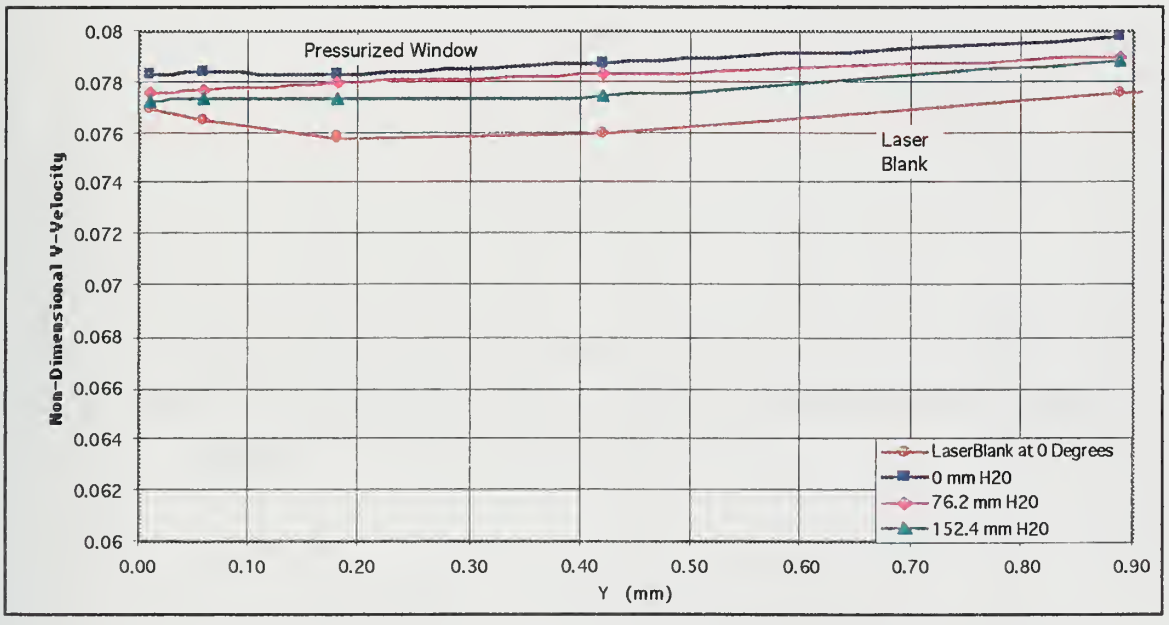

Figure 27b. Comparisons of radial surveys using the laser blank and pressurized LDV window at a Prat of 0.9620

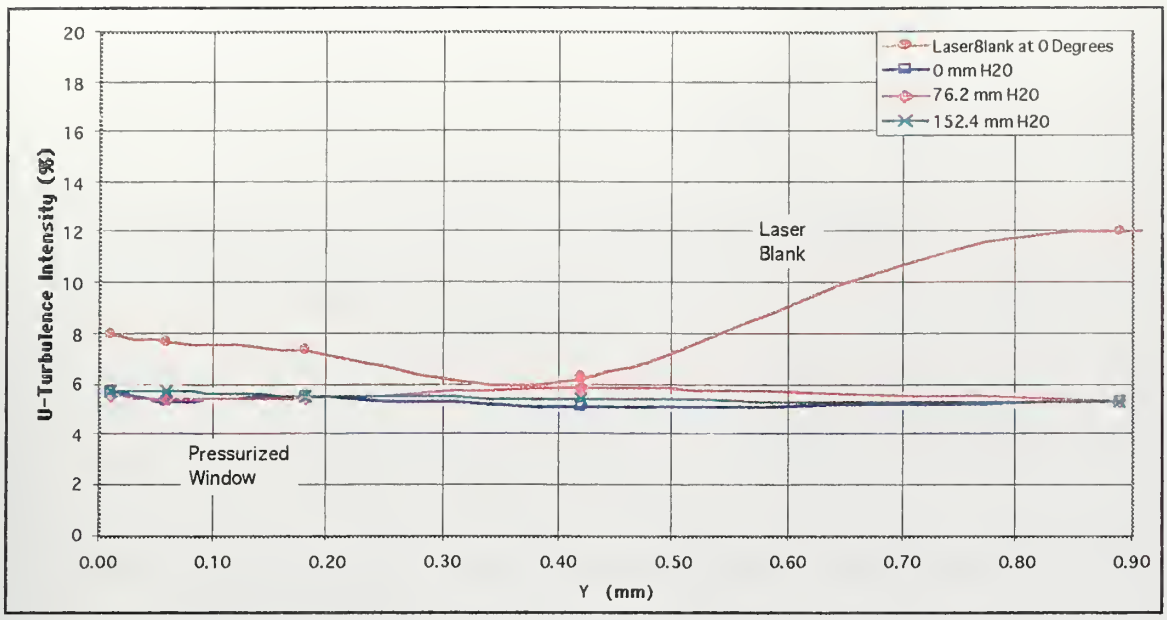

Figure 28a. Comparisons of radial surveys using the laser blank and pressurized LDV window at a Prat of 0.9620

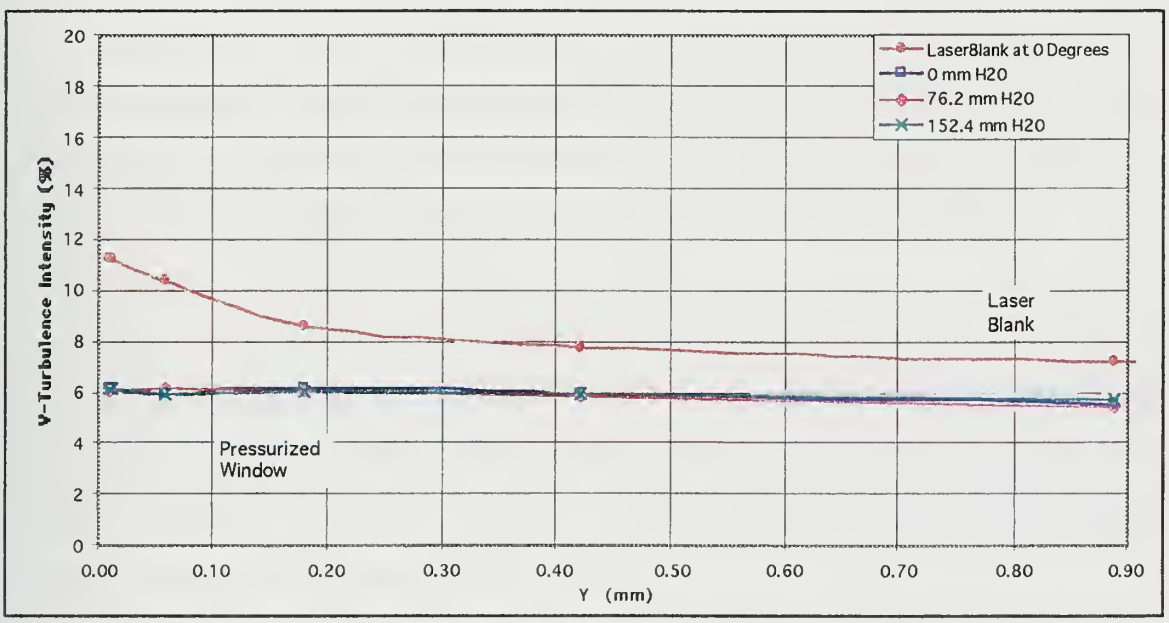

Figure 28b. Comparisons of radial surveys using the laser blank and pressurized LDV window at a Prat of 0.9620

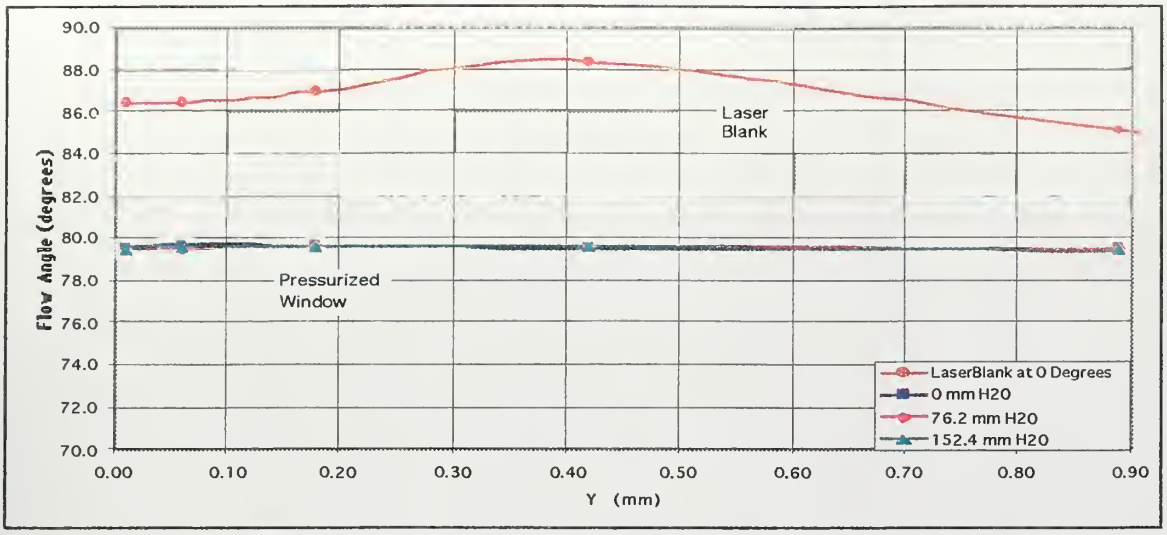

Figure 29. Comparisons of radial surveys using the laser blank and pressurized LDV window at a Prat of 0.9620

5. Effect of Various Chamber Pressures Compared to Laser Blank

Figures 30-32 show a comparison between results obtained with the new pressurized window under various chamber pressures and the laser blank, with the LDV fixed at a point within the flow. Chamber pressures of 0, 76.2, and 152.4 millimeters of water (0, 3, and 6 inches of water) were applied to the new window to determine their effect on flow measurements.

Figure 30a and 30b show the pressurized window velocity data to be significantly above the velocities obtained with the laser blank. This could be due to the flow escaping out of the optical access hole of the laser blank causing a lower-than-actual velocity to be detected by the LDV. Both the horizontal and vertical velocities also showed a slight increase when the pressure was increased within the chamber.

Figures 31a and 31b show reduced turbulence intensities in both the horizontal and vertical directions when utilizing the new LDV window, as previously shown. This reduction in turbulence intensity could be due to the containment of the flow within the new window, reducing the turbulence caused by the flow previously escaping from the optical access hole.

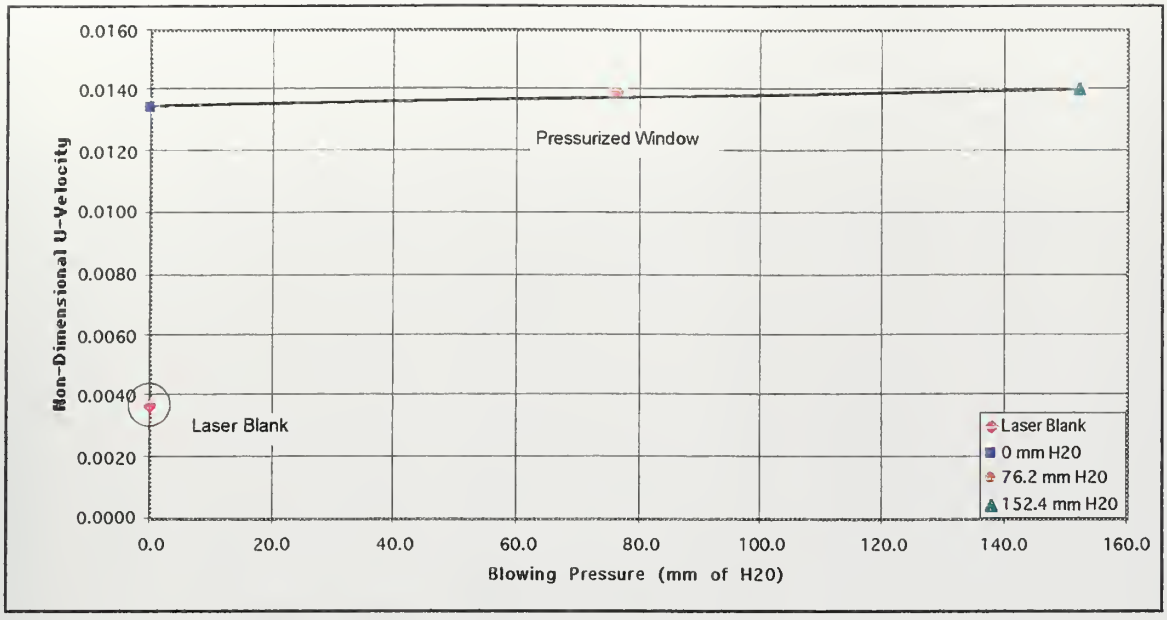

Figure 30a. Pressurized LDV window and laser blank comparisons at Prat of 0.9620

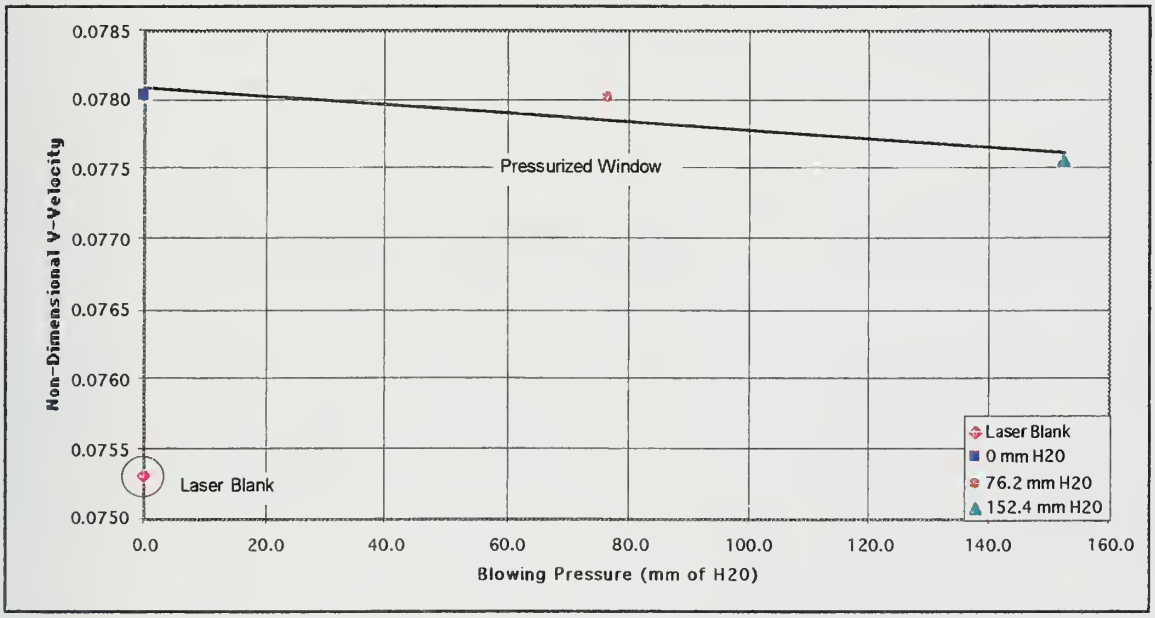

Figure 30b. Pressurized LDV window and laser blank comparisons at Prat of 0.9620

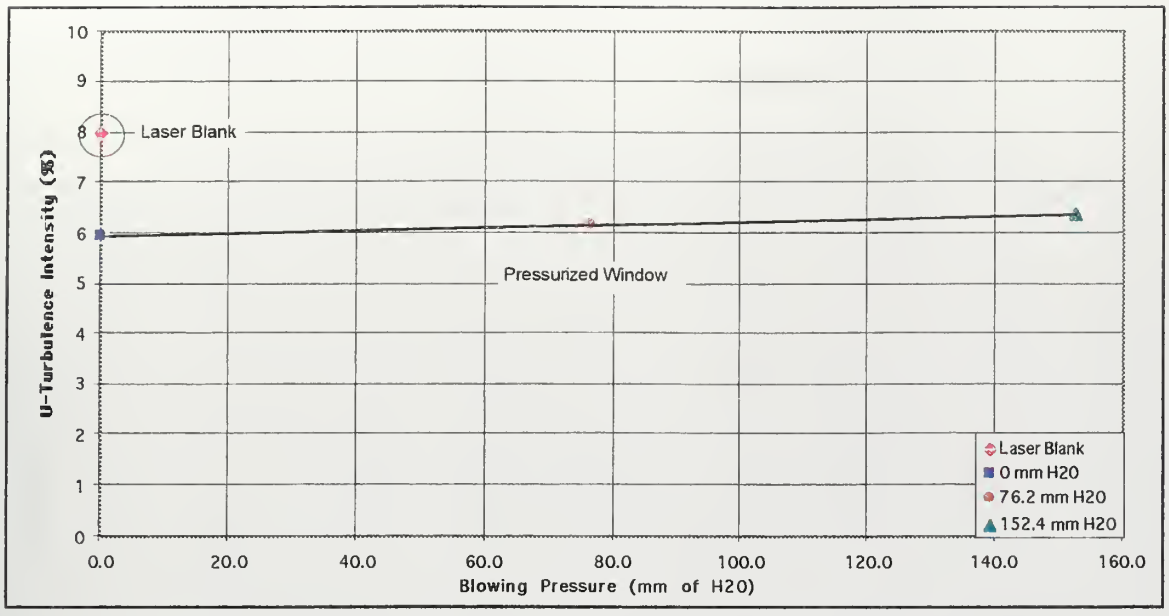

Figure 31a. Pressurized LDV window and laser blank comparisons at Prat of 0.9620

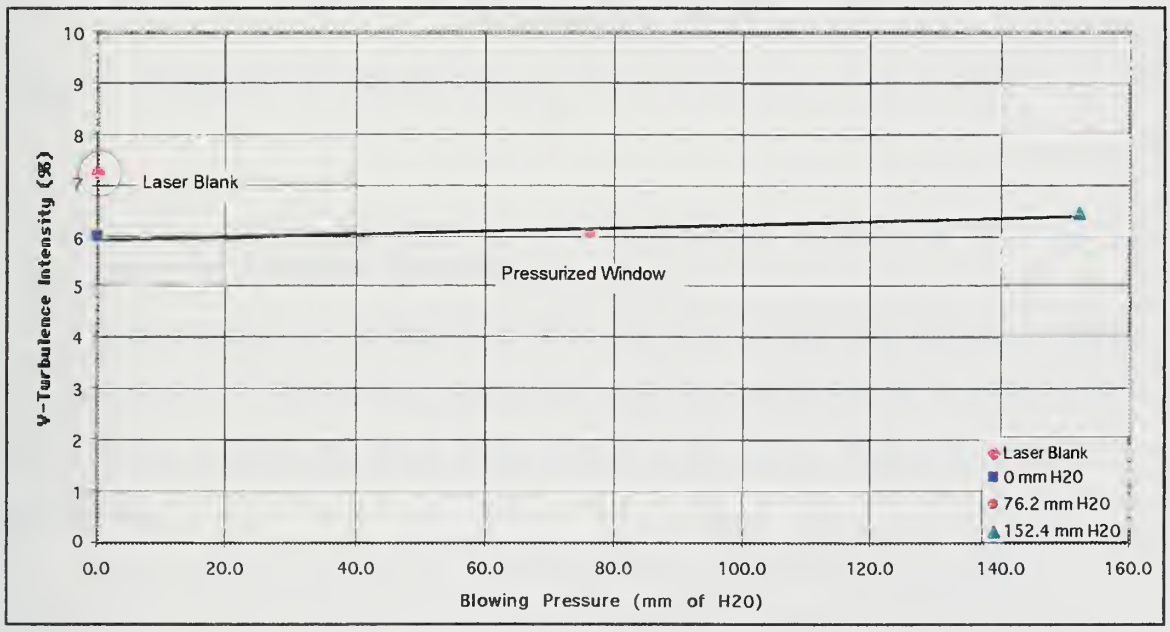

Figure 31b. Pressurized LDV window and laser blank comparisons at Prat of 0.9620

Figure 32 shows a difference in flow angle of about 6 degrees between the laser blank and the pressurized window, with the pressurized window having the lower angle.

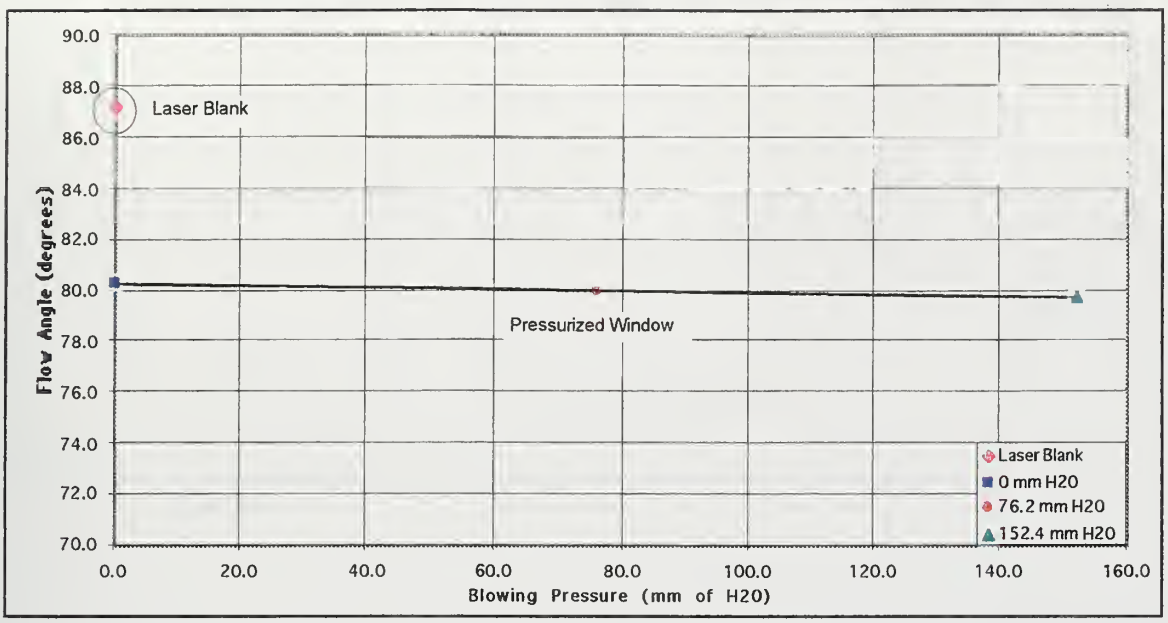

Figure 32. Pressurized LDV window and laser blank comparisons at Prat of 0.9620

6. Circumferential Surveys with Pressurized Window at 76.2 mm (3 in) water Chamber Pressure

Circumferential surveys from -8 to +8 degrees wake position were conducted with the new pressurized LDV window at a constant mid-range chamber pressure of 76.2 mm (3 in) water to further determine the effects of this window on this survey. Figures 33-35 show these results.

Figures 33a and 33b show the velocity profiles over the circumferential range. Similar trends to those in the radial survey also occurred here. The circumferential velocity profiles of the new window were also higher than those obtained with the laser blank (Figures 27a and 27b).

Figures 34a and 34b show the turbulence intensity with the pressurized window again to be lower than the turbulence intensity with the laser blank.

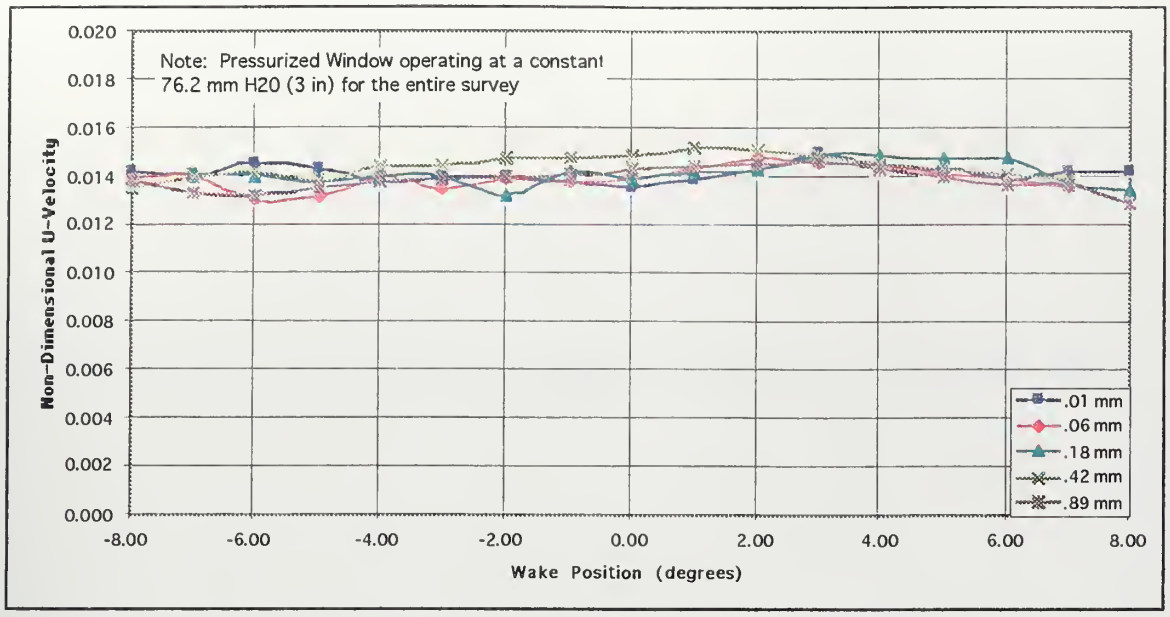

Figure 33a. A circumferential survey through the pressurized LDV window at a Prat of 0.9620

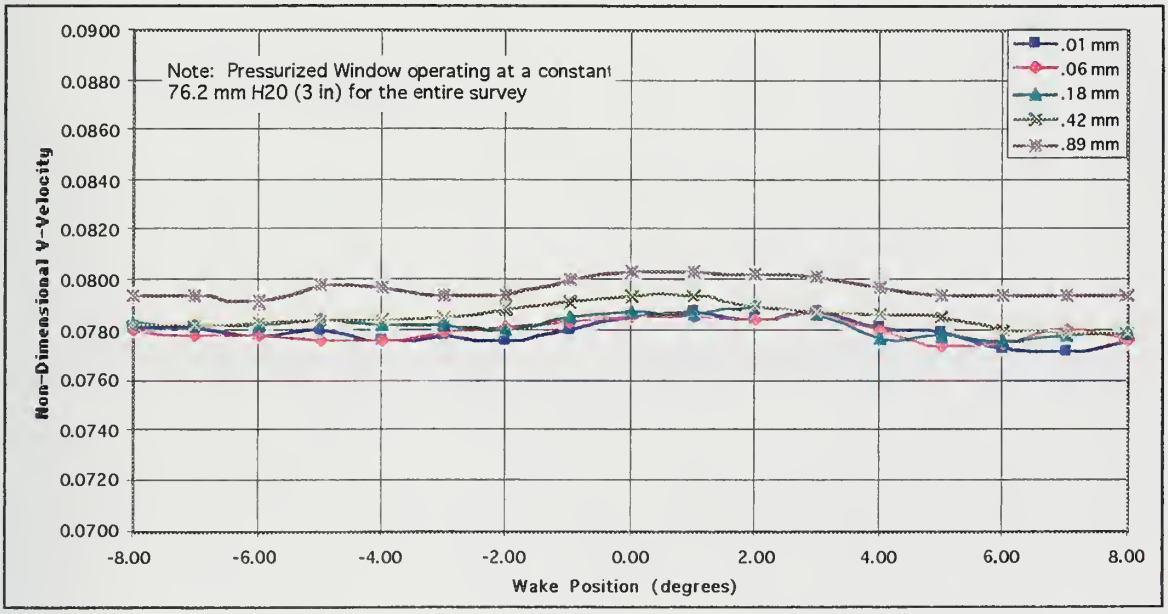

Figure 33b. A circumferential survey through the pressurized LDV window at a Prat of 0.9620

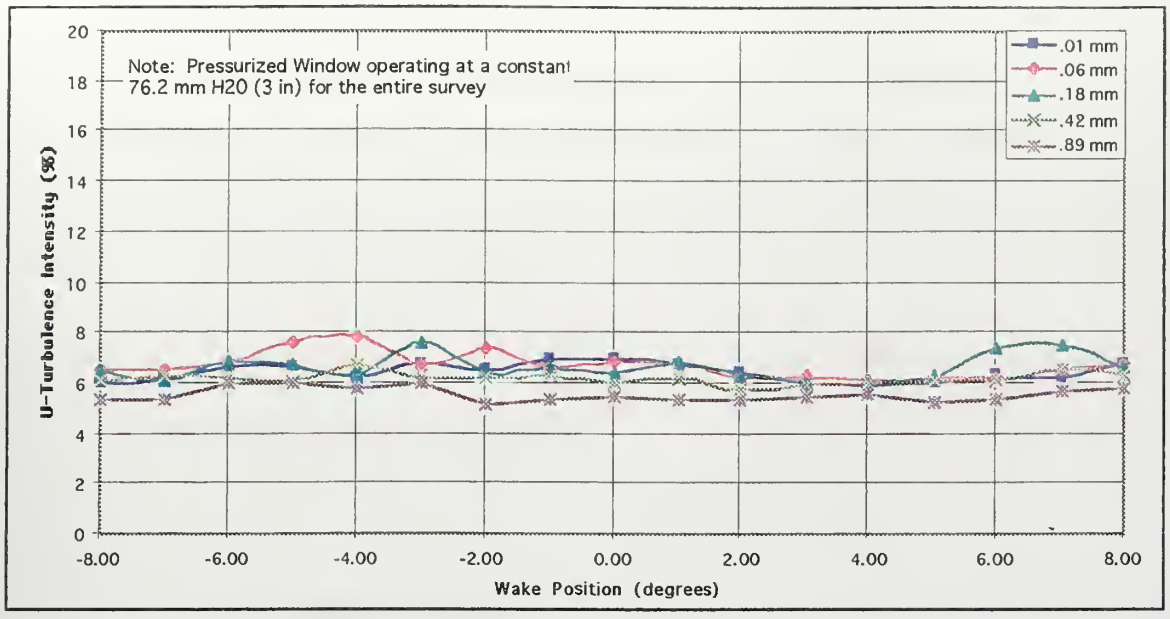

Figure 34a. A circumferential survey through the pressurized LDV window at a Prat of 0.9620

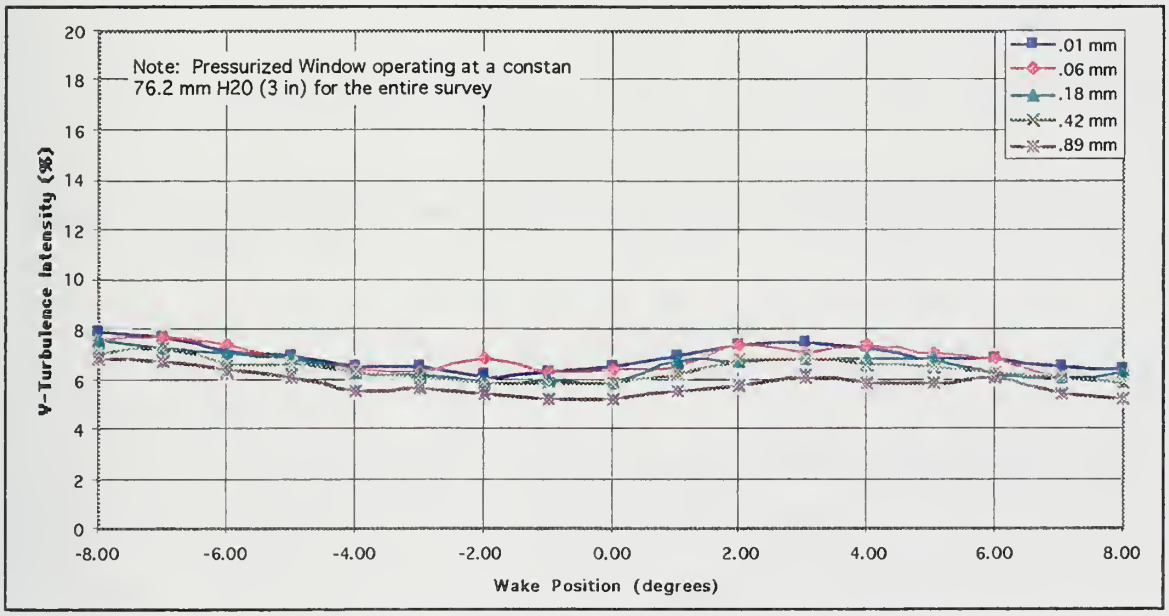

Figure 34b. A circumferential survey through the pressurized LDV window at a Prat of 0.9620

Figure 35 also shows flow angles lower than with the laser blank, which is consistent with the flow angles measured in the previous radial surveys. The results from the circumferential survey were fully consistent with those from the previous radial surveys indicating good repeatability of the one dimensional measuring technique with the new LDV window.

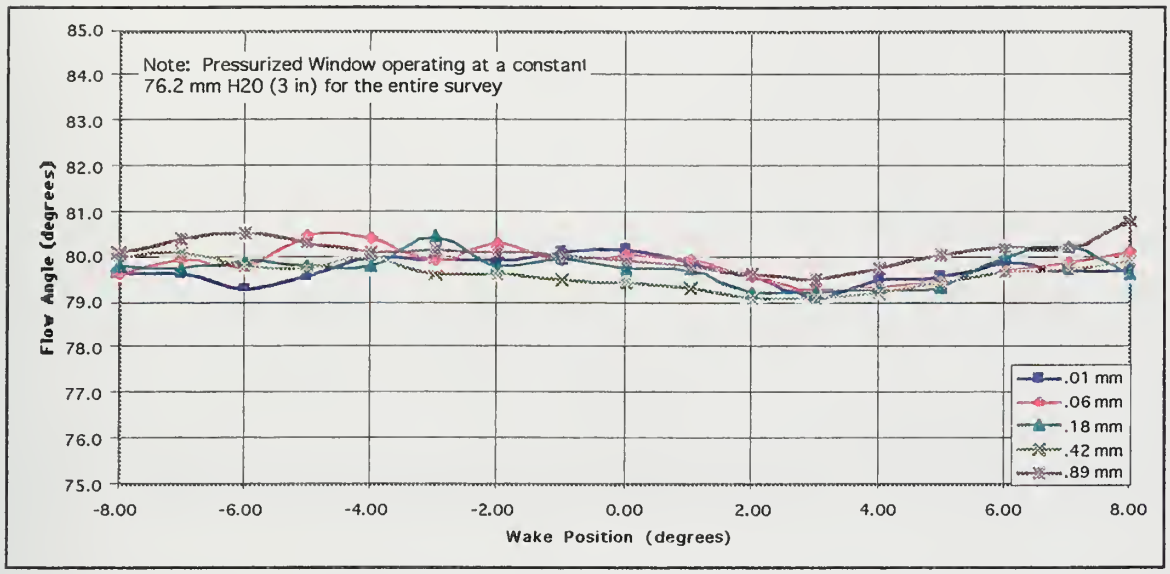

Figure 35. A circumferential survey through the pressurized LDV window at a Prat of 0.9620

7. Final Comparison with Laser Blank, Pressurized LDV Window, and Cobra Probe

Three-hole cobra probe surveys were performed to verify the aforementioned LDV data, with the probe at the same location as the LDV windows (Figure 1). Cobra-probe data were taken at a pressure ratio of 0.9620. Utilizing the equations in Reference 3 and the third-order calibration curve from Figure D1 of Appendix D, the values for (X), total non-dimensional velocity, were calculated from the measurements. Flow angle was read from the vernier scale on the probe holder and recorded in the front panel of the LabView program.

Figures 36 and 37 are the final comparisons of total non-dimensional velocity and flow angle between these three measuring methods. Figure 36 shows the probe velocity increasing as the probe was radially traversed into the ATC.

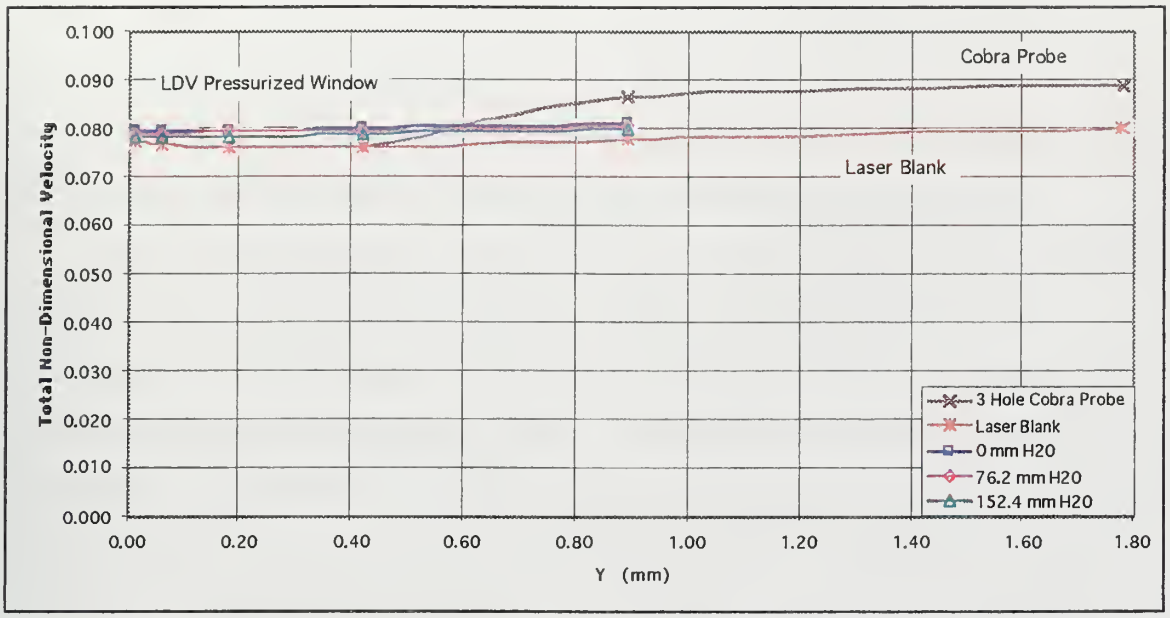

Figure 36. Final total non-dimensional velocity comparison between laser blank, pressurized window, and 3-hole cobra probe at a Prat of 0.9620

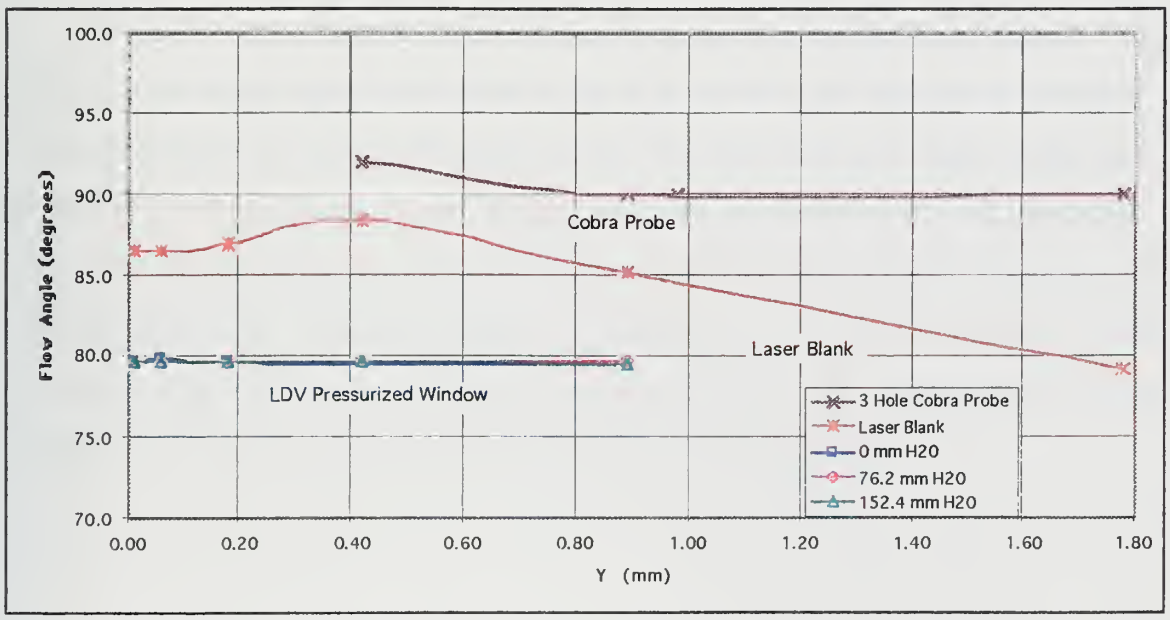

Figure 37. Final flow angle comparison between laser blank, pressurized window, and 3-hole cobra probe at a Prat of 0.9620

Figure 38 is a pictorial illustration of the possible interaction of the probe within the ATC. Figure 38a shows the probe approximately at the 1.78 mm radial position. At this position, the probe stem sealed the hole and the flow did not leak. The internal flow was relatively undisturbed. Figure 38b shows the probe head at the endwall. In this position, the probe no longer sealed the hole and the flow could leak out of the ATC. The LDV windows were in behavior, with the laser blank giving lower velocities due to the flow leakage and the pressurized window giving higher velocities due to no leakage (Figures 39 and 40).

Figure 36 shows the total non-dimensional velocity which was the vectorial sum of the U and V velocities. The cobra probe initially measured a velocity similar to the LDV measurement with the laser blank, since the flow was leaking out at this time. As the probe stem plugged the hole and stopped the leakage, the velocity rose to slightly above the LDV measurement obtained with the pressurized window. This suggested that as the flow leaked out of the optical access hole, the measurements indicated lower velocities due to the flow slowing down within the ATC in order to exit the opening. The higher value of velocity recorded by the cobra probe when set as shown in Figure 38a could be due to wall-proximity effects.

Figure 37 shows the flow angles obtained from the three measurement methods. The probe gave the largest angles which could be due to its intrusion and large size as compared to the non-intrusive and small LDV probe volume. The laser blank gave higher angles near the endwall which decreased to about 79 degrees as the survey progressed. The pressurized window was the most consistent of the two methods, even with varying chamber pressures. It gave approximately 79.5 degrees throughout its radial survey. The flow angles given by the two LDV methods seem to agree well at the final point within the ATC farthest away from the endwall. Both methods measured 79.5 degrees at the 1.78 mm position.

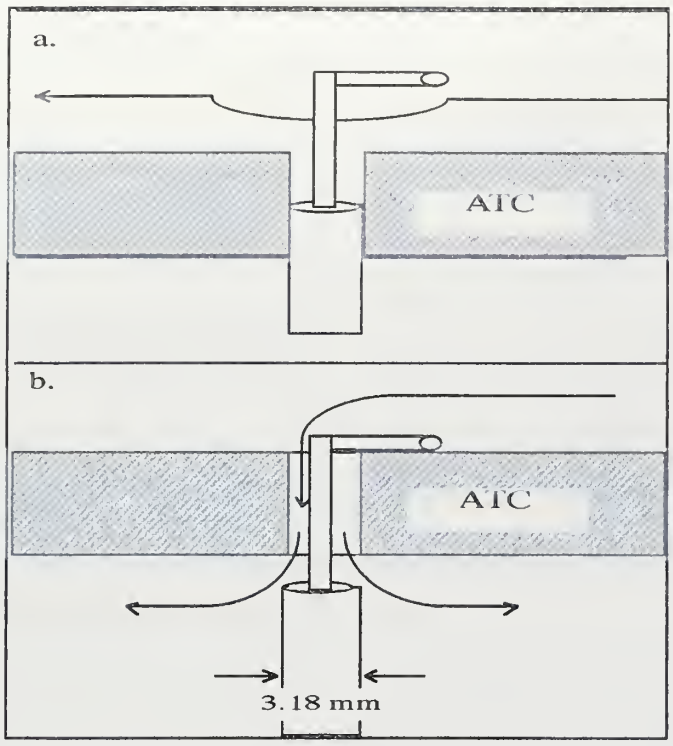

Figure 38. ATC flow depiction - the 3-hole cobra probe

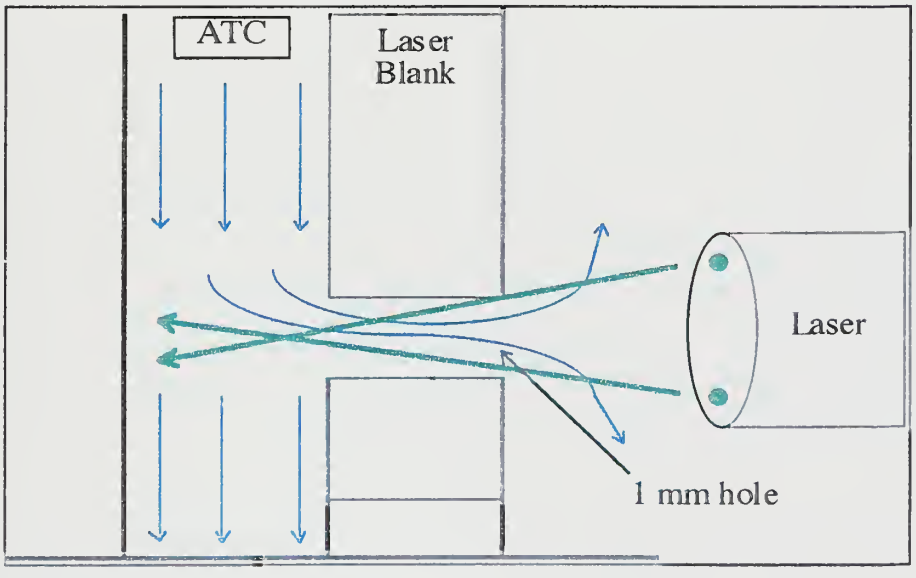

Figure 39. ATC flow depiction - laser blank

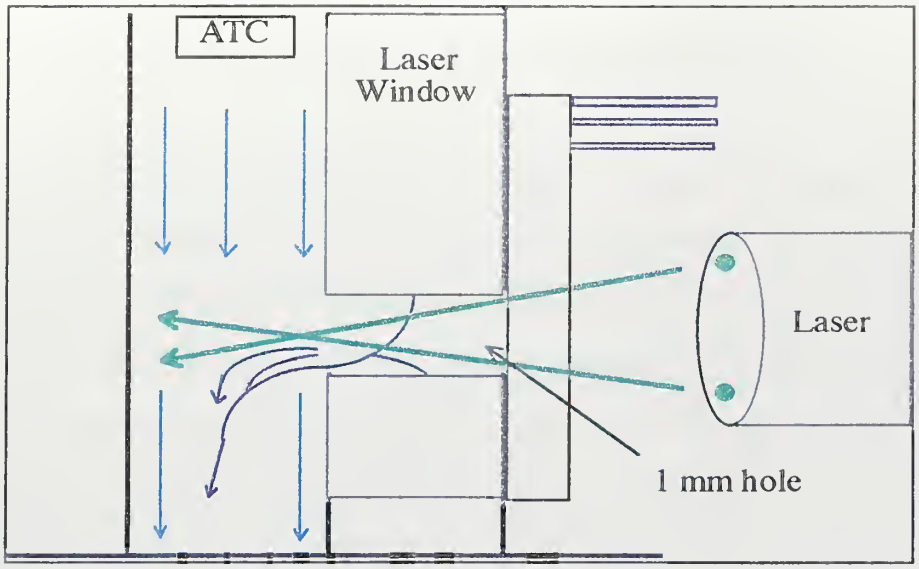

Figure 40. ATC flow depiction - pressurized window

V. CONCLUSIONS AND RECOMMENDATIONS

An experimental investigation with an innovative pressurized LDV window was conducted on the flow through an annular turbine cascade to determine the effects of such a window on laser measurements. A pressure ratio (P_{rat}) of .09620, defined as the downstream hub-static pressure (P_{hub}) divided by the upstream stagnation pressure (P_0), was chosen to test the new window. Three chamber pressures of 0, 76.2 and 152.4 mm (0, 3, and 6 in) of water were applied to the pressurized window resulting in LDV measurements that were compared with those obtained with a laser blank and velocity distributions obtained with a three-hole cobra probe.

An equalized pressure condition of 0 mm of water was considered preferable when measuring. In this condition the pressurized window eliminated any influence that the optical access hole may have had and the internal flow was not then affected by any pressurized air from the window. When the chamber was pressurized, the effect on the ATC flow of the increasing the pressure was found to be surprisingly small up to 152.4 mm (6 in) of water chamber pressure. The ATC flow seemed to be relatively insensitive to this procedure, which could be used to purge the window of any seed build up during the experiment.

LDV alignment and radial survey procedures were devised and repeated. The probe volume passed cleanly through the optical access hole and radial surveys were conducted to provide complete coverage for data recording. Introduction of a second fiber-optic probe for three component measurements would decrease the effective probe volume and increase radial position accuracy.

Initial measurements with the 1-dimensional probe showed good repeatability, but did not compare well with previous 2-component measurements. The previous measurements used a different data acquisition system than the one available for the present experiment, which may have contributed to the discrepancy. However, the 1-D procedure did prove to be both repeatable and accurate, despite the large amount of movement of the laser probe head.

Successful two-dimensional measurements of velocity, flow angle, and turbulence intensity through a 1.092 mm diameter optical access hole were demonstrated using both the 1-dimensional procedure and the new pressurized window. All LDV data were acquired one-half axial chord downstream of the turbine stator over five radial positions and 17 separate circumferential displacements. The range of experimental flow velocities was decreased from that used in Reference 2 due to the unavailability of the former processor and the limitations of the current signal processor.

The coarse circumferential (wake) positioning mechanism needed modification to allow more precise adjustment. Experimental circumferential positioning uncertainties may have contributed to some of the differences in the compared data.

Successful cobra probe measurements were conducted to help verify the measurements taken using the pressurized window. The result of a comparison of all three flow measurement devices was that, when the flow was contained (pressurized window), the measurements indicated higher velocities, lower turbulence intensities, and lower flow angles. If the flow was not contained (laser blank), the measurements indicated lower velocities, higher turbulence intensities, and higher flow angles. As the flow turned to exit the optical access hole, the flow angle increased.

The pressurized window provided accurate and repeatable LDV measurements with fewer disturbances to the flow than the previous laser blank. Future efforts to improve on this initial design would be to modify the shape to accommodate the laser probe volume deeper into the turbine. Increased flow velocities could also be attempted with subsequent increased chamber pressures to determine the benefits of this window on LDV measurements at higher flow speeds.

APPENDIX A. PRESSURE DATA ACQUISITION

The following table relates each Scanivalve port to its respective pressure measurement.

Scanivalve Port Number	Pressure Measured
1	Ambient Pressure
2	Calibration Pressure (set at 20 inches hg)
3	Not Used
4	Upstream Total Pressure (P_0)
5	Downstream Hub Static Pressure (P_{hub})
6	Upstream Static Pressure (P_{static})
7	Not Used
8	Not Used
9	Blade Static Port #1 (at leading edge)
10	Blade Static Port #2 (suction side)
11	Blade Static Port #3 (suction side)
12	Blade Static Port #4 (suction side)
13	Blade Static Port #5 (suction side)
14	Blade Static Port #6 (suction side)
15	Blade Static Port #7 (suction side)
16	Blade Static Port #8 (at leading edge)
17	Blade Static Port #9 (pressure side)
18	Blade Static Port #10 (pressure side)
19	Blade Static Port #11 (pressure side)

Table A1. Pressure data acquisition connections

APPENDIX B. BLADE MIDSPAN SURFACE PRESSURE DATA

Prat of .9825	Date: 04/05/96	Baro=30.06 in Hg	Temp=78 F
Scanivalve Port #	**Scanivalve Port Value**	**Static Pressure (psi)**	**P/Po**
1	P ambient	14.7690	
2	P calibration	15.7554	
4	Po (Ref. Upstream Stagnation)	15.0334	1.0000
5	P hub exit (Static @ 0.5c downstream)	14.7897	
6	P up static (Ref. Upstream Static)	15.0398	
9	P Static Port 1 (@ leading edge)	15.0399	1.0004
10	P Static Port 2	15.0207	0.9992
11	P Static Port 3	14.9188	0.9924
12	P Static Port 4	14.821	0.9859
13	P Static Port 5	14.788	0.9837
14	P Static Port 6	14.8013	0.9846
15	P Static Port 7	14.8046	0.9848
16	P Static Port 8 (@ leading edge)	15.0384	1.0003
17	P Static Port 9	15.0281	0.9996
18	P Static Port 10	14.9838	0.9967
19	P Static Port 11	14.9462	0.9942

Table B1. Surface pressures at 0.9825 pressure ratio

Prat of .9757	Date: 04/05/96	Baro=30.06 in Hg	Tstag=83 F
Scanivalve Port #	Scanivalve Port Value	Static Pressure (psi)	P/Po
1	P ambient	14.7641	
2	P calibration	15.7586	
4	Po (Ref. Upstream Stagnation)	15.1364	1.0000
5	P hub exit (Static @ 0.5c downstream)	14.7923	
6	P up static (Ref. Upstream Static)	15.1430	
9	P Static Port 1 (@ leading edge)	15.1430	1.0004
10	P Static Port 2	15.0970	0.9974
11	P Static Port 3	14.9739	0.9893
12	P Static Port 4	14.8382	0.9803
13	P Static Port 5	14.7836	0.9767
14	P Static Port 6	14.8068	0.9782
15	P Static Port 7	14.811	0.9785
16	P Static Port 8 (@ leading edge)	15.1439	1.0005
17	P Static Port 9	15.1278	0.9994
18	P Static Port 10	15.0646	0.9953
19	P Static Port 11	15.0121	0.9918

Table B2. Surface pressures at 0.9757 pressure ratio

Prat of .9710	Date: 04/05/96	Baro=30.06 in Hg	Tstag=84 F
Scanivalve Port #	Scanivalve Port Value	Static Pressure (psi)	P/Po
1	P ambient	14.7641	
2	P calibration	15.7587	
4	Po (Ref. Upstream Stagnation)	15.2046	1.0000
5	P hub exit (Static @ 0.5c downstream)	14.7981	
6	P up static (Ref. Upstream Static)	15.2119	
9	P Static Port 1 (@ leading edge)	15.2141	1.0006
10	P Static Port 2	15.1462	0.9962
11	P Static Port 3	15.0207	0.9879
12	P Static Port 4	14.8607	0.9774
13	P Static Port 5	14.7972	0.9732
14	P Static Port 6	14.8174	0.9745
15	P Static Port 7	14.8243	0.9750
16	P Static Port 8 (@ leading edge)	15.2113	1.0004
17	P Static Port 9	15.1929	0.9992
18	P Static Port 10	15.1203	0.9945
19	P Static Port 11	15.0582	0.9904

Table B3. Surface pressures at 0.9710 pressure ratio

Prat of .9669	Date: 04/05/96	Baro=30.06 in Hg	Tstag=84 F
Scanivalve Port #	Scanivalve Port Value	Static Pressure (psi)	P/Po
1	P ambient	14.7641	
2	P calibration	15.7586	
4	Po (Ref. Upstream Stagnation)	15.2744	1.0000
5	P hub exit (Static @ 0.5c downstream)	14.8050	
6	P up static (Ref. Upstream Static)	15.2841	
9	P Static Port 1 (@ leading edge)	15.2865	1.0008
10	P Static Port 2	15.2107	0.9958
11	P Static Port 3	15.0609	0.9860
12	P Static Port 4	14.8758	0.9739
13	P Static Port 5	14.8012	0.9690
14	P Static Port 6	14.8283	0.9708
15	P Static Port 7	14.8306	0.9709
16	P Static Port 8 (@ leading edge)	15.2846	1.0007
17	P Static Port 9	15.2625	0.9992
18	P Static Port 10	15.1727	0.9933
19	P Static Port 11	15.1026	0.9888

Table B4. Surface pressures at 0.9669 pressure ratio

Prat of .9621	Date: 04/05/96	Baro=30.06 in Hg	Tstag=85 F
Scanivalve Port #	**Scanivalve Port Value**	**Static Pressure (psi)**	**P/Po**
1	P ambient	14.7641	
2	P calibration	15.7583	
4	Po (Ref. Upstream Stagnation)	15.3525	1.0000
5	P hub exit (Static @ 0.5c downstream)	14.8108	
6	P up static (Ref. Upstream Static)	15.3636	
9	P Static Port 1 (@ leading edge)	15.3639	1.0007
10	P Static Port 2	15.2706	0.9947
11	P Static Port 3	15.1029	0.9837
12	P Static Port 4	14.8922	0.9700
13	P Static Port 5	14.8123	0.9648
14	P Static Port 6	14.8349	0.9663
15	P Static Port 7	14.8383	0.9665
16	P Static Port 8 (@ leading edge)	15.3492	0.9998
17	P Static Port 9	15.3361	0.9989
18	P Static Port 10	15.24	0.9927
19	P Static Port 11	15.1585	0.9874

Table B5. Surface pressures at 0.9621 pressure ratio

Prat of .9575	Date: 04/05/96	Baro=30.06 in Hg	Tstag=86 F
Scanivalve Port #	**Scanivalve Port Value**	**Static Pressure (psi)**	**P/Po**
1	P ambient	14.7641	
2	P calibration	15.7555	
4	Po (Ref. Upstream Stagnation)	15.4209	1.0000
5	P hub exit (Static @ 0.5c downstream)	14.4318	
6	P up static (Ref. Upstream Static)	15.4318	
9	P Static Port 1 (@ leading edge)	15.4335	1.0008
10	P Static Port 2	15.3285	0.9940
11	P Static Port 3	15.1364	0.9816
12	P Static Port 4	14.906	0.9666
13	P Static Port 5	14.8175	0.9609
14	P Static Port 6	14.8389	0.9623
15	P Static Port 7	14.8454	0.9627
16	P Static Port 8 (@ leading edge)	15.4295	1.0006
17	P Static Port 9	15.4039	0.9989
18	P Static Port 10	15.2961	0.9919
19	P Static Port 11	15.2016	0.9858

Table B6. Surface pressures at 0.9575 pressure ratio

Prat of .9527	Date: 04/05/96	Baro=30.06 in Hg	Tstag=87 F
Scanivalve Port #	**Scanivalve Port Value**	**Static Pressure (psi)**	**P/Po**
1	P ambient	14.7641	
2	P calibration	15.7545	
4	Po (Ref. Upstream Stagnation)	15.4937	1.0000
5	P hub exit (Static @ 0.5c downstream)	14.8297	
6	P up static (Ref. Upstream Static)	15.5083	
9	P Static Port 1 (@ leading edge)	15.5087	1.0010
10	P Static Port 2	15.3948	0.9936
11	P Static Port 3	15.1786	0.9797
12	P Static Port 4	14.9241	0.9632
13	P Static Port 5	14.8256	0.9569
14	P Static Port 6	14.8482	0.9583
15	P Static Port 7	14.8526	0.9586
16	P Static Port 8 (@ leading edge)	15.4951	1.0001
17	P Static Port 9	15.477	0.9989
18	P Static Port 10	15.3583	0.9913
19	P Static Port 11	15.2577	0.9848

Table B7. Surface pressures at 0.9527 pressure ratio

Prat of .9483	Date: 04/05/96	Baro=30.06 in Hg	Tstag=88 F
Scanivalve Port #	**Scanivalve Port Value**	**Static Pressure (psi)**	**P/Po**
1	P ambient	14.7641	
2	P calibration	15.7528	
4	Po (Ref. Upstream Stagnation)	15.5657	1.0000
5	P hub exit (Static @ 0.5c downstream)	14.8287	
6	P up static (Ref. Upstream Static)	15.5851	
9	P Static Port 1 (@ leading edge)	15.5843	1.0012
10	P Static Port 2	15.4564	0.9930
11	P Static Port 3	15.2216	0.9779
12	P Static Port 4	14.9405	0.9598
13	P Static Port 5	14.8176	0.9519
14	P Static Port 6	14.8631	0.9549
15	P Static Port 7	14.8673	0.9551
16	P Static Port 8 (@ leading edge)	15.5804	1.0009
17	P Static Port 9	15.5473	0.9988
18	P Static Port 10	15.4147	0.9903
19	P Static Port 11	15.3053	0.9833

Table B8. Surface pressures at 0.9483 pressure ratio

Prat of .9445	Date: 04/05/96	Baro=30.06 in Hg	Tstag=89 F
Scanivalve Port #	Scanivalve Port Value	Static Pressure (psi)	P/Po
1	P ambient	14.7641	
2	P calibration	15.7510	
4	Po (Ref. Upstream Stagnation)	15.6278	1.0000
5	P hub exit (Static @ 0.5c downstream)	14.8335	
6	P up static (Ref. Upstream Static)	15.6487	
9	P Static Port 1 (@ leading edge)	15.6442	1.0010
10	P Static Port 2	15.5066	0.9922
11	P Static Port 3	15.2518	0.9759
12	P Static Port 4	14.951	0.9567
13	P Static Port 5	14.8355	0.9493
14	P Static Port 6	14.857	0.9507
15	P Static Port 7	14.8619	0.9510
16	P Static Port 8 (@ leading edge)	15.6258	0.9999
17	P Static Port 9	15.6073	0.9987
18	P Static Port 10	15.4658	0.9896
19	P Static Port 11	15.3467	0.9820

Table B9. Surface pressures at 0.9445 pressure ratio

Prat of .9392	Date: 04/05/96	Baro=30.06 in Hg	Tstag=90 F
Scanivalve Port #	Scanivalve Port Value	Static Pressure (psi)	P/Po
1	P ambient	14.7641	
2	P calibration	15.7517	
4	Po (Ref. Upstream Stagnation)	15.7097	1.0000
5	P hub exit (Static @ 0.5c downstream)	14.8411	
6	P up static (Ref. Upstream Static)	15.7266	
9	P Static Port 1 (@ leading edge)	15.731	1.0014
10	P Static Port 2	15.5861	0.9921
11	P Static Port 3	15.307	0.9744
12	P Static Port 4	14.9793	0.9535
13	P Static Port 5	14.8469	0.9451
14	P Static Port 6	14.8718	0.9467
15	P Static Port 7	14.8752	0.9469
16	P Static Port 8 (@ leading edge)	15.7156	1.0004
17	P Static Port 9	15.6932	0.9989
18	P Static Port 10	15.5362	0.9890
19	P Static Port 11	15.4039	0.9805

Table B10. Surface pressures at 0.9392 pressure ratio

Prat of .9359	Date: 04/05/96	Baro=30.06 in Hg	Tstag=91 F
Scanivalve Port #	Scanivalve Port Value	Static Pressure (psi)	P/Po
1	P ambient	14.7641	
2	P calibration	15.7495	
4	Po (Ref. Upstream Stagnation)	15.7679	1.0000
5	P hub exit (Static @ 0.5c downstream)	14.8419	
6	P up static (Ref. Upstream Static)	15.7873	
9	P Static Port 1 (@ leading edge)	15.7941	1.0017
10	P Static Port 2	15.6366	0.9917
11	P Static Port 3	15.3413	0.9729
12	P Static Port 4	14.9785	0.9499
13	P Static Port 5	14.8416	0.9413
14	P Static Port 6	14.8748	0.9434
15	P Static Port 7	14.8762	0.9434
16	P Static Port 8 (@ leading edge)	15.79	1.0014
17	P Static Port 9	15.7491	0.9988
18	P Static Port 10	15.5812	0.9882
19	P Static Port 11	15.4452	0.9795

Table B11. Surface pressures at 0.9359 pressure ratio

Prat of .9312	Date: 04/05/96	Baro=30.06 in Hg	Tstag=92 F
Scanivalve Port #	Scanivalve Port Value	Static Pressure (psi)	P/Po
1	P ambient	14.7641	
2	P calibration	15.7478	
4	Po (Ref. Upstream Stagnation)	15.8447	1.0000
5	P hub exit (Static @ 0.5c downstream)	14.8544	
6	P up static (Ref. Upstream Static)	15.8694	
9	P Static Port 1 (@ leading edge)	15.8735	1.0018
10	P Static Port 2	15.7070	0.9913
11	P Static Port 3	15.3889	0.9712
12	P Static Port 4	15.0051	0.9470
13	P Static Port 5	14.8559	0.9376
14	P Static Port 6	14.8856	0.9395
15	P Static Port 7	14.89	0.9397
16	P Static Port 8 (@ leading edge)	15.8606	1.0010
17	P Static Port 9	15.8372	0.9995
18	P Static Port 10	15.6559	0.9881
19	P Static Port 11	15.5034	0.9785

Table B12. Surface pressures at 0.9312 pressure ratio

APPENDIX C. LDV DATA

Date	Prat	Run #	Depth	U-Velocity	U-Non	V-Velocity	V-Non	U-Turbulence	V-Turbulence	Flow Angle
			(mm)	(m/s)	Dimensionalized	(m/s)	Dimensionalized	(%)	(%)	degrees
4/16/96	0.9054	1	0.0090	7.7263	0.0098	70.6980	0.0896	9.2920	10.8338	83.9859
			0.0590	7.6138	0.0096	70.8067	0.0897	8.8283	10.7080	84.0281
			0.1790	6.3443	0.0080	72.6799	0.0921	9.1375	10.3136	84.6274
			0.4200	6.6946	0.0085	74.0324	0.0938	8.8455	9.6086	84.6887
			0.8890	7.0147	0.0089	76.1521	0.0965	8.8078	8.0782	84.2938
			1.7790	7.6428	0.0097	79.3038	0.1005	8.5545	6.5872	83.8449
		2	0.0090	7.3401	0.0093	75.1028	0.0951	8.8467	8.1487	
			0.0590	7.3422	0.0093	74.7188	0.0946	8.8773	8.3646	
			0.1790	6.9598	0.0088	75.0067	0.0950	8.6105	8.4808	
			0.4200	6.5290	0.0083	76.0889	0.0964	8.7808	7.8535	
			0.8890	7.5725	0.0096	77.8091	0.0986	8.8516	7.4860	
			1.7790	8.9538	0.0113	80.0626	0.1014	8.9554	7.1723	
		3	0.0090	7.7023	0.0098	70.3165	0.0891	8.6246	11.2738	
			0.0590	7.7153	0.0098	71.1984	0.0902	8.7844	10.9511	
			0.1790	7.4003	0.0094	72.4658	0.0918	8.6960	10.2123	
			0.4200	7.6315	0.0097	74.2093	0.0940	9.2821	9.4072	
			0.8890	8.4376	0.0107	76.4671	0.0969	9.5977	7.9965	
			1.7790	9.1613	0.0116	79.4832	0.1007	9.3782	6.4372	

Table C1. 04/16/96 Laser blank radial survey at 0.9054 pressure ratio

Date	Prat	Wake Position	Depth	U-Velocity	U-Non	V-Velocity	V-Non	U-Turbulence	V-Turbulence	Flow Angle
		(degrees)	(mm)	(m/s)	Dimensionalized	(m/s)	Dimensionalized	(%)	(%)	degrees
4/26/96	0.9054	0	0.0090	7.5867	0.0096	67.3459	0.0850	8.2461	13.3413	83.5726
			0.0590	7.5842	0.0096	66.5375	0.0840	8.4709	12.4993	83.4973
			0.1790	8.0933	0.0102	65.5193	0.0827	7.9839	12.1199	82.9582
			0.4200	8.1258	0.0103	65.0528	0.0821	8.3899	10.9839	82.8800
			0.8890	7.7965	0.0098	65.1411	0.0822	8.8630	9.8928	83.1749
			1.7790	9.4393	0.0119	75.2531	0.0950	8.4856	9.9922	82.8505
		Pinned (-2 deg)	0.0090	7.9418	0.0100	67.4893	0.0852	8.5371	12.4886	83.2886
			0.0590	7.9699	0.0101	67.1699	0.0848	8.6211	11.9539	83.2333
			0.1790	8.5587	0.0108	66.3405	0.0837	8.3250	11.4469	82.6488
			0.4200	8.1064	0.0102	65.8481	0.0831	8.2266	10.3691	82.9818
			0.8890	7.7319	0.0098	65.4274	0.0826	8.7679	9.6328	83.2603
			1.7790	10.4489	0.0132	74.7139	0.0943	8.9899	9.8799	82.0387

Table C2. 04/26/96 Laser blank radial survey at 0.9054 pressure ratio

Date	Prat	Depth	Wake Position	U-Velocity	U-Non	V-Velocity	V-Non	U-Turbulence	V-Turbulence	Flow Angle
		(mm)	(degrees)	(m/s)	Dimensionalized	(m/s)	Dimensionalized	(%)	(%)	degrees
4/26/96	0.9054	0.01	8.0000	8.7570	0.0111	61.0770	0.0776	6.5409	11.9974	81.9703
			7.0000	8.9116	0.0113	61.7911	0.0785	6.7514	12.6270	81.9236
			6.0000	8.7271	0.0110	61.8813	0.0787	6.6094	12.4939	82.1000
			5.0000	8.7370	0.0110	61.7979	0.0786	6.4054	12.3947	82.0806
			4.0000	9.0774	0.0115	62.0636	0.0789	5.8996	12.6903	81.8110
			3.0000	8.8678	0.0112	62.3786	0.0793	5.7717	12.1044	82.0375
			2.0000	8.9612	0.0113	62.4936	0.0794	5.8697	12.6623	81.9693
			1.0000	8.9421	0.0113	62.4349	0.0794	6.3205	12.8076	81.9788
			0.0000	8.9111	0.0113	61.4553	0.0781	6.7566	12.5069	81.8805
			-1.0000	8.9763	0.0113	62.5559	0.0795	6.5990	13.1067	81.9639
			-2.0000	8.7992	0.0111	62.9436	0.0800	6.6703	12.7317	82.1683
			-3.0000	8.8903	0.0112	60.7911	0.0773	6.5965	11.9403	81.8119
			-4.0000	8.7644	0.0111	61.6588	0.0784	6.9645	12.3777	82.0384
			-5.0000	8.9914	0.0114	61.1861	0.0778	6.7237	11.5065	81.7728
			-6.0000	9.2114	0.0116	61.4081	0.0781	6.4447	13.3419	81.6043
			-7.0000	9.0160	0.0114	61.7278	0.0785	6.3016	13.9456	81.8220
			-8.0000	9.1600	0.0116	63.1058	0.0802	6.1572	14.4980	81.8721
		0.06	8.0000	9.2007	0.0116	61.8903	0.0787	6.7256	12.9828	81.6110
			7.0000	9.1781	0.0116	61.4019	0.0781	6.5109	13.0005	81.5657
			6.0000	9.1200	0.0115	62.0508	0.0789	6.8248	13.3862	81.7048
			5.0000	9.1354	0.0115	61.5695	0.0783	6.1339	12.9443	81.6269
			4.0000	8.8697	0.0112	61.2918	0.0779	6.0526	12.5114	81.8308
			3.0000	9.1518	0.0116	61.4036	0.0781	5.9164	12.5012	81.5898
			2.0000	8.9826	0.0113	61.2838	0.0779	5.8574	12.4938	81.7272
			1.0000	9.1263	0.0115	61.2486	0.0779	6.1394	12.9263	81.5920
			0.0000	8.9294	0.0113	61.2309	0.0778	6.3844	12.9888	81.7685
			-1.0000	9.3722	0.0118	61.2948	0.0779	6.8244	12.7725	81.3752
			-2.0000	9.0669	0.0115	60.6321	0.0771	6.8014	12.1949	81.5622
			-3.0000	9.1668	0.0116	61.4783	0.0782	6.6025	13.0070	81.5863
			-4.0000	9.0649	0.0115	61.1101	0.0777	6.5926	12.9230	81.6291

Date	Prat	Depth	Wake Position	U-Velocity	U-Non	V-Velocity	V-Non	U-Turbulence	V-Turbulence	Flow Angle
		(mm)	(degrees)	(m/s)	Dimensionalized	(m/s)	Dimensionalized	(%)	(%)	degrees
			-5.0000	9.2264	0.0117	59.3996	0.0755	6.9049	13.2696	81.2406
			-6.0000	9.1726	0.0116	60.3660	0.0767	6.5442	12.5975	81.4282
			-7.0000	9.4620	0.0120	60.3353	0.0767	6.5880	13.7378	81.1575
			-8.0000	9.4617	0.0120	60.3312	0.0767	5.7620	12.5894	81.1572
		0.18	8.0000	9.1225	0.0115	58.3371	0.0742	6.6463	10.8126	81.1590
			7.0000	9.6565	0.0122	58.9808	0.0750	6.6811	10.5627	80.7506
			6.0000	9.0252	0.0114	58.6529	0.0746	6.3091	10.8814	81.2982
			5.0000	9.2633	0.0117	58.7839	0.0747	6.4421	10.7820	81.0918
			4.0000	9.3896	0.0119	59.4559	0.0756	5.9659	10.4109	81.0727
			3.0000	9.3258	0.0118	59.3763	0.0755	5.6890	9.8853	81.1207
			2.0000	9.3122	0.0118	59.3969	0.0755	5.8731	10.6835	81.1365
			1.0000	9.3414	0.0118	60.3910	0.0768	6.2334	10.2768	81.2532
			0.0000	9.4195	0.0119	59.8481	0.0761	6.5733	9.7079	81.1025
			-1.0000	9.3607	0.0118	59.6495	0.0758	6.7631	10.0447	81.1282
			-2.0000	9.2666	0.0117	59.6625	0.0758	6.8001	10.1740	81.2179
			-3.0000	9.5436	0.0121	59.9614	0.0762	6.7823	10.7888	81.0040
			-4.0000	9.4871	0.0120	59.8467	0.0761	6.8254	10.8933	81.0395
			-5.0000	9.2245	0.0117	59.6104	0.0758	6.9121	11.4045	81.2496
			-6.0000	9.6519	0.0122	59.3545	0.0755	6.5618	10.9097	80.8121
			-7.0000	9.6546	0.0122	59.7283	0.0759	6.2292	11.0594	80.8662
			-8.0000	9.6308	0.0122	59.6301	0.0758	5.9114	10.0893	80.8735
		0.42	8.0000	9.6093	0.0121	58.6440	0.0745	6.9475	8.5302	80.7268
			7.0000	9.6198	0.0122	58.8849	0.0749	6.4806	8.3530	80.7542
			6.0000	9.7546	0.0123	59.0213	0.0750	6.5286	9.0157	80.6482
			5.0000	9.8126	0.0124	59.3508	0.0754	6.3175	8.7052	80.6448
			4.0000	9.6658	0.0122	59.6109	0.0758	5.8641	8.3807	80.8219
			3.0000	9.8621	0.0125	60.2217	0.0766	6.2545	9.2189	80.7321
			2.0000	10.0930	0.0128	59.7916	0.0760	6.2871	8.4031	80.4520
			1.0000	9.7961	0.0124	59.6883	0.0759	7.1465	8.6011	80.7122
			0.0000	9.5456	0.0121	59.6467	0.0758	7.0418	8.2379	80.9395
			-1.0000	9.4079	0.0119	59.4290	0.0755	7.0671	8.0504	81.0359

Date	Prat	Depth	Wake Position	U-Velocity	U-Non	V-Velocity	V-Non	U-Turbulence	V-Turbulence	Flow Angle
		(mm)	(degrees)	(m/s)	Dimensionalized	(m/s)	Dimensionalized	(%)	(%)	degrees
			-2.0000	9.8236	0.0124	58.6927	0.0746	7.3689	8.2178	80.5314
			-3.0000	9.6044	0.0121	58.4125	0.0743	6.8753	8.4234	80.6954
			-4.0000	9.8322	0.0124	58.3281	0.0741	6.6871	8.3061	80.4651
			-5.0000	9.8835	0.0125	58.5983	0.0745	6.5970	8.6453	80.4597
			-6.0000	9.8131	0.0124	58.8232	0.0748	6.5794	8.5165	80.5620
			-7.0000	10.0289	0.0127	58.4140	0.0743	6.3373	8.6078	80.2920
			-8.0000	9.9161	0.0125	59.0151	0.0750	6.4582	8.2266	80.4952
		0.8900	8.0000	9.9965	0.0126	60.0407	0.0763	6.5887	7.6467	80.5802
			7.0000	10.5149	0.0133	59.4985	0.0756	6.5281	7.6588	80.0127
			6.0000	10.5122	0.0133	59.8526	0.0761	6.4432	8.4151	80.0731
			5.0000	10.8461	0.0137	60.2165	0.0765	6.4400	8.2750	79.8250
			4.0000	10.6144	0.0134	60.4791	0.0769	5.9827	8.4440	80.0803
			3.0000	10.7056	0.0135	61.0712	0.0776	6.1018	8.2774	80.0919
			2.0000	10.3515	0.0131	61.1472	0.0777	6.3947	8.0605	80.4251
			1.0000	10.4739	0.0132	60.7170	0.0772	6.3898	8.1937	80.2467
			0.0000	10.3550	0.0131	60.1497	0.0765	7.0236	7.1155	80.2661
			-1.0000	10.0215	0.0127	60.0845	0.0764	6.8388	7.0750	80.5638
			-2.0000	9.9767	0.0126	60.1453	0.0765	7.1133	7.0830	80.6146
			-3.0000	10.2565	0.0130	60.0480	0.0763	6.9256	7.2871	80.3409
			-4.0000	10.2692	0.0130	59.8772	0.0761	6.9702	7.4479	80.3021
			-5.0000	10.3514	0.0131	59.7628	0.0760	6.6431	7.5250	80.2076
			-6.0000	10.6230	0.0134	59.7802	0.0760	6.6676	8.1968	79.9587
			-7.0000	10.3550	0.0131	60.1413	0.0765	6.7896	8.2124	80.2648
			-8.0000	10.2497	0.0129	59.9124	0.0762	6.7121	7.7260	80.3258
		1.7800	8.0000	10.5075	0.0133	61.5419	0.0782	3.7752	6.5907	80.3447
			7.0000	10.7380	0.0136	61.3728	0.0780	3.6736	6.9605	80.1103
			6.0000	11.0958	0.0140	61.3041	0.0779	3.4421	6.9224	79.7764
			5.0000	10.9327	0.0138	62.2611	0.0791	3.6119	7.2509	80.0754
			4.0000	10.8737	0.0137	61.8806	0.0787	3.5696	7.5447	80.0684
			3.0000	11.1308	0.0141	62.5371	0.0795	3.5140	7.5943	79.9429
			2.0000	11.1401	0.0141	62.4859	0.0794	3.6464	7.2865	79.9266

Date	Prat	Depth	Wake Position	U-Velocity	U-Non	V-Velocity	V-Non	U-Turbulence	V-Turbulence	Flow Angle
		(mm)	(degrees)	(m/s)	Dimensionalized	(m/s)	Dimensionalized	(%)	(%)	degrees
			1.0000	11.0462	0.0140	62.4443	0.0794	3.7845	7.2656	80.0033
			0.0000	11.0897	0.0140	62.3987	0.0793	3.7912	6.3280	79.9575
			-1.0000	10.4026	0.0131	62.2212	0.0791	3.8873	6.3911	80.5418
			-2.0000	10.7487	0.0136	62.1578	0.0790	3.6834	6.2852	80.2233
			-3.0000	10.8329	0.0137	62.1273	0.0790	3.6855	6.4667	80.1434
			-4.0000	11.0899	0.0140	61.4829	0.0782	3.6068	6.6467	79.8108
			-5.0000	10.6160	0.0134	61.9295	0.0787	3.6791	7.4993	80.3068
			-6.0000	10.8497	0.0137	61.4407	0.0781	3.4613	7.0579	80.0203
			-7.0000	10.6387	0.0134	61.8889	0.0787	3.6087	7.5119	80.2802
			-8.0000	10.4167	0.0132	61.7202	0.0785	3.8202	7.5143	80.4537

Table C3. 04/26/96 Laser blank circumferential survey at 0.9054 pressure ratio

Date	Prat	Wake Position	Depth	U-Velocity	U-Non	V-Velocity	V-Non	U-Turbulence	V-Turbulence	Flow Angle
		(degrees)	(mm)	(m/s)	Dimensionalized	(m/s)	Dimensionalized	(%)	(%)	degrees
4/19/92	0.9620	-8	0.0090	5.7456	0.0073	61.1444	0.0781	9.5115	12.2320	84.6701
			0.0590	5.2821	0.0067	60.9264	0.0778	9.2503	11.1208	85.0804
			0.1790	4.4444	0.0056	59.8129	0.0764	9.9199	9.5370	85.7808
			0.4200	0.8329	0.0011	59.9625	0.0766	10.1712	8.0492	89.2099
			0.8890	3.2516	0.0041	60.8124	0.0777	14.3875	8.4654	86.9612
			1.7790	12.7285	0.0161	61.3428	0.0783	7.0233	7.6633	78.3593
		0	0.0090	3.7604	0.0048	60.2522	0.0769	8.0066	11.3192	86.4543
			0.0590	3.7736	0.0048	59.9021	0.0765	7.6785	10.3852	86.4211
			0.1790	3.2045	0.0041	59.3887	0.0758	7.3043	8.6216	86.9335
			0.4200	1.7476	0.0022	59.4696	0.0759	6.2254	7.8045	88.3288
			0.8890	5.2735	0.0067	60.7388	0.0776	12.1140	7.2078	85.0733
			1.7790	11.8807	0.0151	61.7119	0.0788	7.2294	6.7558	79.1791
		7	0.0090	5.6170	0.0071	59.7457	0.0761	8.7389	11.1699	84.6530
			0.0590	5.3221	0.0067	59.8740	0.0762	8.9340	10.6864	84.9430
			0.1790	4.4359	0.0056	59.3469	0.0756	9.4625	9.8103	85.7444
			0.4200	1.7372	0.0022	59.3350	0.0756	9.3038	7.9928	88.3305
			0.8890	1.9976	0.0025	60.1984	0.0767	13.0173	7.8159	88.1079
			1.7790	12.4215	0.0157	61.1662	0.0779	7.3607	6.7633	78.5706

Table C4. 04/19/96 Laser blank radial survey at 0.9620 pressure ratio

Date	Prat	LDV Window	Depth	U-Velocity	U-Non	V-Velocity	V-Non	U-Turbulence	V-Turbulence	Flow Angle
			(mm)	(m/s)	Dimensionalized	(m/s)	Dimensionalized	(%)	(%)	degrees
4/30/96	0.0962	Laser Blank								
			1.78	2.9374	0.0037	59.2896	0.0753	8.0094	7.2784	87.1837
		Pressurized Window								
		Chamber Pressure (mm water)								
		0	1.78	10.5493	0.0134	61.4338	0.0780	5.9229	5.9988	80.2563
			1.78	10.7358	0.0136	61.7900	0.0785	6.2899	6.3154	80.1435
			1.78	10.5558	0.0134	61.7046	0.0784	5.8820	6.0196	80.2924
		76.2	1.78	10.9306	0.0139	61.4216	0.0780	6.1382	6.0059	79.9093
			1.78	11.1289	0.0141	61.3917	0.0780	6.1905		79.7252
		152.4	1.78	11.0337	0.0140	61.0734	0.0776	6.3454	6.4562	79.7592
			1.78	10.6817	0.0136	61.0624	0.0776	6.2015	6.5576	80.0776
			1.78	10.8223	0.0137	61.0932	0.0776	6.2952	6.4242	79.9546

Table C5. 04/30/96 Laser blank and pressurized window comparison at 0.9620 pressure ratio

Date	Prat	Chamber Pressure	Depth	U-Velocity	U-Non	V-Velocity	V-Non	U-Turbulence	V-Turbulence	Flow Angle
		(mm water)	(mm)	(m/s)	Dimensionalized	(m/s)	Dimensionalized	(%)	(%)	degrees
5/14/96	0.9620	0.0	0.01	11.3153	0.0144	61.4396	0.0782	5.7016	6.1415	79.5648
			0.06	11.1038	0.0141	61.5593	0.0784	5.3944	6.0199	79.7752
			0.18	11.2528	0.0143	61.5071	0.0783	5.5404	6.2028	79.6323
			0.42	11.4629	0.0146	61.8782	0.0788	5.1256	6.0154	79.5050
			0.89	11.6201	0.0148	62.6365	0.0798	5.2979	5.5779	79.4902
		76.2	0.01	11.2395	0.0143	60.9537	0.0776	5.5153	6.1021	79.5524
			0.06	11.2783	0.0144	61.0378	0.0777	5.4226	6.2064	79.5312
			0.18	11.1969	0.0143	61.2629	0.0780	5.4023	6.0874	79.6425
			0.42	11.3190	0.0144	61.4613	0.0783	5.8823	5.8672	79.5651
			0.89	11.4433	0.0146	62.0443	0.0790	5.3822	5.4518	79.5499
		152.4	0.01	11.2041	0.0143	60.6618	0.0773	5.7209	6.1861	79.5355
			0.06	11.1788	0.0142	60.8026	0.0774	5.7005	5.9003	79.5823
			0.18	11.1890	0.0142	60.7868	0.0774	5.6005	6.0612	79.5703
			0.42	11.2060	0.0143	60.8454	0.0775	5.4155	5.8966	79.5647
			0.89	11.5008	0.0146	61.9084	0.0788	5.3217	5.7021	79.4761

Table C6. 05/14/96 Pressurized window radial survey at 0.9620 pressure ratio

Date	Prat	Depth	Wake Position	U-Velocity	U-Non	V-Velocity	V-Non	U-Turbulence	V-Turbulence	Flow Angle
		(mm)	(degrees)	(m/s)	Dimensionalized	(m/s)	Dimensionalized	(%)	(%)	degrees
5/10/96	0.9620	0.01	8.0000	11.0861	0.0142	60.5957	0.0781	6.7788	6.3624	79.6756
			7.0000	11.0617	0.0142	60.2982	0.0781	6.2881	6.4858	79.6951
			6.0000	10.8376	0.0139	60.3806	0.0778	6.3130	6.7593	79.8574
			5.0000	11.1738	0.0143	60.8723	0.0779	6.0381	6.8219	79.5699
			4.0000	11.1802	0.0144	61.0850	0.0776	5.9255	7.2357	79.5155
			3.0000	11.6389	0.0149	61.5732	0.0778	6.0512	7.4339	79.1231
			2.0000	11.1058	0.0143	61.3176	0.0776	6.4217	7.3818	79.5825
			1.0000	10.8577	0.0139	61.5985	0.0781	6.7730	6.9236	79.8743
			0.0000	10.5965	0.0136	61.3842	0.0785	7.0034	6.5053	80.1707
			-1.0000	10.7282	0.0138	61.0189	0.0788	6.9105	6.2937	80.0849
			-2.0000	10.8710	0.0140	60.6274	0.0784	6.4827	6.1376	79.9105
			-3.0000	10.9138	0.0140	60.7931	0.0788	6.8093	6.4816	79.9128
			-4.0000	10.7318	0.0138	60.6350	0.0781	6.2998	6.4638	79.9999
			-5.0000	11.1605	0.0143	60.9237	0.0779	6.6291	6.9364	79.5735
			-6.0000	11.3366	0.0146	60.8027	0.0772	6.6302	7.1385	79.3284
			-7.0000	10.9661	0.0141	61.0615	0.0771	6.1756	7.7685	79.6557
			-8.0000	11.0737	0.0142	61.0783	0.0775	6.0276	7.8965	79.6066
		0.06	8.0000	10.6049	0.0136	60.6716	0.0780	6.7477	6.2782	80.0954
			7.0000	10.8258	0.0139	61.0110	0.0777	6.5411	6.0737	79.8620
			6.0000	11.0348	0.0142	60.5802	0.0777	6.2427	6.7982	79.6688
			5.0000	11.2538	0.0144	60.4480	0.0776	6.2123	6.9744	79.4498
			4.0000	11.3640	0.0146	60.9431	0.0775	6.1308	7.3983	79.3402
			3.0000	11.4905	0.0148	61.4391	0.0779	6.2727	7.0536	79.2714
			2.0000	11.2120	0.0144	61.2874	0.0781	6.2841	7.3942	79.5552
			1.0000	10.8348	0.0139	61.3993	0.0783	6.7771	6.4902	79.9281
			0.0000	10.7220	0.0138	61.3756	0.0785	6.8299	6.3781	80.0552
			-1.0000	10.8578	0.0139	61.2227	0.0785	6.6362	6.2870	79.9356
			-2.0000	10.4609	0.0134	61.0440	0.0784	7.3379	6.7577	80.2790
			-3.0000	10.8944	0.0140	60.8677	0.0786	6.7118	6.3131	79.9088
			-4.0000	10.2737	0.0132	60.5953	0.0780	7.8991	6.3998	80.3968

Date	Prat	Depth	Wake Position	U-Velocity	U-Non	V-Velocity	V-Non	U-Turbulence	V-Turbulence	Flow Angle
		(mm)	(degrees)	(m/s)	Dimensionalized	(m/s)	Dimensionalized	(%)	(%)	degrees
			-5.0000	10.1044	0.0130	60.6457	0.0773	7.6505	6.7548	80.4762
			-6.0000	10.8841	0.0140	60.7547	0.0775	6.8597	7.3858	79.7782
			-7.0000	10.8120	0.0139	60.7642	0.0780	6.5578	7.6616	79.9147
			-8.0000	11.1036	0.0143	60.9563	0.0776	6.4700	7.6099	79.5919
		0.18	8.0000	11.1550	0.0143	60.9096	0.0783	6.6639	6.2432	79.6373
			7.0000	10.4836	0.0135	60.8135	0.0782	7.4879	6.0941	80.2337
			6.0000	10.7189	0.0138	60.6506	0.0782	7.3565	6.2274	80.0229
			5.0000	11.4711	0.0147	60.8506	0.0784	6.2985	6.7699	79.3577
			4.0000	11.4936	0.0148	60.6999	0.0782	6.0864	6.8460	79.3072
			3.0000	11.5860	0.0149	61.5427	0.0782	6.0431	6.8308	79.2290
			2.0000	11.5742	0.0149	61.7487	0.0780	6.3205	6.7067	79.2196
			1.0000	11.1058	0.0143	61.4916	0.0786	6.8451	6.7057	79.7129
			0.0000	11.0723	0.0142	61.5494	0.0787	6.4086	5.9227	79.7655
			-1.0000	10.8194	0.0139	61.4134	0.0787	6.6536	5.9922	79.9852
			-2.0000	11.0569	0.0142	61.0091	0.0790	6.3994	5.9264	79.8117
			-3.0000	10.2833	0.0132	61.1258	0.0787	7.6460	6.1764	80.4799
			-4.0000	10.8825	0.0140	61.0929	0.0777	6.3354	6.3096	79.7994
			-5.0000	10.8749	0.0140	61.2694	0.0778	6.6958	6.8377	79.8311
			-6.0000	10.7556	0.0138	61.1553	0.0776	6.8500	6.9766	79.9079
			-7.0000	10.9347	0.0140	61.1300	0.0778	6.1544	7.3216	79.7702
			-8.0000	10.9434	0.0141	61.2254	0.0779	6.4989	7.5780	79.7781
		0.42	8.0000	10.8198	0.0139	60.8680	0.0782	6.3564	5.9064	79.9323
			7.0000	11.0187	0.0141	60.8881	0.0782	6.5599	6.1607	79.7423
			6.0000	11.1054	0.0143	60.9793	0.0783	6.1107	6.2789	79.6854
			5.0000	11.3813	0.0146	61.4073	0.0784	6.1293	6.5042	79.4451
			4.0000	11.6059	0.0149	61.4833	0.0784	6.0045	6.6340	79.2347
			3.0000	11.7501	0.0151	61.5629	0.0785	5.9691	6.8528	79.1265
			2.0000	11.8026	0.0152	61.7421	0.0788	5.7982	6.7589	79.1191
			1.0000	11.5990	0.0149	62.0785	0.0792	6.2782	6.2087	79.3445
			0.0000	11.5013	0.0148	62.1005	0.0794	6.0864	5.8889	79.4699
			-1.0000	11.4812	0.0147	61.8740	0.0794	6.3339	5.8225	79.4843

Date	Prat	Depth	Wake Position	U-Velocity	U-Non	V-Velocity	V-Non	U-Turbulence	V-Turbulence	Flow Angle
		(mm)	(degrees)	(m/s)	Dimensionalized	(m/s)	Dimensionalized	(%)	(%)	degrees
			-2.0000	11.2359	0.0144	61.6250	0.0790	6.2023	5.9311	79.6492
			-3.0000	11.2614	0.0145	61.3933	0.0788	6.2638	6.0684	79.5967
			-4.0000	10.7825	0.0138	61.2641	0.0787	6.7192	6.2615	80.0174
			-5.0000	11.0639	0.0142	61.3047	0.0786	6.1684	6.6100	79.7499
			-6.0000	10.9187	0.0140	61.2438	0.0780	6.2538	6.6426	79.8121
			-7.0000	10.5358	0.0135	61.1104	0.0779	6.3814	7.2848	80.1478
			-8.0000	10.6614	0.0137	61.1637	0.0779	6.1093	7.0585	80.0295
		0.8900	8.0000	10.0277	0.0129	62.0759	0.0794	5.7614	5.1875	80.7935
			7.0000	10.6607	0.0137	62.0445	0.0794	5.7103	5.4611	80.2189
			6.0000	10.6607	0.0137	62.0245	0.0792	5.3766	6.0886	80.1896
			5.0000	10.8725	0.0140	62.0361	0.0798	5.2425	5.8680	80.0732
			4.0000	11.2029	0.0144	62.2824	0.0797	5.5270	5.9209	79.7747
			3.0000	11.4020	0.0146	62.6499	0.0794	5.4977	6.1510	79.5471
			2.0000	11.3183	0.0145	62.6955	0.0794	5.4092	5.76476	79.6292
			1.0000	11.2296	0.0144	62.7916	0.0800	5.3590	5.55178	79.7830
			0.0000	11.1532	0.0143	62.7952	0.0803	5.4640	5.21952	79.8925
			-1.0000	10.9629	0.0141	62.5333	0.0803	5.3997	5.21232	80.0610
			-2.0000	10.9209	0.0140	62.0724	0.0802	5.2171	5.44242	80.0834
			-3.0000	10.8128	0.0139	62.0292	0.0801	5.9833	5.64056	80.1726
			-4.0000	10.7911	0.0139	62.3329	0.0797	5.8139	5.52799	80.1352
			-5.0000	10.5377	0.0135	62.3519	0.0794	6.0813	6.1604	80.3249
			-6.0000	10.2973	0.0132	61.8777	0.0793	5.9863	6.32056	80.5399
			-7.0000	10.4477	0.0134	62.0669	0.0794	5.4399	6.73985	80.4073
			-8.0000	10.8125	0.0139	62.0948	0.0794	5.4240	6.87407	80.0838

Table C7. 05/10/96 Pressurized window circumferential survey at 76.2 mm water chamber pressure and 0.9620 pressure ratio

APPENDIX D. 3 HOLE COBRA PROBE DATA

Date	Tare	Cal	Pt1,1	Pt1,2	p1	p23	Pt2	p2	Patmos	Pt2/p2	Mach	X	Beta
8/7/96	-0.086	67.933	3.804	3.746	3.454	0.303	3.708	0.084	29.920	1.009	0.113	0.050	0.008
	-0.067	67.603	7.640	7.600	6.897	0.335	7.643	-0.007	29.920	1.019	0.163	0.073	0.016
	-0.078	67.899	11.496	11.532	10.048	0.562	11.604	-0.036	29.920	1.029	0.201	0.090	0.023
	-0.075	67.915	15.539	15.474	13.626	0.769	15.659	-0.074	29.920	1.039	0.234	0.104	0.031
	-0.085	67.915	19.541	19.522	17.195	1.170	19.499	-0.072	29.920	1.048	0.260	0.116	0.038
	-0.073	67.919	24.205	24.055	20.972	1.355	24.208	-0.168	29.920	1.060	0.290	0.129	0.046
	-0.097	67.901	27.631	27.559	24.177	1.539	27.914	-0.240	29.920	1.069	0.311	0.138	0.053
	-0.112	67.639	28.200	28.160	24.648	1.343	27.655	-0.310	29.920	1.069	0.310	0.137	0.054
	-0.080	67.895	27.720	27.618	24.136	1.254	27.007	-0.386	29.920	1.067	0.307	0.136	0.053
	-0.113	67.924	23.534	23.476	20.440	1.071	23.893	-0.266	29.920	1.059	0.289	0.128	0.045
	-0.100	67.903	19.473	19.394	17.050	0.924	19.138	-0.181	29.920	1.048	0.259	0.115	0.038
	-0.084	67.885	15.712	15.568	13.623	0.709	15.383	-0.122	29.910	1.038	0.232	0.103	0.031
	-0.034	67.827	11.540	11.480	10.387	0.563	11.856	-0.094	29.910	1.029	0.204	0.091	0.024
	0.035	67.809	7.852	7.781	6.934	0.321	7.889	-0.056	29.910	1.020	0.167	0.074	0.016
	0.157	67.661	3.723	3.737	3.281	0.015	3.815	-0.032	29.910	1.009	0.116	0.052	0.008

Table D1. 3-Hole cobra probe calibration data

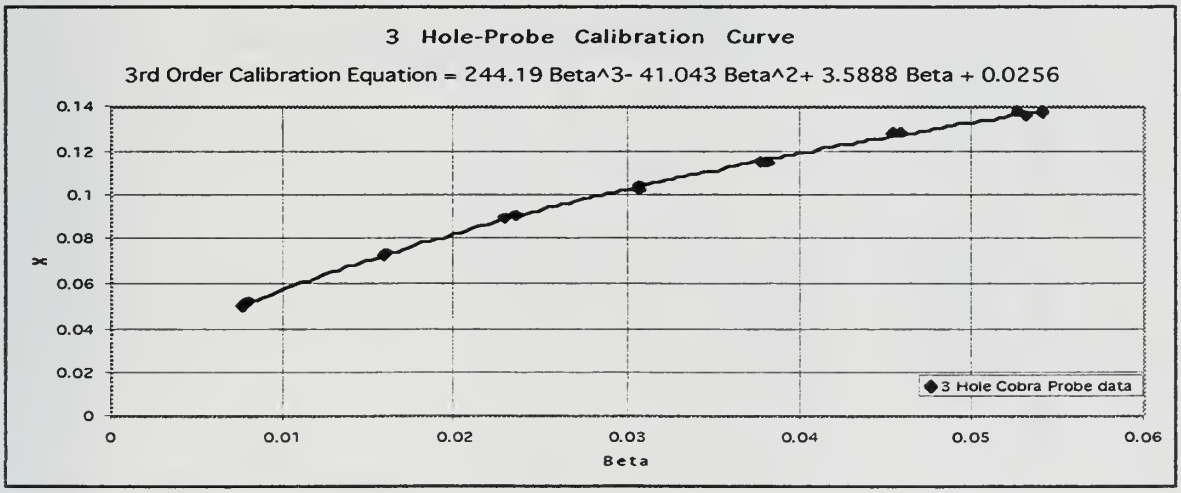

Figure D1. 3-Hole cobra probe calibration curve

Date	Tare	Cal	Pt1,1	Pt1,2	p1	p23	Pt2	p2	Flow Angle	Patmos	Pt2/p2	Beta	Y (mm)	X
8/12/96	0.047	67.483	15.839	15.781	9.622	2.583	-0.006	0.058	92.000	29.830	1.000	0.017	0.420	0.076
	0.046	67.434	15.709	15.244	12.154	3.119	-0.007	0.061	90.000	29.830	1.000	0.022	0.890	0.087
	0.047	67.398	15.632	15.281	12.827	3.312	-0.119	0.055	90.000	29.830	1.000	0.023	1.780	0.089
	0.023	67.469	15.712	15.556	12.847	3.297	-0.212	0.049	91.000	29.830	0.999	0.023	1.780	0.089
	-0.007	67.493	15.713	15.352	12.499	3.142	-0.213	0.043	91.000	29.830	0.999	0.022	0.890	0.088
	-0.019	67.531	15.638	15.252	9.904	2.547	-0.007	0.062	94.600	29.830	1.000	0.018	0.420	0.078
	-0.030	67.450	15.505	15.249	10.106	2.601	-0.137	0.056	92.000	29.825	1.000	0.018	0.420	0.079
	-0.062	67.532	15.671	15.315	12.534	3.168	-0.052	0.053	90.000	29.825	1.000	0.022	0.890	0.088
	-0.074	67.535	15.732	15.435	13.195	3.343	-0.208	0.047	90.000	29.820	0.999	0.024	1.780	0.091

Table D2. A radial survey utilizing the 3-hole cobra probe at a Prat of 0.9620

APPENDIX E. PRESSURIZED WINDOW DRAWINGS

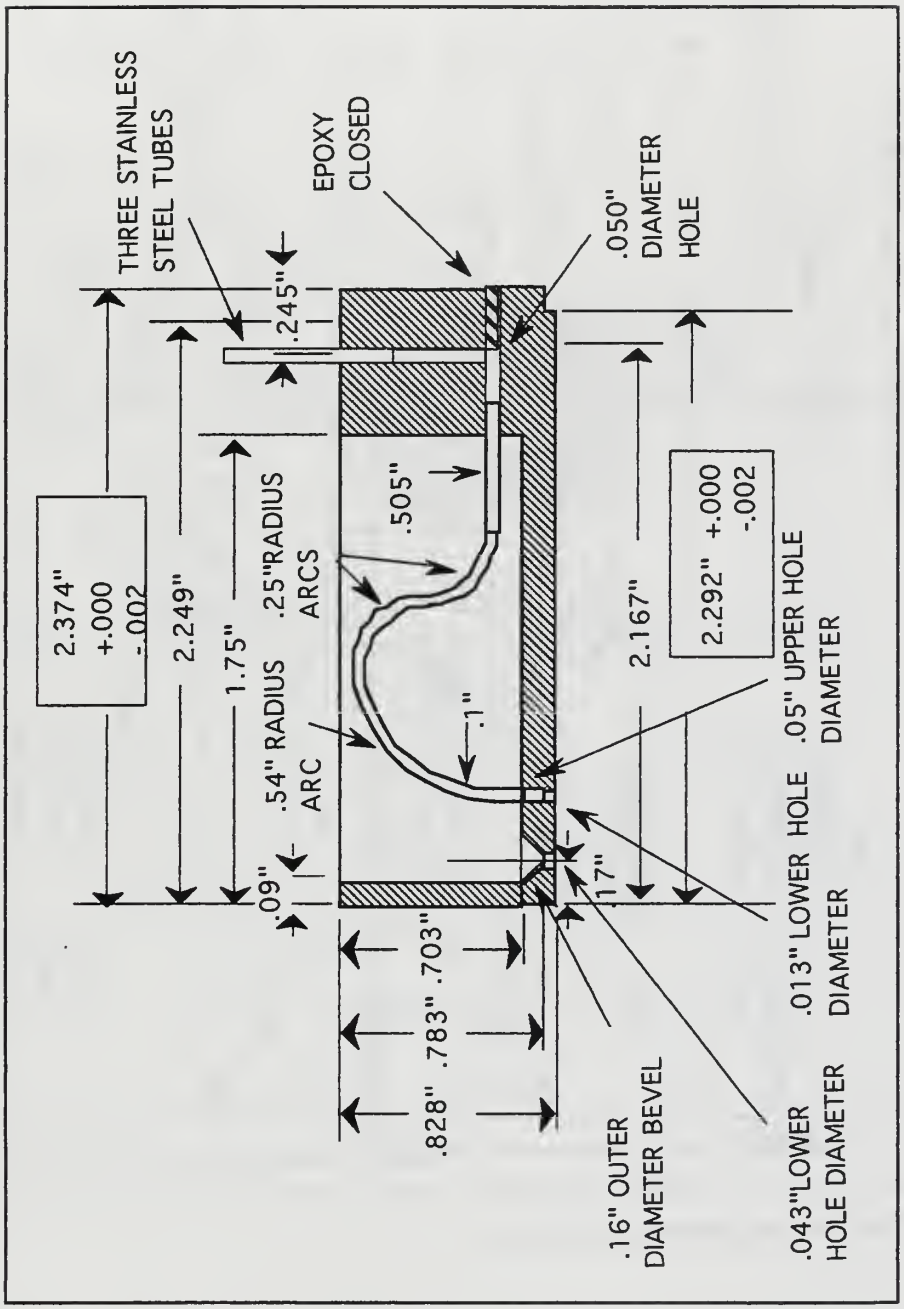

Figure E1. Side view of pressurized window

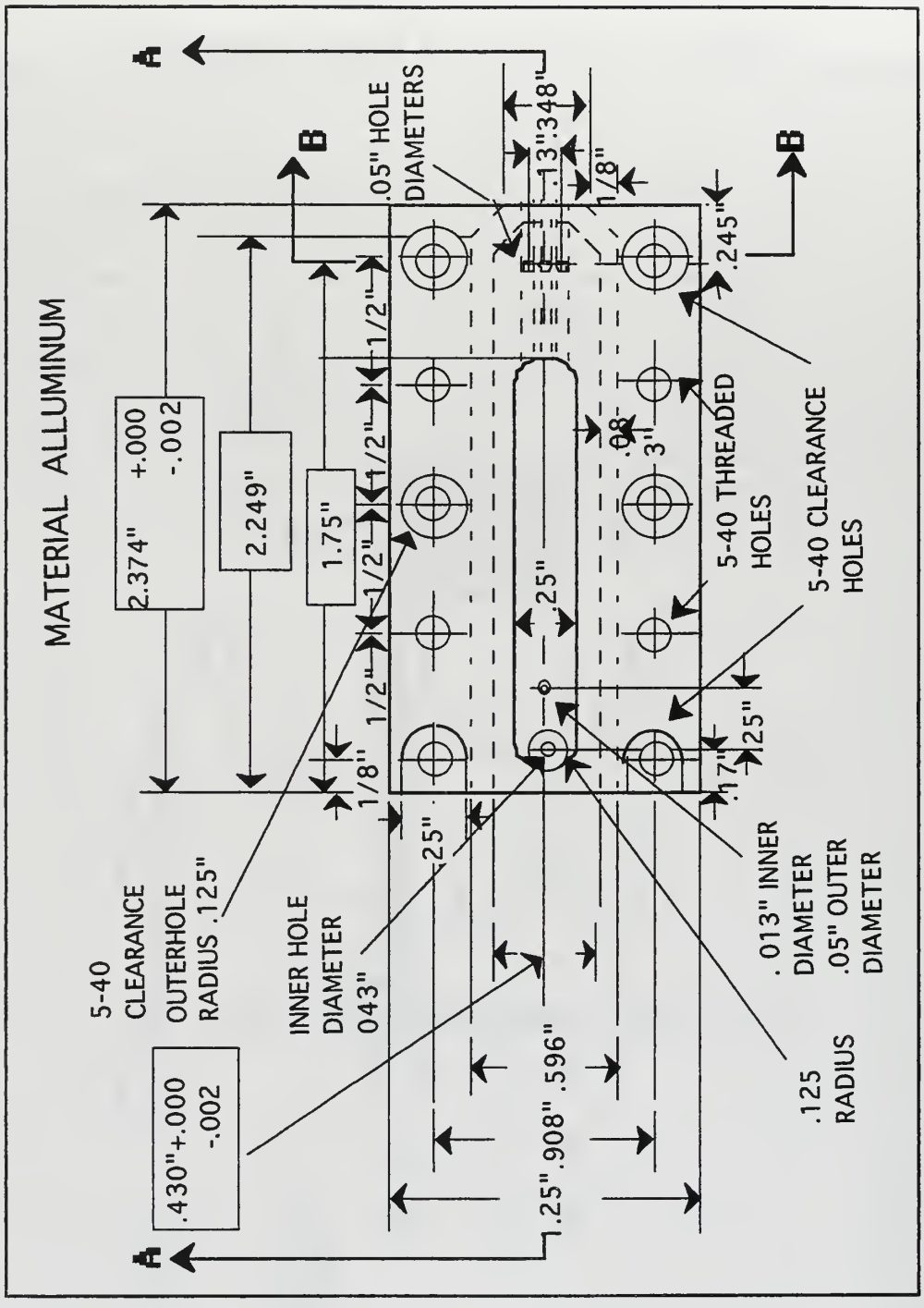

Figure E2. Top view of pressurized window

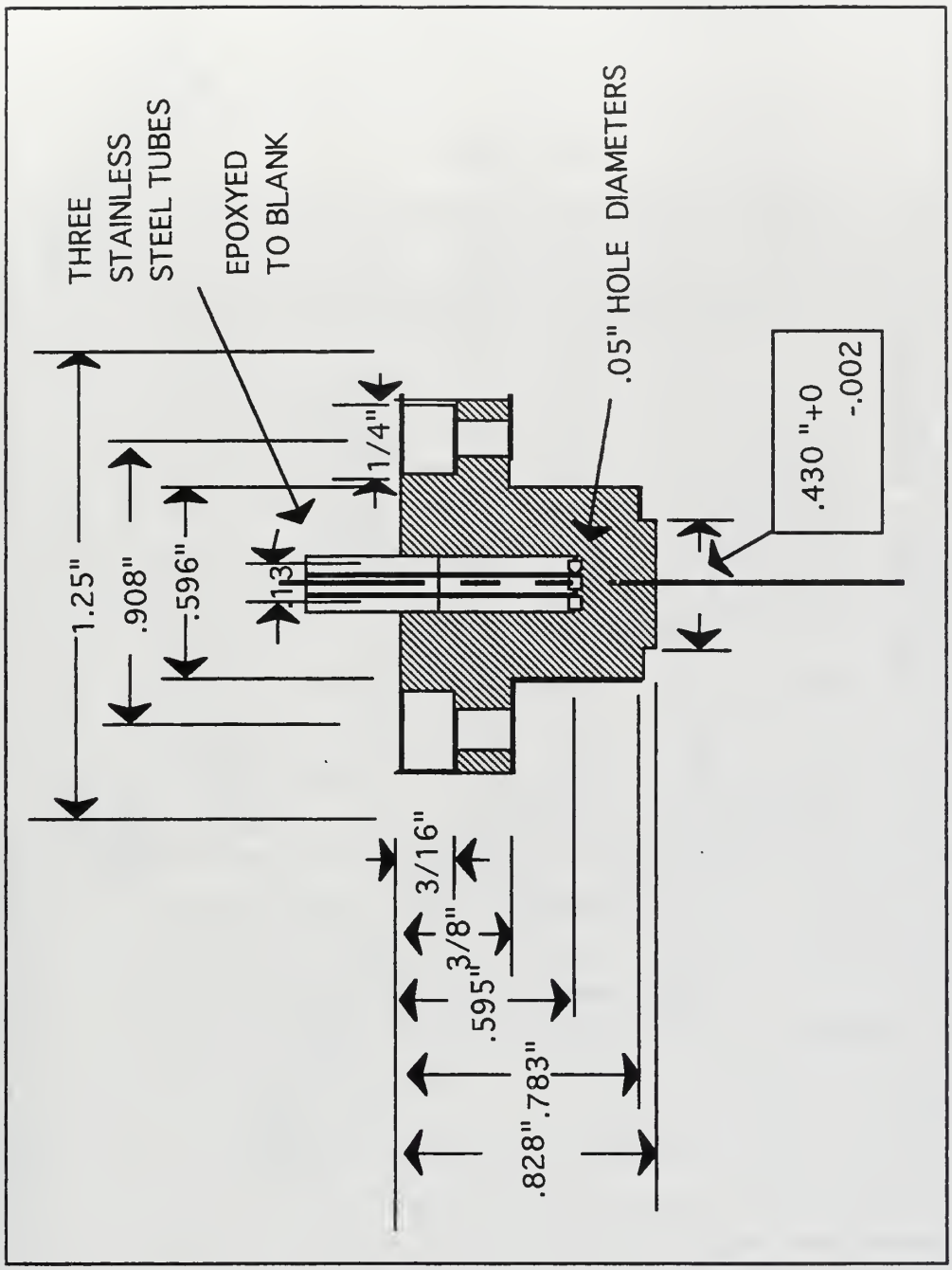

Figure E3. Front view of pressurized window

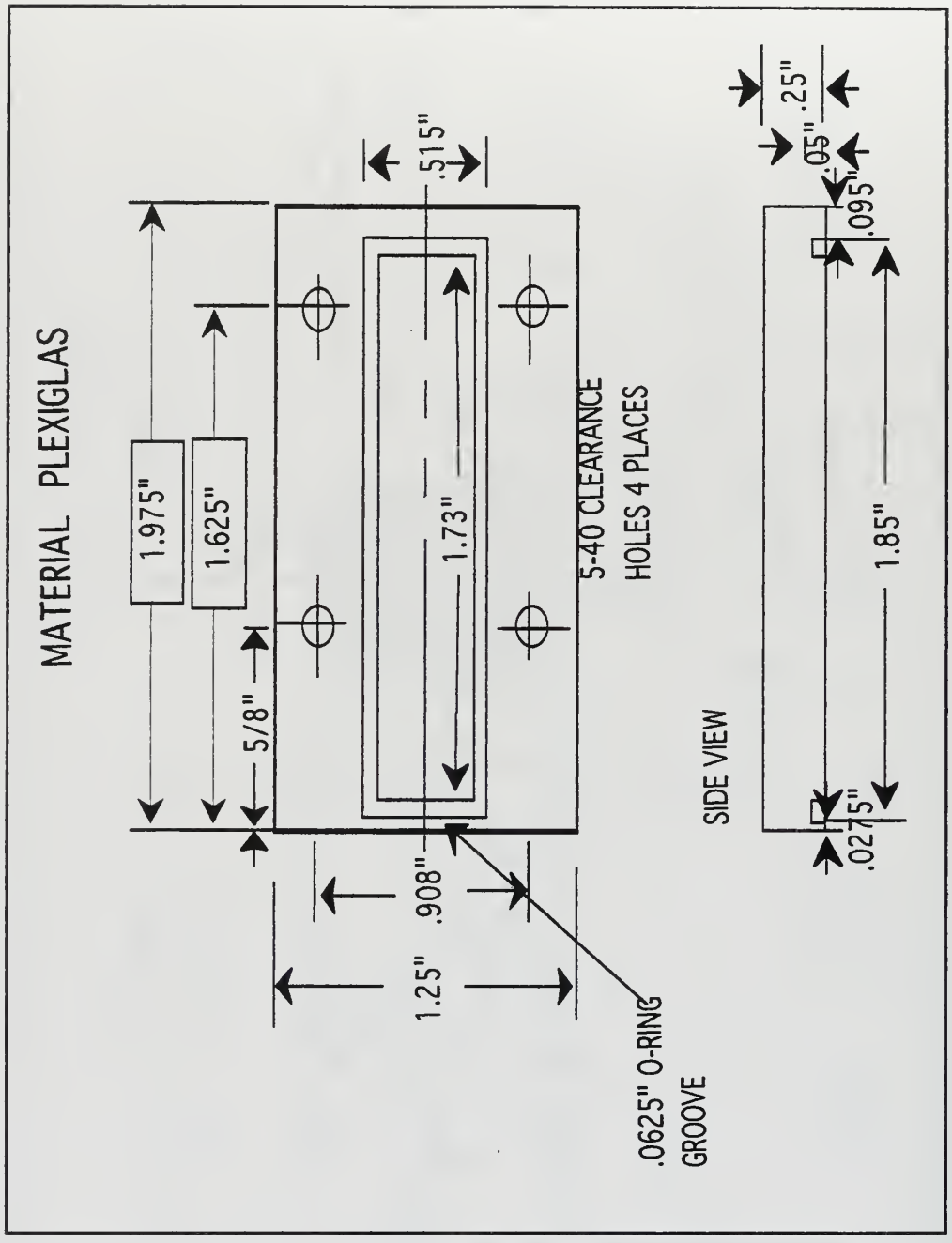

Figure E4. Plexiglas window cover

APPENDIX F. FREEJET

Date	Prat	Temp (F)	X	Height	U-Velocity	V-Velocity	UV-Mag. Mean	U-Turb.Intensity	V-Turb.Intensity	Flow Angle
			(mm)	(mm)	(m/s)	(m/s)	(m/s)	(%)	(%)	(degrees)
3/8/96	0.9900	110	-20.00	-50.00	25.878	26.256	36.865	3.026	3.237	36.865
			-20.00	-40.00	25.903	25.994	36.697	2.469	2.671	36.697
			-20.00	-30.00	25.908	25.713	36.502	2.365	2.457	36.502
			-20.00	-20.00	26.054	25.847	36.700	2.615	3.070	36.700
			-20.00	-10.00	26.041	26.156	36.909	2.534	2.900	36.909
			-20.00	0.00	26.016	26.036	36.806	2.439	2.794	36.806
			-20.00	10.00	26.010	26.113	36.857	2.696	2.877	36.857
			-20.00	20.00	26.079	26.142	36.925	2.377	2.485	36.925
			-20.00	30.00	26.080	26.252	37.004	2.515	2.812	37.004
			-20.00	40.00	26.116	26.173	36.974	2.285	2.527	36.974
			-20.00	50.00	26.038	26.224	36.954	2.442	2.468	36.954
	0.9615	112	-20.00	-50.00	56.127	57.501	80.353	1.771	3.367	45.693
			-20.00	-40.00	56.426	57.120	80.290	1.753	3.666	45.350
			-20.00	-30.00	56.925	56.971	80.536	2.016	3.433	45.023
			-20.00	-20.00	57.266	56.839	80.685	1.984	4.788	44.786
			-20.00	-10.00	57.291	57.064	80.862	2.114	6.188	44.886
			-20.00	0.00	56.547	58.077	81.059	1.780	2.501	45.765
3/14/96	0.9900	105	-20.00	-50.00	27.523	28.189	39.397	2.232	2.474	45.416
			-20.00	-40.00	27.716	28.187	39.530	2.106	2.363	45.100
			-20.00	-30.00	27.822	28.403	39.759	2.293	2.249	44.784
			-20.00	-20.00	27.874	28.136	39.605	2.816	2.900	44.771
			-20.00	-10.00	27.866	28.039	39.531	2.218	2.694	45.126
			-20.00	0.00	27.886	28.095	39.585	2.572	2.794	45.022
			-20.00	10.00	27.855	28.277	39.692	2.625	2.768	45.113
			-20.00	20.00	27.926	28.157	39.657	2.403	2.742	45.069

Date	Prat	Temp (F)	X	Height	U-Velocity	V-Velocity	UV-Mag. Mean	U-Turb.Intensity	V-Turb.Intensity	Flow Angle
			(mm)	(mm)	(m/s)	(m/s)	(m/s)	(%)	(%)	(degrees)
			-20.00	30.00	28.038	28.103	39.698	2.560	2.836	45.188
			-20.00	40.00	27.957	27.863	39.471	3.568	3.894	45.063
			-20.00	50.00	27.394	27.091	38.528	4.739	5.366	45.204
	0.9615	112	-20.00	-30.00	60.079	61.490	85.968	2.058	1.994	45.665
			-20.00	-20.00	60.445	61.340	86.118	1.879	2.116	45.421
			-20.00	-10.00	60.878	61.377	86.448	1.648	1.859	45.234
			-20.00	0.00	61.056	61.222	86.463	1.628	1.628	45.078
			-20.00	10.00	61.543	61.222	86.808	1.456	1.740	44.850
			-20.00	20.00	61.295	61.610	86.907	1.561	1.937	45.147

Table F1. Freejet data

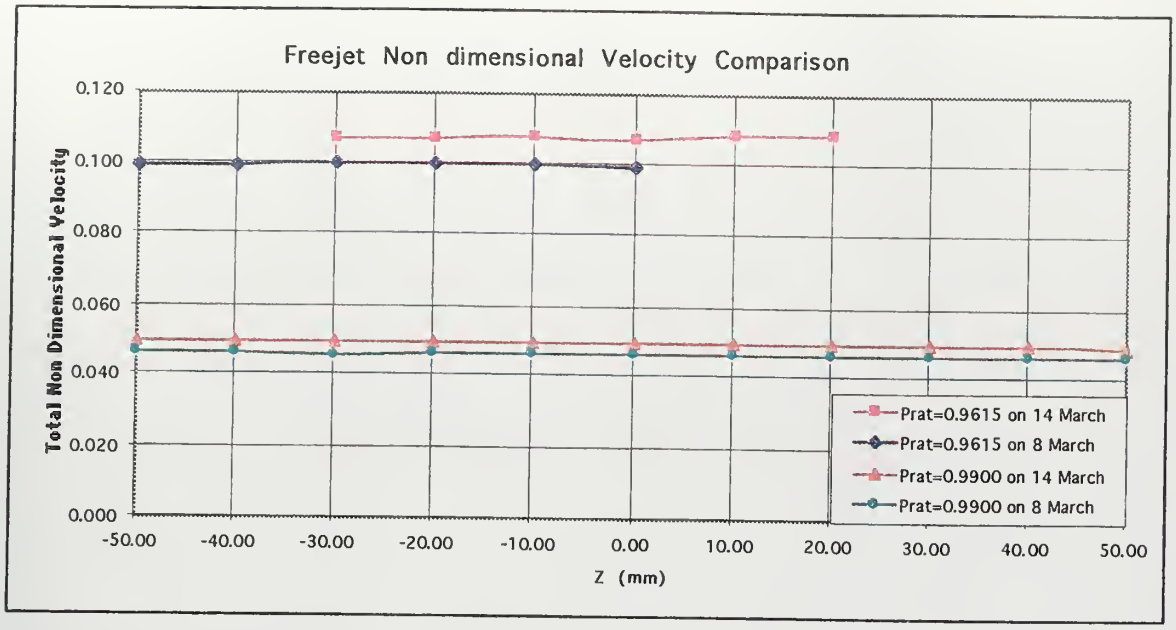

Figure F1. Freejet Survey

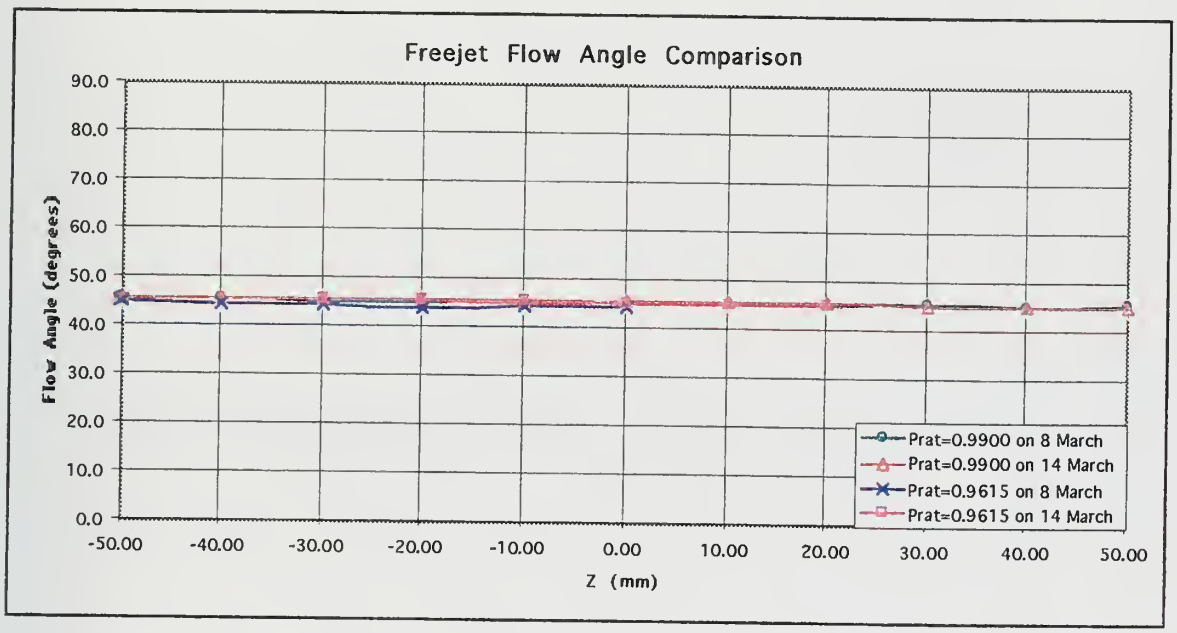

Figure F2. Freejet Survey

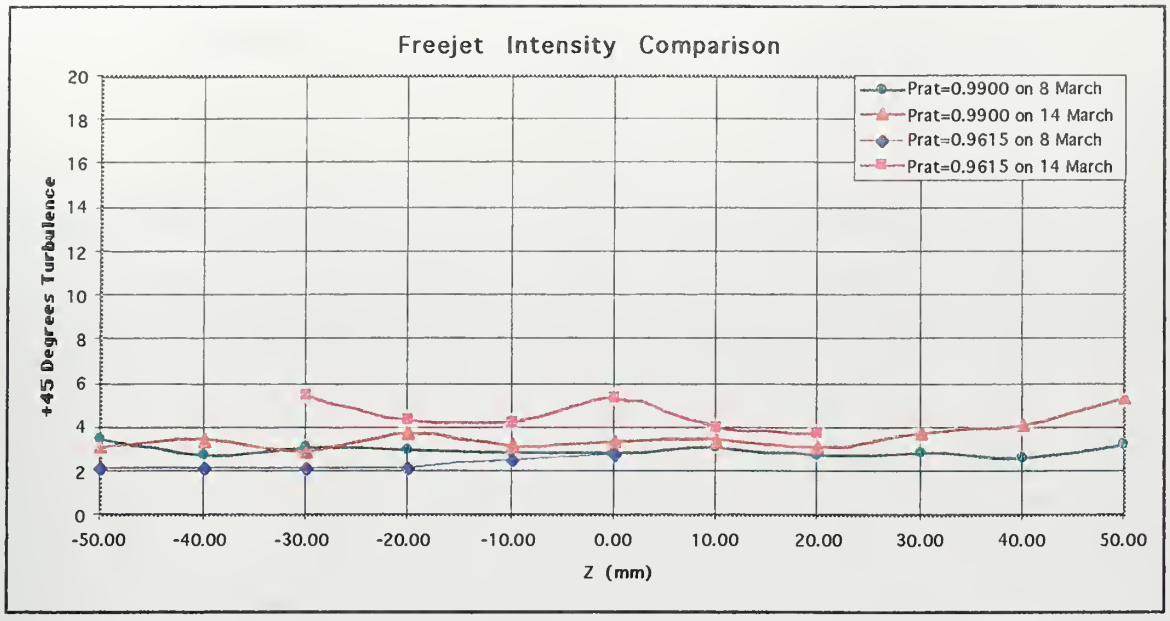

Figure F3a. Freejet Survey

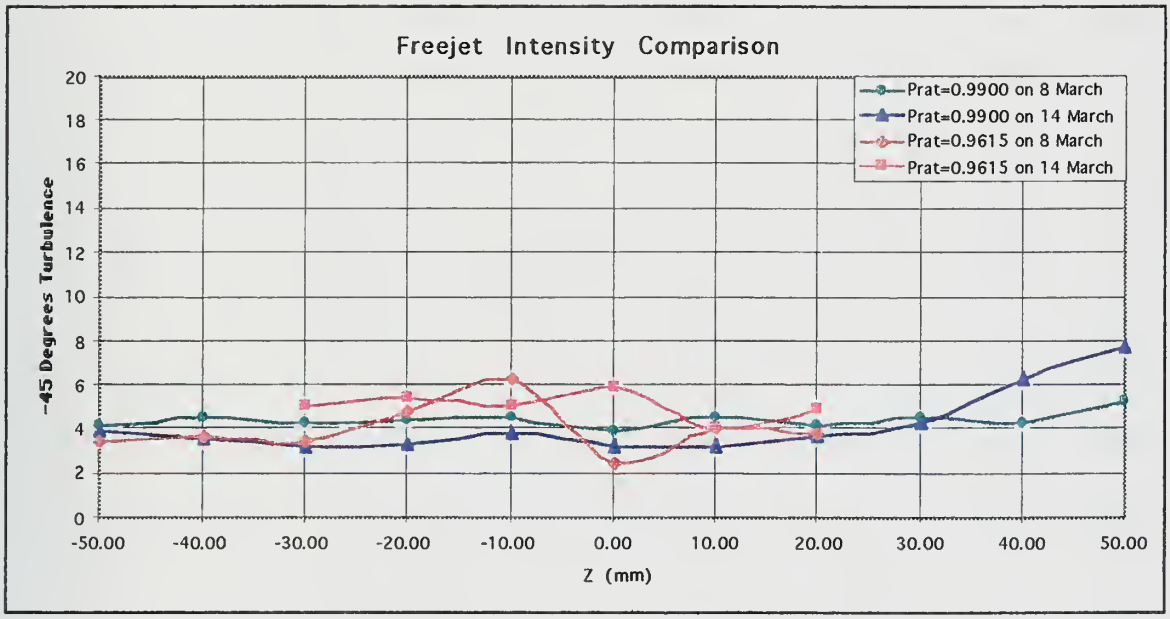

Figure F3b. Freejet Survey

APPENDIX G. PRESSURIZED WINDOW AT PRAT OF 0.9054

Date	Prat	Chamber Pressure	Run	Depth	U-Velocity	U-Non dim.	V-Velocity	V-Non dim.	U-Turbulence Intensity	V-Turbulence Intensity	Flow Angle
		(in mm water)	#	(mm)	(m/s)	Velocity	(m/s)	Velocity	(%)	(%)	(degrees)
5/7/96	.9054	3	1	0.01	3.398	.0043	67.975	.0866	8.022	11.862	87.14
				0.06	3.001	.0038	68.373	.0872	7.692	12.266	87.49
				0.18	5.117	.0065	69.404	.0885	8.898	12.292	85.78
				0.42	3.407	.0043	71.727	.0914	8.270	11.362	87.28
				0.89	11.631	.0148	69.201	.0882	9.309	9.388	80.46
			2	0.01	2.081	.0026	67.502	.0860	6.561	12.056	88.23
				0.06	1.818	.0023	67.970	.0866	6.389	12.073	88.47
				0.18	2.674	.0034	68.722	.0876	7.628	12.274	87.77
				0.42	1.296	.0016	71.341	.0909	5.686	10.785	88.96
				0.89	11.644	.0148	72.996	.0930	8.657	9.788	80.94
		6	1	0.01	.521	.0007	67.324	.0858	3.696	12.163	89.56
				0.06	.256	.0003	67.376	.0859	2.848	12.338	89.78
				0.18	.347	.0004	68.554	.0874	3.293	11.846	89.71
				0.42	.738	.0009	70.991	.0905	4.489	11.210	89.40
				0.89	11.505	.0147	74.124	.0945	9.041	9.520	81.18
			2	0.01	.529	.0007	67.633	.0862	3.854	12.645	89.55
				0.06	.396	.0005	68.027	.0867	3.478	12.197	89.67
				0.18	0.4929	.0006	68.055	.0867	3.740	11.884	89.59
				0.42	3.5915	.0046	70.609	.0900	8.548	11.835	87.09
				0.89	11.69	.0149	71.031	.0905	8.772	11.681	80.65

Table G1. Pressurized window data at a Prat of 0.9054

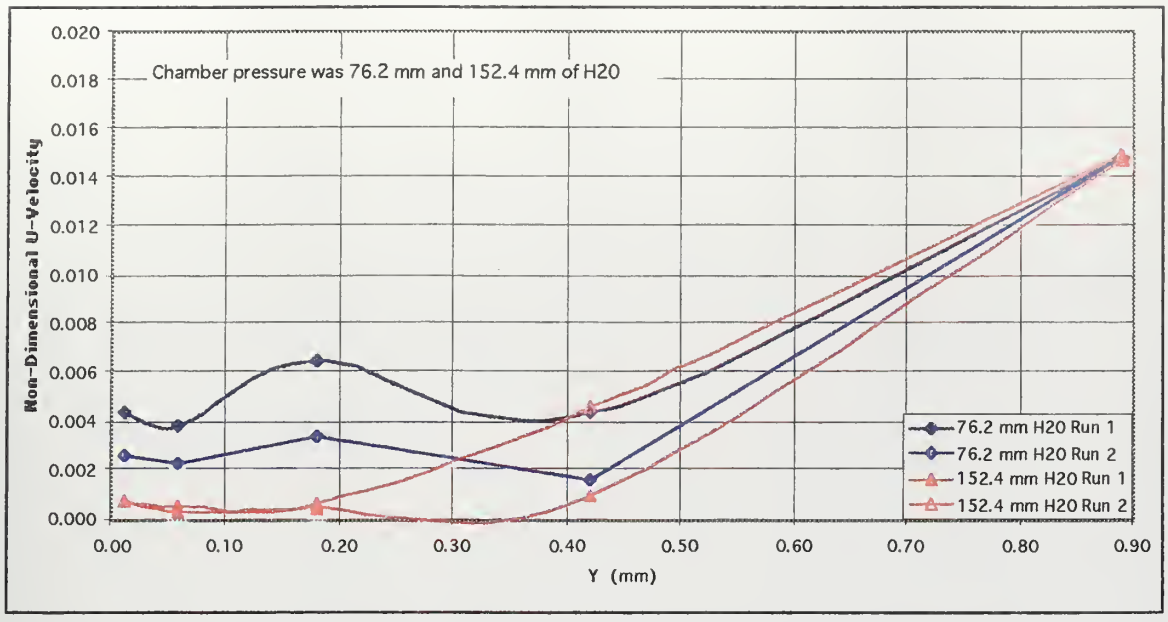

Figure G1a. A radial survey through the pressurized window at a Prat of 0.9054

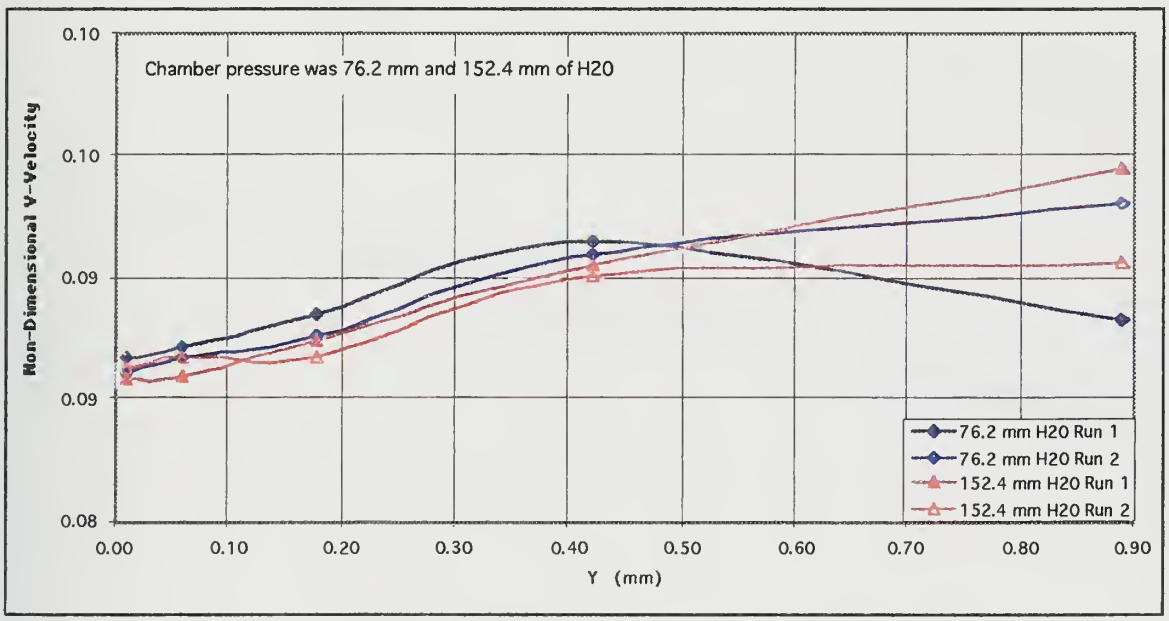

Figure G1b. A radial survey through the pressurized window at a Prat of 0.9054

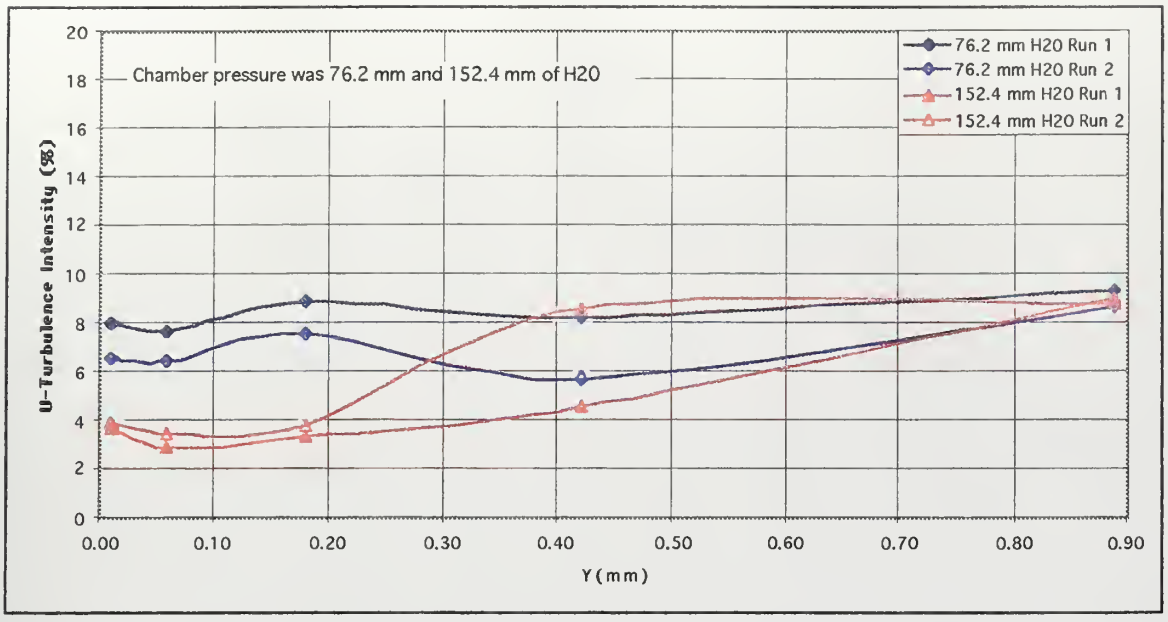

Figure G2a. A radial survey through the pressurized window at a Prat of 0.9054

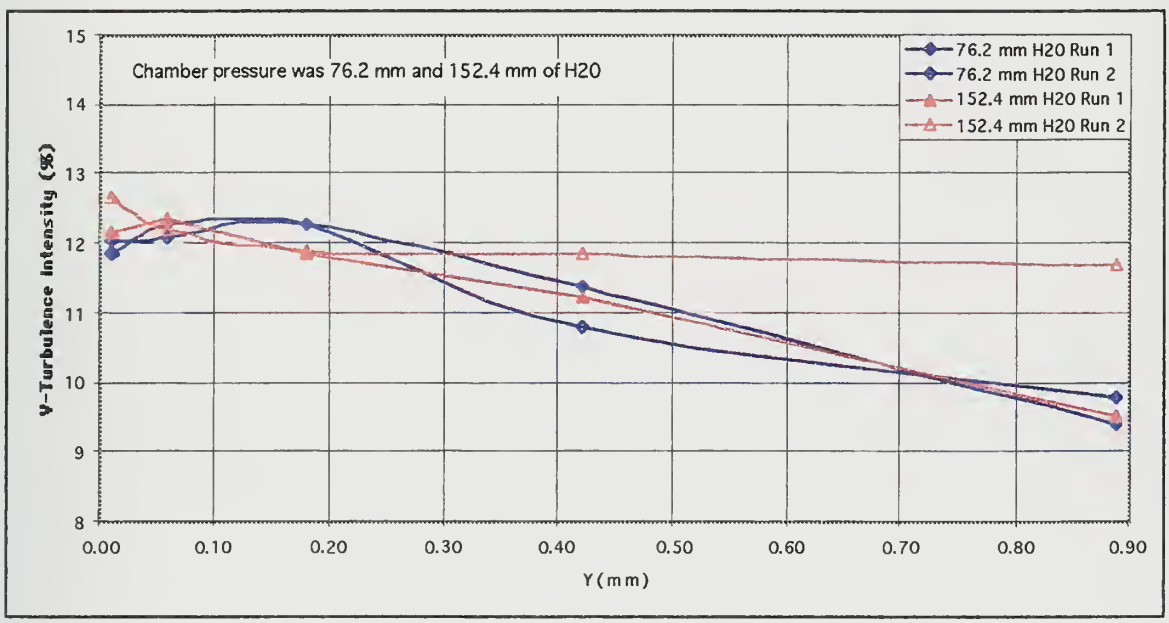

Figure G2b. A radial survey through the pressurized window at a Prat of 0.9054

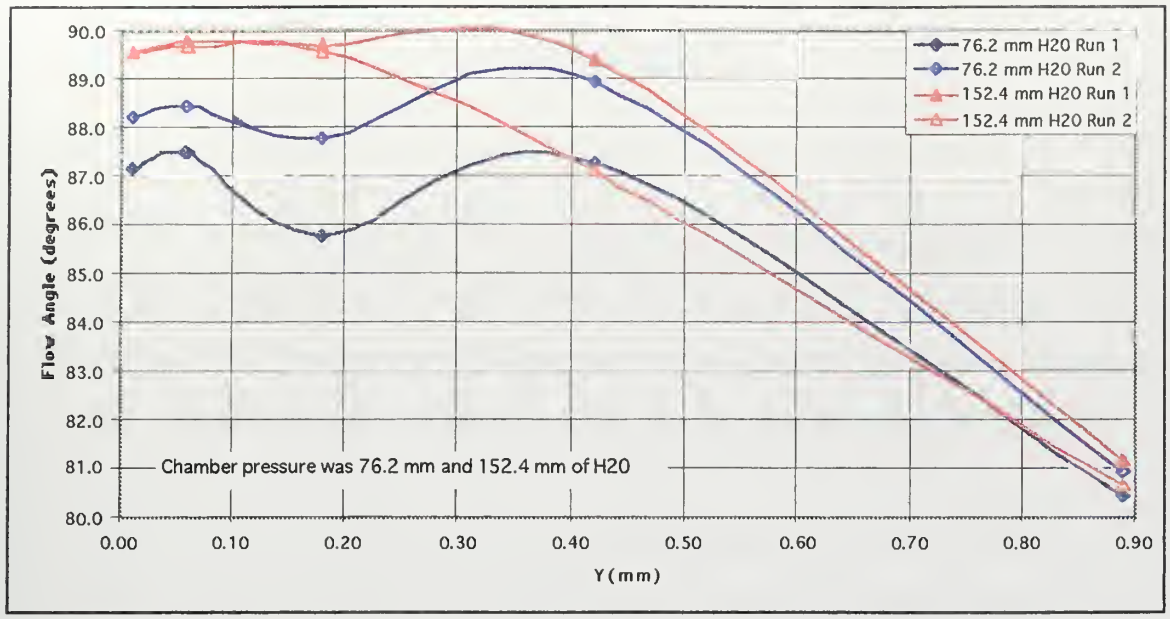

Figure G3. A radial survey through the pressurized window at a Prat of 0.9054

LIST OF REFERENCES

1. Chima, R. V. and Yokota, J. W., "Numerical Analysis of Three-Dimensional Viscous Flows in Turbomachinery," AIAA Journal, Vol. 28, No. 5, May 1990, pp. 798-806.
2. Donovan, B.H., "Experimental and Computational Investigation of the Flow Through an Annular Turbine Cascade," Master's Thesis, Naval Postgraduate School, Monterey, CA, June 1995.
3. Spitz, J.D., "Laser Anemometry and Viscous Computation of the Flow Through an Annular Turbine Cascade," Master's Thesis, Naval Postgraduate School, Monterey, CA, March 1994.
4. Thomas, G. D., "Measurement and Prediction of the Flow Through an Annular Turbine Cascade," Master's Thesis, Naval Postgraduate School, Monterey, CA, June 1993.

INITIAL DISTRIBUTION LIST

		No. Copies
1.	Defense Technical Information Center 8725 John J. Kingman Road., Ste 0944 Ft. Belvoir, VA 22060-6218	2
2.	Dudley Knox Library Naval Postgraduate School 411 Dyer Rd. Monterey, CA 93943-5101	2
3.	Professor Daniel J. Collins Department of Aeronautics and Astronautics Code AA/CO Naval Postgraduate School 699 Dyer Road-Room 137 Monterey, CA 93943-5106	1
4.	Professor Garth V. Hobson Department of Aeronautics and Astronautics Code AA/HG Naval Postgraduate School 699 Dyer Road-Room 137 Monterey, CA 93943-5106	10
5.	Professor Raymond P. Shreeve Department of Aeronautics and Astronautics Code AA/SF Naval Postgraduate School 699 Dyer Road-Room 137 Monterey, CA 93943-5106	1
6.	Naval Air Systems Command AIR-4.4.T (Attn: Mr. C. Gordon) Washington, DC 20361-5360	1
7.	Naval Air Warfare Center Aircraft Division AIR-4.4.3.1(Attn: D. Parish) Propulsion and Power Engineering, Building 106 Patuxent River, MD 20670-5304	1
8.	Michael H. Guerrera 94-419 Noholoa Loop Mililani Town, HI, 96789	3